AD-A150 794 SPATIAL ACQUISITION ALGORITHMS AND SYSTEMS FOR INTERSATELLITE OPTICAL COM..(U) MASSACHUSETTS INST OF TECH LEXINGTON LINCOLN LAB P VAN HOVE ET AL. 27 NOV 84 1/2

UNCLASSIFIED TR-667 ESD-TR-84-016 F19628-85-C-0002 F/G 17/2 NL

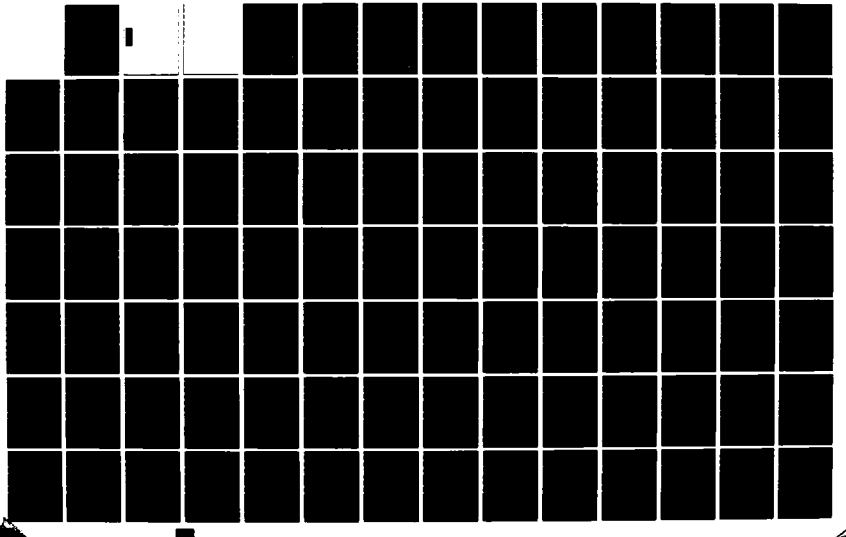

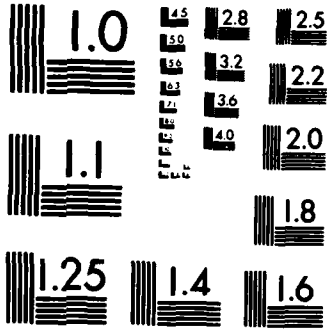

MICROCOPY RESOLUTION TEST CHART
NATIONAL BUREAU OF STANDARDS-1963-A

MASSACHUSETTS INSTITUTE OF TECHNOLOGY
LINCOLN LABORATORY

SPATIAL ACQUISITION ALGORITHMS AND SYSTEMS FOR INTERSATELLITE OPTICAL COMMUNICATION LINKS

P. VAN HOVE
V.W.S. CHAN
Group 68

TECHNICAL REPORT 667

27 NOVEMBER 1984

LEXINGTON MASSACHUSETTS

ABSTRACT

Spatial acquisition strategies and technologies are analyzed for optical communication systems. Theoretical analysis is followed by examples and comparisons to aid system design. Examples are given for state-of-the-art technology appropriate for space applications.

TABLE OF CONTENTS

TABLE OF CONTENTS (Con't)

LIST OF FIGURES

LIST OF FIGURES (Continued)

LIST OF FIGURES (Continued)

INTRODUCTION

Optical communications offer attractive advantages for intersatellite communications and their implementation has been investigated [1]. Our primary interest is in two-way links where both satellites have a transmitter laser and a receiving system. A crucial advantage of optical waves for communications is their short wavelength, allowing very large bandwidths and very high antenna gains. This in turn permits the use of low power transmitter lasers without sacrificing the throughput rate of the channel.

The use of large antenna gains induces very narrow transmission beams. The system performance therefore relies strongly on the correct pointing of the transmitter and receiver optics. The initial uncertainty on the positioning is usually much larger than the value required for establishing the link. The function of a spatial acquisition system is to estimate the position of the partner satellite to within a desired uncertainty bound. The tracking system then upgrades this estimate and compensates for further fluctuations in time. Although the spatial acquisition may be coupled with the acquisition of other parameters such as time and frequency, we are concerned here primarily about spatial acquisition and will consider the other parameters only for as far as they interact with the spatial acquisition.

The spatial acquisition problem considered as a whole is very involved and the performance may depend on a large number of parameters. The goal of the analysis presented in this report is to clarify the tradeoffs between various designs and to serve as a guide towards sensible engineering

choices. These choices include the selection between direct and heterodyne detection technologies and between parallel, serial or zooming strategies. The problem will be idealized, resulting in mathematical expressions which may compare to the real world figures only through multiplicative constants, but which are suitable for comparisons. The idealization of the problem includes ignoring the relative motion, ignoring synchronization issues, discretizing the parameters, and modeling as a fixed sample size Bayes test. The rationale behind these hypotheses is developed in the preliminaries.

The appropriate technology must be chosen keeping also in mind that the spatial acquisition unit is an ancillary package. It should therefore not dominate the transmission system performance, weight and power requirement.

1. PRELIMINARIES

This chapter presents some notation and vocabulary used through this report, addresses some hypotheses and idealizations made in the sequel, and outlines the structure of the next chapters.

1.1 Notations

The two satellites are denoted A and B. These symbols appear as a right subscript to specify which satellite a parameter describes. Right superscripts are used to specify some parameters more explicitly. Integer arguments on the parameters designate the zooming stage, from 0 to I-1, when performing a zooming acquisition. A list of the main parameters follows.

D_B^T	Diameter of the transmitter output lens on B
D_A^R	Diameter of the receiver input lens on A
e	The electronic charge
f_o	Central frequency of the IF signal
F	Noise factor of the photomultiplying detector
H_{ijk}	Hypothesis, ijk, meaning the signal is present in spatial slot i, time slot j, frequency slot k
H_p	Hypothesis p, meaning the signal is present in spatial slot p
$h_f(t)$	Transfer function of the IF filter
$H_f(\omega)$	Frequency response of the IF filter
h	Planck's constant

I	Number of zooming stages
k	Boltzmann's constant
K_A	Number of sensors of the reveiver on A
$K_x(t,u)$	Covariance function of the process x(t)
L	Distance between both satellites
l_{ijk}	Sufficient statistic for the spatial slot i, time slot j, frequency slot k
$\underline{l}$	Array combining all the sufficient statistics
M_A	$= \Omega_B^U/\Omega_B^D$. Desired accuracy improvement in solid angle. Also the dimension of the M-ary detection problem for the receiver on A
m_n	Mean value of the sufficient statistic when only noise is present
m_s	Mean value of the sufficient statistic when the signal is present
N_A^T	$= \Omega_A^U/\Omega_B^B$. Ratio of the uncertainty solid angle to the illumination solid angle from B. This is also the number of time slots for the receiver on A
N_A^{F*}	$= W/W^S$. Maximal value of N_A^F
$N_o/2$	Double sided spectral density of the noise
P_B^L	Power of the transmitter laser on B
P_A^S	Signal power received by A, averaged over the total acquisition time
PE	Probability of an erroneous acquisition
$PE(2)$	Probability of error in a binary test
PAC	Probability of a correct acquisition

$S_x(\omega)$	Power spectral density of the process x(t)
t_o	Starting time of the acquisition
T_i, T_f	Time limits for the signal integration
T_A	Total spatial acquisition time for the receiver on A
W	Maximum frequency shift between the received signal and the local oscillator signal
W^F	Bandwidth of the IF filters
W^S	Short time bandwidth of the IF signal
Z	Input impedance of the photodiode amplifier
η	Quantum efficiency of the optical detector
λ	Optical wavelength
λ_b	Noise photon count rate
λ_s	Signal photon count rate
λ_{bo}	Background noise photon count rate per spatial mode
ν	Optical frequency
Ω_A^U	Solid angle representing the uncertainty B has on the position of A
Ω_A^R	Solid angle representing the resolution limit of the receiver on A
Ω_B^D	Solid angle representing the desired uncertainty range on the position of B. This is usually equal to Ω_A^R
Ω_B^B	Solid angle of the beam emitted by B. The power density of the beam is assumed uniform over Ω_B^B

σ_n^2	Variance of the sufficient statistic when only noise is present
σ_s^2	Variance of the sufficient statistic when the signal is present
θ_A	Half aperture of the cone subtending Ω_A^U

Some abbreviations and definitions are listed below.

APD	Avalanche photo diode
AWGN	Additive White Gaussian Noise
PMT	Photo Multiplier Tube
PSD	Power Spectral Density

A parallel illumination consists of illuminating the whole uncertainty zone Ω_A^U uniformly from B.

A sequential illumination consists of scanning Ω_A^U with a beam of width $\Omega_B^B \leq \Omega_A^U$. Satellite A then receives a signal burst of duration T_A/N_A^T, and only noise during the rest of T_A.

A parallel receiver operation consists of mapping the total uncertainty zone Ω_B^U onto the receiver array in the focal plane of the imaging system on A, and collecting the data from the sensors simultaneously.

A sequential receiver operation consists of scanning the image of Ω_B^U in in the focal plane, with the K_A available sensors.

A zooming acquisition consists of reducing $\Omega_B^U = \Omega_B^U(o)$ down to Ω_B^D in several steps. At each step i, $\Omega_B^U(i)$ is reduced to $\Omega_B^U(i+1)$.

1.2 Idealizing the Problem

We discuss in this section some issues of concern for the spatial acquisition and develop the rationale behind the adopted solutions.

1.2.1 Modeling as a Bayes M-ary Detection

The acquisition system is faced with a non-linear estimation problem, since the parameter is imbedded in the received signal in a non-linear way. A problem of this kind is usually separated into two steps [2]; a) the range of the parameter is divided into slots of appropriate width and the receiver decides in which of the slots the parameter lies; b) a maximum likelihood (ML) or minimum mean square error (MMSE) estimator provides a closer estimate of the parameter. In the present analysis, we assume that task b) of the estimation problem is assigned to the tracking system. The acquisition can be therefore modeled as an M-ary detection problem. Furthermore, we consider the simplifying approximation that the parameters imbedded in the received signal are also discrete, each value corresponding to one of the receiver slots; see Sec. 1.2.5. We assign the a-priori probabilities and choose the costs for minimum probability of error. The test is therefore a Bayes M-ary detection.

1.2.2 Sample Size Choice

Once a spatial acquisition procedure is initiated, it should always succeed. The appropriate statistical test may therefore be the sequential test [3]. In a sequential test, the data is collected and continuously

tested until a decision can be made with a sufficient certainty. The test duration is therefore data dependent and is a random variable. We consider in this report fixed sample size tests however (Bayes tests in this case). We evaluate for these tests, the mean probability of error for fixed data acquisition times. The duration required to achieve a desired mean probability of error with the fixed sample size test is longer than the average duration required by a sequential test for the same error probability. We assume here the ratio between both durations does not depend appreciably on the acquisition strategy and on the signal statistics. The fixed sample size Bayes test therefore gives useful results for comparing the various strategies.

1.2.3 Relative Motion

The relative position of the satellites may be derived from ephemerides data, but fluctuations in the orbits induce uncertainties of the order of 10^{-3} rad on both azimuth and elevation. Diffraction limited communication beams may have a divergence as low as 10^{-5} rad. This is much smaller than the uncertainty regions and the desired improvement in accuracy is on the order of 10^{4}, when expressed as solid angles. The positions of both satellites are not fixed in time, but ephemerides give an estimate of the relative angular velocity of the satellites. The largest relative angular velocity is 200 μrad/sec and may be known to within a fractional error of 10^{-4}. If ephemerides position and velocity data are used by an open loop spatial tracking system, a 100 sec acquisition will incur a tracking error of only 2×10^{-6} rad which is smaller than the diffraction limited resolution of

the optics of either satellite. The relative motion is therefore neglected in this analysis, assuming ephemerides velocity data is available and used by an open loop tracking system during the acquisition.

1.2.4 Coupling of the Parameters

Before the optical communication link can be established, not only the optics must be correctly pointed, but also the frequency, polarization and timing must be acquired and tracked to within tight uncertainty bounds.

The acquisition of any of the four parameters may depend on the knowledge of the other parameters. The optimal acquisition scheme can therefore involve a simultaneous acquisition of all the parameters. Our primary concern here is spatial acquisition but we will examine briefly the coupling of the spatial parameter with the other parameters. The starting time of the acquisition sequence and the schedule of the acquisition is assumed to be known a priori or received through another communication link, with an accuracy sufficient to assume that a coordinated two-way acquisition is possible. If direct detection is used for the spatial acquisition system, polarization and frequency are irrelevant parameters as long as the signal frequency is within the bandwidth of the optical filter of the receiver. Spatial acquisition is therefore decoupled from these parameters in direct detection. When heterodyne detection is used, quadrature polarization detectors may be used to decouple the polarization parameter. However, the frequency mismatch between the received beam and the local oscillator may be large and unknown before the acquisition proceeds, for heterodyne detection.

Spatial and frequency acquisitions are therefore coupled in this case. In our analysis, we consider several signal models and cover separate as well as simultaneous frequency and spatial acquisitions.

1.2.5 Idealizing the Geometry and the Signals

We assume here the illumination beam has a uniform power density over its opening and its geometry permits a scanning of the uncertainty zone without any overlap. This assumption is unrealistic but the overlap and diffraction effects may be accounted for by a single correction factor on the laser power.

We consider all bandlimited signals to have a rectangular power spectral density and all bandpass filters to have a rectangular frequency response. Other power spectral densities or filter responses are accommodated through correctly defining the bandwidths involved.

1.2.6 *Parallel Receiver, Sequential Illumination*

We concentrate our analysis in Chapters 2 and 3 on a parallel receiver operation and a sequential illumination strategy. The initial uncertainty zone Ω_A^U is divided into N_A^T subcells with an area of Ω_B^B each, and the transmitter on B illuminates each cell for a duration T_A/N_A^T. The receiver on maps the uncertainty zone Ω_B^U onto its detector array and analyzes the outputs of the sensors simultaneously.

The acquisition time for a sequential receiver operation is obtained from the parallel receiver acquisition time through a simple multiplication. Specifically, if Ω_B^U is divided into M_A resolution cells and if only $K_A < M_A$ cells are analyzed simultaneously, the acquisition time is M/K times the acquisition time for an M-sensor parallel receiver.

The acquisition time for a parallel illumination corresponds to the particular case $N_A^T = 1$, $\Omega_B^B = \Omega_A^U$.

The sequential illumination and parallel receiver strategy therefore provides the figures for the other non-zooming strategies.

1.2.7 Average Illumination Power

ince the probability of presence of A has a uniform density over Ω_A^U, the beam illuminating this region from B must investigate all the area uniformly. Averaging over the search time T_A, the transmitter laser power is therefore uniformly distributed over the uncertainty zone Ω_A^U. If θ_A is the half angle opening of the cone subtending Ω_A^U, then $\Omega_A^U \simeq \pi\theta_A^2$ for small θ_A and the average signal power density received by A is $P_B^L/\pi\theta_A^2 L^2$. The effective aperture area of the receiver is $\pi/4\ (D_A^R)^2$ and collects an average power given by

$$P_A^S = \frac{P_B^L}{4}\left(\frac{D_A^R}{L\theta_A}\right)^2 \tag{1.1}$$

The average signal photon count rate λ_s is given by

$$\lambda_s = \frac{\eta P^s}{h\nu} = \frac{\eta P_B^L}{4h\nu}\left(\frac{D_A^R}{L\theta_A}\right)^2 \tag{1.2}$$

1.3 Report Outline

We concentrate our analysis on parallel receiver operation and sequential illumination. From our discussion in Sec. 1.2.6, the results obtained for this strategy are easily applied to the other non-zooming strategies. We discuss this strategy in Chapter 2 for heterodyne detection, and in Chapter 3 for direct detection.

When a parallel receiver structure is used, the search reduces the uncertainty zone to a solid angle $\Omega^U(1) = \frac{1}{K}\,\Omega^U(0)$. The proper acquisition requires the number of sensors to be $M = \Omega^U(0)/\Omega^D$, which is typically 10^4. If $K < M$, the sensors may be scanned along the image of $\Omega^U(0)$ in the focal plane, and the results of Chapters 2 and 3 may be used when multiplied by the factor M/K. For some detector technologies, the maximum number of sensors may be on the order of 10. In a typical situation, the parallel acquisition time is multiplied by a factor of about 10^3 and the total acquisition time may become much larger than one minute, which is excessive. The strategies considered above consist of a single data collection part followed by a single decision.

Another approach is to conduct a zooming acquisition. At the i^{th} step of the zooming, the initial uncertainty zone $\Omega^U(i)$ is mapped onto the K-sensor array in the focal plane and is reduced to $\Omega^U(i+1) = 1/K\ \Omega^U(i)$ by the decision made after the partial search time T(i). If the acquisition proceeds in a cooperative two-way fashion, each satellite illuminates only the residual uncertainty zone $\Omega^U(i)$ at step i; the signal to noise ratio therefore increases significantly at each stage. Zooming acquisition is

discussed in Chapter 4. Finally, a review and a discussion of the results is presented in Chapter 5.

2. SPATIAL ACQUISITION - HETERODYNE DETECTION - ONE-STEP SEARCH

2.1 Organization

We discuss in this chapter the implementation and the performance of the one-way spatial acquisition performed with heterodyne detection, a sequential illumination and a parallel receiver operation. A statement of the problem is given in Sec. 2.2. A mathematical model of the problem is given in Sec. 2.3. Solutions are given in Sec. 2.4 for various assumptions. Numerical results are given in Sec. 2.5. Extensions to other search strategies are addressed in Sec. 2.6.

2.2 Statement of the Problem

Let two satellites A and B perform a mutual spatial acquisition procedure starting at the same time t_o. Both satellites have transmitter lasers of powers P_A^L, P_B^L respectively, operating at the same wavelength λ, and have beamforming optics of diameters D_A^T, D_B^T. The on-board receivers consist of optical imaging systems of aperture sizes D_A^R, D_B^R and heterodyne receiver arrays of K_A and K_B elements respectively.

The satellites are separated by a distance L and the a priori knowledge that B has on the relative position of A is summarized by a uniform probability of presence density in the solid angle Ω_A^U. Conversely, Ω_B^U is the solid angle of the zone which represents the a priori uncertainty that A has on the position of B; see Fig. 2.1. From our previous discussion, we consider a reference frame where there is negligible relative angular motion.

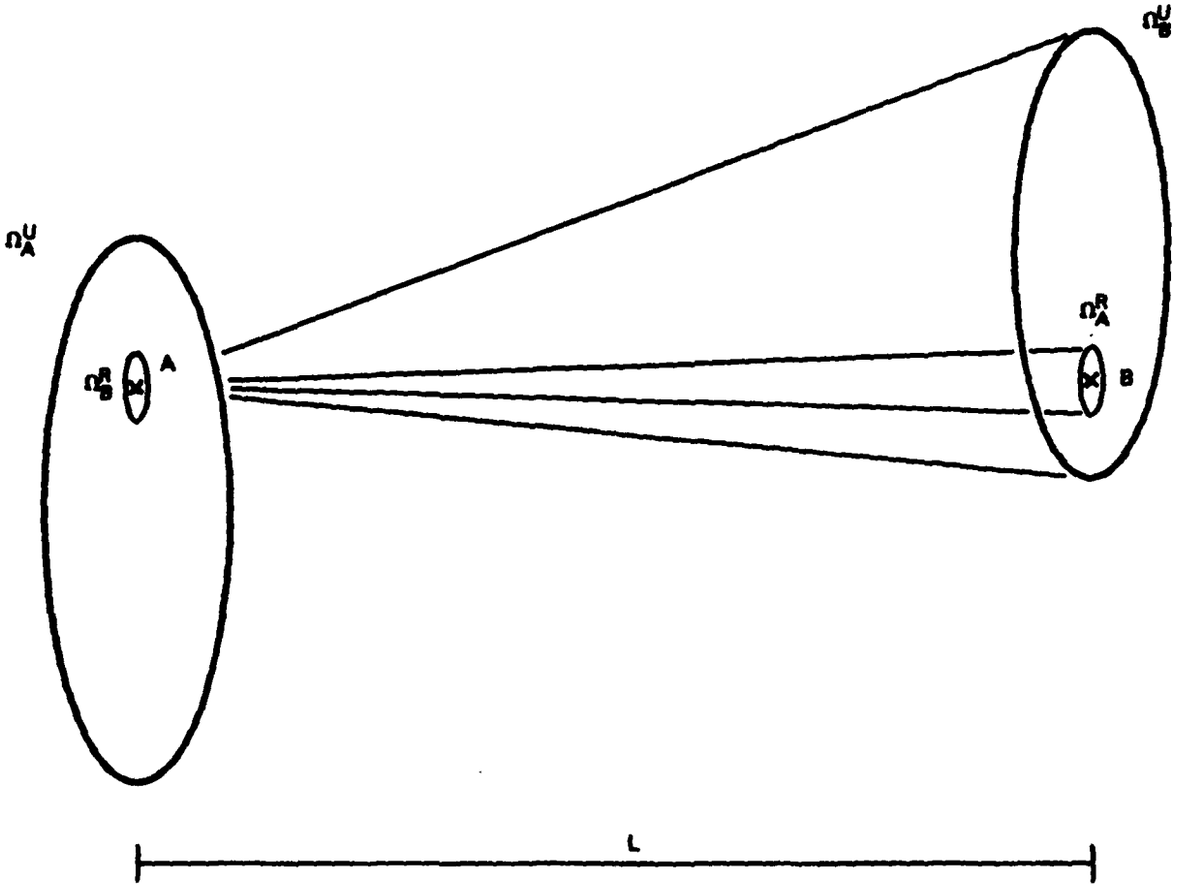

131148N

Fig. 2.1. Geometry of the acquisition problem.

The spatial acquisition procedure is considered complete when the spatial uncertainty zones have been narrowed from their initial values Ω_A^U and Ω_B^U, down to the desired values, Ω_B^D and Ω_A^D. We consider in the sequel the case where $\Omega_A^D = \Omega_B^R$, the resoltuion limit of the receiver on B. We assume a fixed time search, and consider the cost criterium to be minimum probability of error. The problem then becomes a Bayes hypothesis testing problem because all a priori probabilities and costs are assigned. We may then derive optimum receivers and their probability of error PE. Subsequently we may invert this result to obtain an expression for the acquisition time required to achieve a defined probability of correct acquisition PAC = 1 - PE.

We consider in this chapter, only two simultaneous but independent one-way acquisitions. Since the two acquisitions are equivalent, we only evaluate the acquisition time T_A, defined as the data collection time required for the receiver on A to locate the position of B with a probability PAC. The duration T_A depends essentially on the signal models, the signal to noise ratios, and on the dimension of the detection problem. The averaged signal level is given by P_A^S in Eq. (1.1) and the dimension of the problem is characterized by the resolution gain M_A, the number of timeslots N_A^T and the number of detectors K_A. We find in this chapter, expressions for T_A as a function of P_A^S, M_A, N_A^T, K_A and the signal and noise models. Since the same expressions hold for T_B, the subscripts will be sometimes omitted.

2.3 Mathematical Model of the Problem

We assume first that the one-way acquisition is performed with a parallel processing in one step. This means that the number of sensors K_A must be no less than the desired resolution gain $M_A = \Omega_B^U/\Omega_A^D$. If this is not the case, either a sequential, a zooming or a combination of both receiver operations must be used; see Sec. 2.6. We assume in the following discussion that $K_A = M_A$.

The illumination strategy consists of sequentially illuminating from B, the whole uncertainty zone Ω_A^U with a beam of solid angle $\Omega_B^B \geq \Omega_B^D$. The uncertainty zone Ω_A^U is therefore divided into $N_A^T = \Omega_A^U/\Omega_B^B$ non-overlapping cells and the acquisition duration T_A is divided into N_A^T time slots. During each timeslot, the beam illuminates one cell and then is switched to the next cell for the duration of the next timeslot; see Fig. 2.2. The signal received at A is therefore a burst with a duration T_A^T/N_A.

The receiver optics in A map Ω_B^U onto the array of M elements in the image plane. Each sensor cell corresponds to the resolution limit of the optical system and has therefore the size of the Airy disk; see Fig. 2.2. The incoming light is mixed with a local oscillator to produce a heterodyne signal. We assume that there is a perfect spatial match between incoming and reference waves.

Three models for representing the IF waveform due to the received signal after heterodyne detection will be considered. All bandwidths given are one-sided.

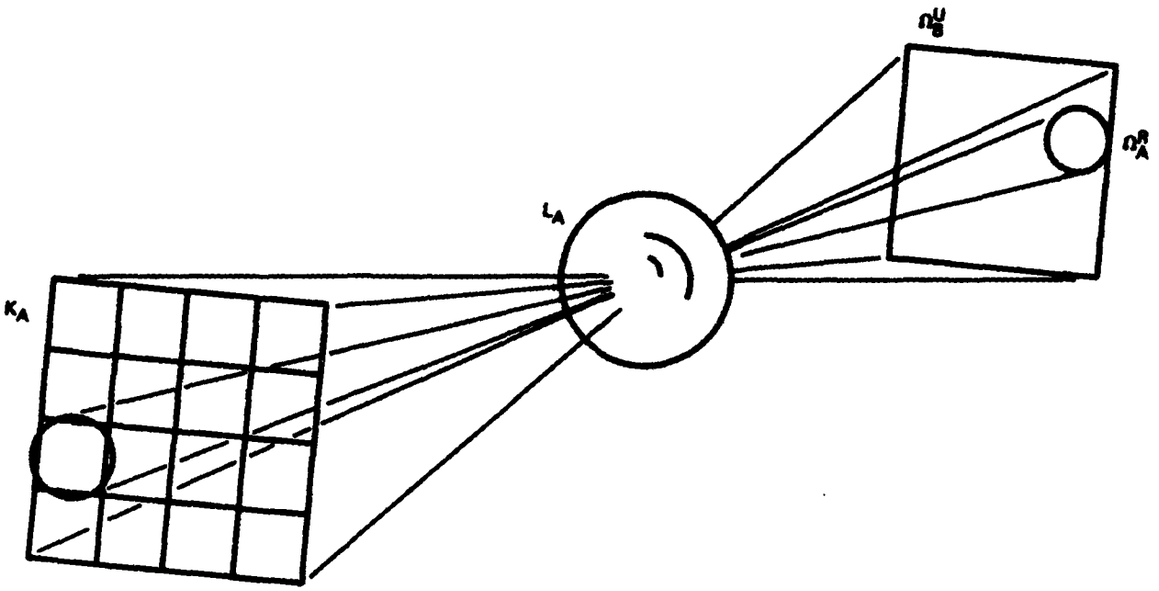

131149N

Fig. 2.2. Mapping of the uncertainty zone Ω_B^u to the focal plane of the receiver in A.

a) The signal is modeled as a zero-mean narrowband Gaussian process of bandwidth W_s with a random center frequency f_o (constant over time) which is uniformly distributed over a frequency interval W.

b) The signal is a sine wave with a frequency jitter such that the instantaneous frequency is uniformly distributed over a bandwidth W_s the center frequency of which (f_o constant over time) is in turn uniformly distributed over $W > W_s$.

c) The signal is a pure sinusoid with random phase and frequency f_o uniformly distributed over the bandwidth W; see Fig. 2.3.

The noise at the receiver is dominated by quantum shot noise. It may be modeled as an additive white Gaussian noise (AWGN) of double-sided spectral height $N_o/2 = h\nu/2\eta$. The rationale behind these signal models is the following. The optimum receiver for model c) gives an upper bound on the performance because it is equivalent to assuming an instantaneous frequency acquisition and an error-free frequency tracking during the spatial acquisition. Model b) is a closer representation of semiconductor lasers noise, although the actual power spectral density (PSD) of the frequency noise may not be rectangular. Model a) is an approximation to model b) which leads easily to optimum receiver designs and which is completely characterized by second order moments. This model introduces signal amplitude fluctuations however, which may not acccurately model the real signal when the lasers are very coherent. For all models, the center frequency f_o is random due to the frequency uncertainties between the transmitter laser in satellite B and the

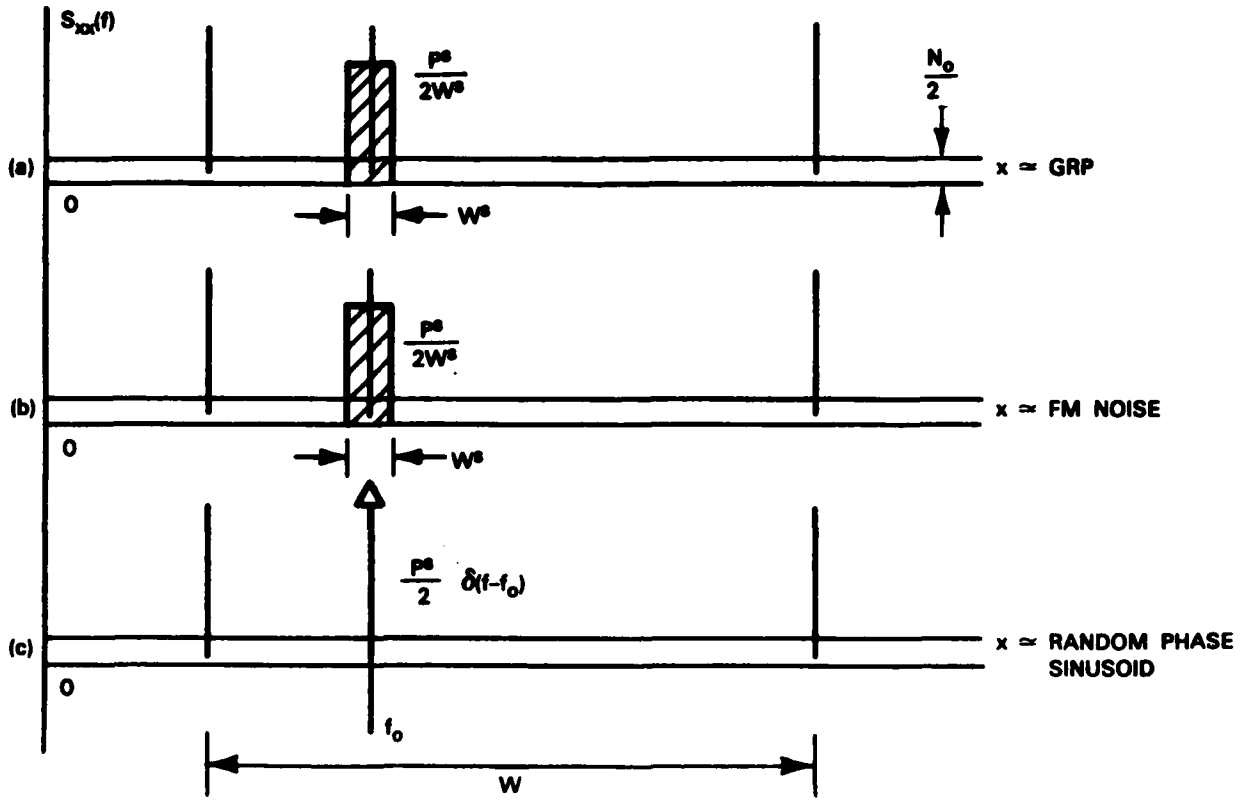

131150N

Fig. 2.3. Spectra of signal models.

local oscillator in satellite A. The mismatch, due mainly to temperature changes and doppler shifts, may be large so that $W \gg W_s$. However, the acquisition time is assumed to be short enough so that f_o does not change during the entire acquisition process.

2.4 Solution of the Problem

2.4.1 Reduction of the Problem

According to the discussion in Chapter 1, we consider only discrete values of the random parameters. It is therefore assumed that the incoming signal energy is concentrated into only one of the M sensors, the signal is a pulse of duration T/N^T starting at a discrete valued random time $t_o + i\ T/N^T$, and the frequency spectrum lies completely in one out of N^F non-overlapping frequency bands. Under the above mentioned assumptions, the incoming wave may be one of $M \times N^T \times N^F$ orthogonal signals, which are equiprobable. Since the spatial acquisition is not concerned with the estimation of the frequency and time of arrival of the signal, our problem is a composite M-ary detection with a set of unwanted parameters which may take $N^T \times N^F$ values on each hypothesis.

The received waveform in each spatial, time and frequency slot may be characterized by a sufficient statistic ℓ_{ijk}, where $i\varepsilon[1,M]$ labels the spatial array cell, $j\varepsilon[1,N^T]$ labels the timeslot, $k\varepsilon[1,N^F]$ labels the frequency slot. The random variables ℓ_{ijk} are statistically independent and have probability densities, conditional to the signal being in spatial, time and frequency slots (p,q,r) given by

$$P_{\ell_{ijk}|H_{pqr}}(L_{ijk}|H_{pqr}) = [p_s(L_{ijk}) - p_n(L_{ijk})]\ \delta_{ip}\delta_{jq}\delta_{kr} + p_n(L_{ijk}) \qquad (1)$$

where $p_s(\cdot)$ is the density when the signal is present in slot (ijk) and $p_n(\cdot)$ is the noise density. The received waveform is completely characterized by the array $\underline{\ell} = \{\ell_{ijk}\}$. The probability density of the sufficient statistics $\underline{\ell}$, averaged over the unwanted parameter set, conditional on the spatial hypothesis H_p is given by:

$$P_{\underline{\ell}|H_p}(\underline{L}|H_p) = \frac{1}{N^T N^F} \sum_{q=1}^{N^T} \sum_{r=1}^{N^F} \frac{p_s(L_{pqr})}{p_n(L_{pqr})} \prod_{\text{all (ijk)}} p_n(L_{ijk}) \qquad (2)$$

The optimum decision rule for minimum PE, with equal a priori probabilities, is the maximum likelihood decision rule,

$$\max_{P} \sum_{q=1}^{N^T} \sum_{r=1}^{N^F} \frac{p_s(L_{pqr})}{p_n(L_{pqr})} \qquad (3)$$

For high signal to noise ratios, the function $p_s(L_{pqr})/p_n(L_{pqr})$ has an exponential dependence on L_{pqr}. This implies that the suboptimal rule:

$$\max_{p} \left[\max_{q} \max_{r} \frac{p_s(L_{pqr})}{p_n(L_{pqr})}\right] \qquad (4)$$

is close to optimal. This rule is the optimal decision when the costs are assigned for the simultaneous acquisition of position, frequency and time of arrival. If the function $p_s(\cdot)/p_n(\cdot)$ is monotonically increasing, the rule in Eq. (4) is equivalent to finding the largest L_{pqr}:

$$\max_{p} \left[\max_{q} \max_{r} L_{pqr} \right] \tag{5}$$

and declaring hypothesis H_s if $p = s$ is the spatial cell corresponding to the largest L_{pqr}. The decision rule in (5), as opposed to (3), does not require the knowledge of the signal parameters. The performance of the suboptimal receiver in (4) or (5) is well approximated by the union bound in the case of low PE and AWGN. An error is likely to occur when one of the $(M-1) \times N^T \times N^F$ variables ℓ_{ijk} corresponding to spatial cells which receive only noise exceeds the variable which contains the signal component. The probability of error is bounded as:

$$PE \leq (M-1) \times N^T \times N^F \times PE^{(2)} \tag{6}$$

where $PE^{(2)}$ is the probability of error in a binary hypothesis testing with the same probability assignments and no unwanted parameters. Our remaining work in this section consists of finding expressions for ℓ_{pqr} as a function of the received signal $\underline{r}(t)$ and computing the binary detection performance $PE^{(2)}$.

2.4.2.1 Signal Model (a): Gaussian Noise with a Flat PSD Over W_s

The sufficient statistic in this case corresponds to the detection of a zero-mean Gaussian process in additive white Gaussian noise and is given in [4], Eq. (2.31) as

$$\ell_{ijk} = \frac{1}{N_o} \int_{T_i}^{T_f} r_i(t)\, h_1(t,u)\, r_i(u)\, dtdu \; ; \quad T_f - T_i = T/N^T \tag{7}$$

where $r_i(t)$ is the received signal in the spatial cell i. The function $h_i(t,u)$ satisfies the integral equation ([4], Eq. (2.23)

$$\frac{N_o}{2} h_i(t,u) + \int_{T_i}^{T_f} h_i(t,z)\, K_s(z,u)dz = K_s(t,u) \tag{8}$$

for $T_i \leq t, \quad u \leq T_f$

where $K_s(t,u)$ is the signal covariance function. Under the SPLOT (Stationary Process, Long Observation Time) condition, Eq. (8) is approximated by [4],

$$\ell_{ijk} = \frac{1}{N_o} \int_{T_i}^{T_f} (r(t) * h_f(t))^2 \, dt \tag{9}$$

with

$$\left|H_f(\omega)\right|^2 = \frac{S_s(\omega)}{S_s(\omega) + N_o/2} \tag{10}$$

Since our signal spectrum $S_s(\omega)$ is modeled as rectangular, (11) is equivalent to within a multiplicative constant to

$$\left|H_f(\omega)\right| = 1 \qquad \text{for } |\omega| \in [f_o - \frac{W}{2}, f_o + \frac{W}{2}]$$

$$0 \qquad \text{otherwise.}$$

The optimal receiver front end is shown in Fig. 2.4. The probability density of the sufficient statistic is shown in Appendix 1 to be conditionally Gaussian under the assumption $W^S T/N^T \gg 1$. When a signal is present,

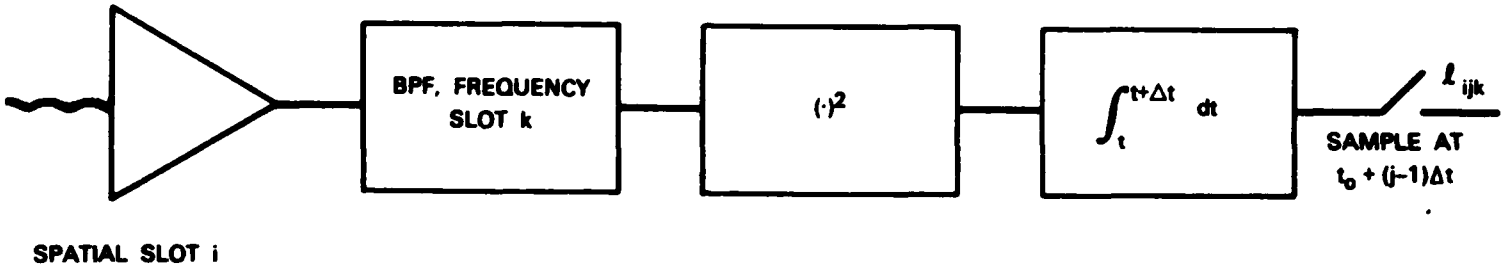

Fig. 2.4. Receiver front-end block diagram.

$$\ell \approx N(m_s, \sigma_s^2)$$

$$m_s = \frac{N_o W_s T}{N^T} + P^s T$$

$$\sigma_n^2 = \frac{N_o^2 W_s T}{N^T} + 2N_o P^s T + \frac{P^{s2} N^T T}{W_s} \qquad (11)$$

where P^s is defined in Eq. 1.1. When only noise is present,

$$\ell \approx N(m_n, \sigma_n^2)$$

$$m_n = N_o \frac{W_s T}{N^T}$$

$$\sigma_n^2 = \frac{N_o^2 W_s T}{N^T} \qquad (12)$$

The optimum receiver requires the implementation of $N^{F*} = W/W^s$ frequency filters for each of the M array cells. If a suboptimal receiver is designed with $N^F < N^{F*}$ filters, then expressions (11) are shown in Appendix 1 to become

$$m_s = \frac{N_o WT}{N^T N^F} + P^s T \; ; \; \sigma_s^2 = \frac{N_o^2 WT}{N^T N^F} + 2N_o P^S T + \frac{P^{s2} N^T T}{W_s} \qquad (13)$$

The expressions for m_n and σ_n^2 are obtained by setting $P^s = 0$ in Eq. (13). With this model, the ratio $P_s(L)/P_n(L)$ is not a monotonically increasing

function so that the decision rule of choosing the largest ℓ_{ijk} is even more suboptimal than Eq. (4) (see Appendix 2). The "pick max" decision rule has a probability of error given in Appendix 2 for the binary case by

$$PE^{(2)} = \text{erfc}\sqrt{\frac{m_s - m_n}{\sigma_s^2 + \sigma_n^2}} \tag{14}$$

Inserting Eqs. (13) and (14) in (6) gives

$$PE \leq (M - 1)\, N^T N^F\, \text{erfc}\left[\frac{P^s\sqrt{T}}{\sqrt{\frac{2N_o^2 W}{N^F N^T} + 2N_o P^s + \frac{P^{s\,2} N^T}{W_s}}}\right] \tag{15}$$

this approximation is accurate when $WT/N^F N^T > 100$ and the bound is tight when the right hand side is $\ll 1$. This last condition prevails when the system has good performance. The first condition may not be satisfied when full frequency processing is performed, $N^F = N^{F*}$, and the illumination beam has the diffraction limited opening $N^T = M$.

2.4.2.2 Signal Model (b): FM Noise with Flat PSD over W_s

Because the random process is not Gaussian, exact computations are far less trivial in this case. It may however be intuitively argued that the receiver front-end in Fig. 2.4 must be close to optimal. The probability density of ℓ_{ijk} in the presence of a signal in slot ijk is evaluated in Appendix 1 as

$$\ell_{ijk}\Big|_{H_{ijk}} \sim N(m_s,\ \sigma_s^2)$$

$$m_s = \frac{N_o WT}{N^T N^F} + P^S T$$

$$\sigma_s^2 = \frac{N_o^2 WT}{N^T N^F} + 2N_o P^S T \qquad (16)$$

Comparing Eqs. (16) and (13), we notice that the expressions of m_s are the same and that σ_s^2 in Eq. (13) contains three terms. The first term corresponds to the noise fluctuations, the second term to the cross correlation between signal and noise, and the third term to signal fluctuations. The third term is absent from Eq. (16) as may be expected and both other terms have exactly the same expression in Eqs. (13) and (16). Expression (16) is a general formulation of the mean and variance after energy detection in a bandwidth W/N^F for a signal with no amplitude noise. The bound for the probability of erroneous spatial acquisition with a signal which has no amplitude fluctuations is

$$PE \leq (M-1)\, N^T N^F\, \mathrm{erfc}\left[\frac{P^S\sqrt{T}}{\sqrt{\frac{2N_o^2 W}{N^F N^T} + 2N_o P^S}}\right] \qquad (17)$$

2.4.2.3 Signal Model (c): Random Phase Sinusoid

The waveform due to the received signal is

$$s(t) = \sqrt{2P^S}\sin(2\pi f_o t + \theta) \qquad T_i < t < T_i + T/N^T$$

$$P_\theta(\theta) = \frac{1}{2\pi} \qquad -\pi < \theta \leq \pi \tag{18}$$

The sufficient statistic is given in [5] as,

$$\ell_{ijk} = \sqrt{R^2_{c_{ijk}} + R^2_{s_{ijk}}}$$

$$R_{c_{ijk}} = \int_{T_i}^{T_f} \sqrt{\frac{2}{T_f - T_i}} \cos(2\pi f_o t)\, r(t)\, dt$$

$$R_{s_{ijk}} = \int_{T_i}^{T_f} \sqrt{\frac{2}{T_f - T_i}} \sin(2\pi f_o t)\, r(t)\, dt \tag{19}$$

and has the following conditional probability densities

$$P_s(L_{ijk}) = \frac{2}{N_o} L_{ijk}\, e^{-\frac{1}{N_o}(L^2_{ijk} + E)} I_o\left(\frac{2\sqrt{E}}{N_o} L_{ijk}\right)$$

$$p_n(L_{ijk}) = \frac{2}{N_o} L_{ijk}\, e^{-\frac{1}{N_o}(L_{ijk})^2} \tag{20}$$

The exact probability of error for the receiver structure in Eq. (5) is computed in Appendix 3 and is well approximated by

$$PE \leq 2WT\,(M - 1)\, e^{-\frac{P^S T}{2N_o}} \tag{21}$$

which is independent of the illumination strategy.

2.5 Discussion of the Result

The expressions obtained in this chapter and in the following chapters apply for any problem geometry and hardware. The present work was conducted as a part of the LASERCOM project, and we have therefore used the related state-of-the-art figures to generate the examples and graphs. The communication lasers are solid state GaAlAs, operate at wavelengths of 0.8 μm, and are limited in power to approximately 10 mW. Frequency stabilized lasers may attain short time bandwidths of about 10 MHz. A heterodyne receiver bandwidth of 1 GHz is assumed.

The doppler frequency shifts may be even larger and must be compensated. The maximal distance occurs for a communication between two geostationary satellites and may be as large as twice the radius of the orbits. Since the optics must have diffraction limited resolution and must meet some weight limits, their apertures are limited to about 0.1 m. We therefore generate all the examples of this report with the following figures which represent the state of the art for coherent detection hardware.

$$P^L = 10^{-2}\text{W}$$

$$\lambda = 0.8\ 10^{-6}\text{m}$$

$$D = 7\ 10^{7}\text{m}$$

$$D^R = D^B = 10^{-1}\text{m}$$

$$\theta = 10^{-3}\text{rad}$$

$$W = 10^{9}\ \text{Hz}\ (1\ \text{GHz})$$

$$W_s = 10^{7}\ \text{Hz}\ (10\ \text{MHz})$$

$$\eta = 1$$

As a consequence,

$$N_o = 2.48\ 10^{-19} J$$

$$P^s = 5.1\ 10^{-15} W$$

$$M = 1.05\ 10^4$$

We use the same figures for comparison with direct detection in the next chapters, although these numbers may not reflect the state-of-the-art for direct detection technology.

The time required to perform the acquisition with PE = 10^{-4}, one way, is computed according to formulas (15), (17), (21) for the three signal models. Curves giving T as a function of $\Omega^B/\Omega^U = 1/N^T$ are displayed in Fig. 2.5 for different values of the number of filters N^F used. We draw the following comments on these curves. When the signal model includes amplitude fluctuations, the curves display first a decrease of the acquisition time T when the beamwidth Ω^B is decreased. The acquisition time reaches a minimum for

$$N^T = \frac{N_o}{P^s} \sqrt{\frac{2WW^s}{N^F}} \qquad (22)$$

and then increases for larger values of N^T. This effect may be attributed to the increase in signal variance when it is integrated over a duration comparable to its temporal coherence. However, the Gaussian approximation is no longer valid in this circumstance and exact Chi-square distribution figures should be used instead.

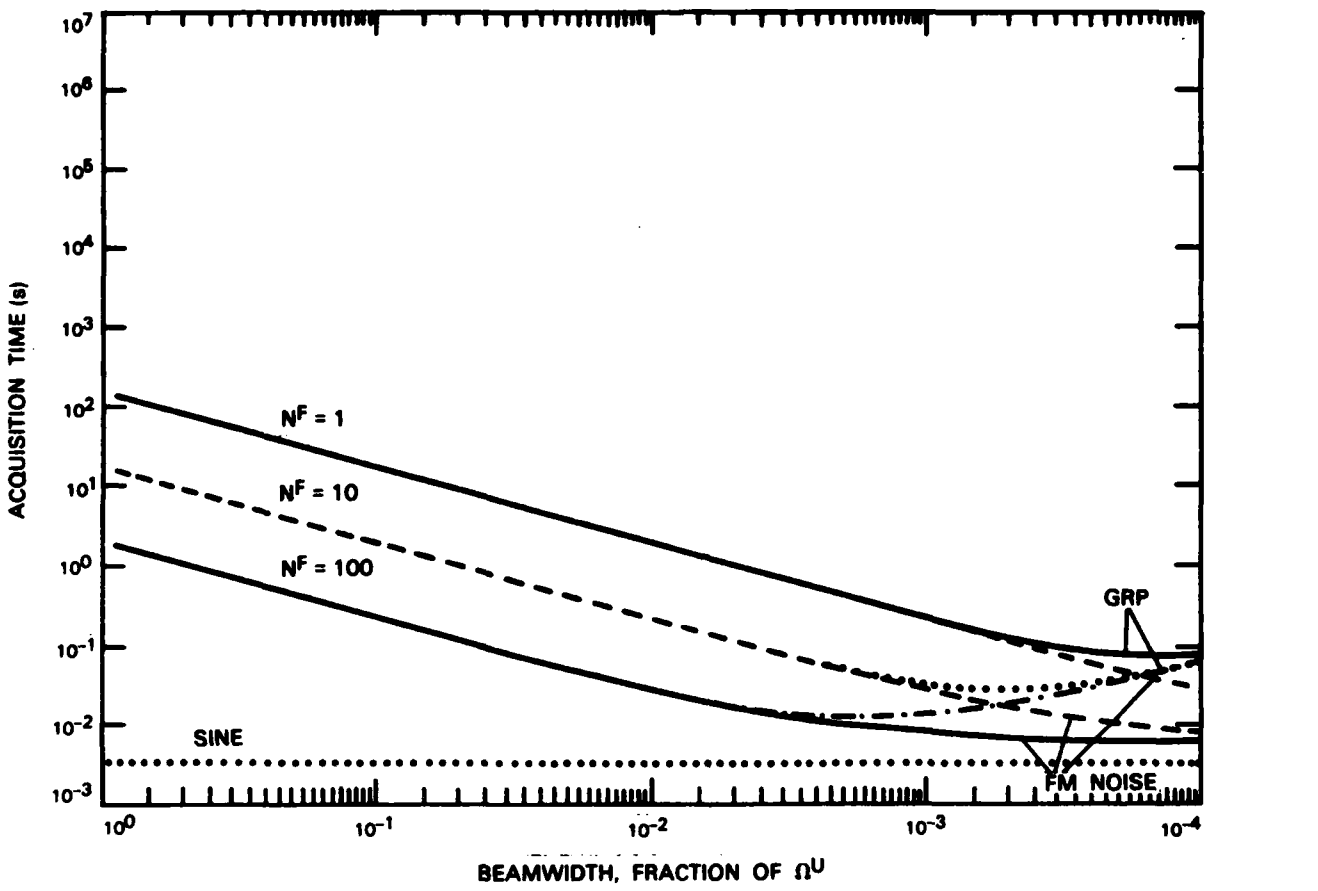

Fig. 2.5. Acquisition times for parallel receiver operation.

When no amplitude fluctuations are modeled in the signal, the function $T(N^T)$ is monotonically decreasing and the minimum occurs at $N^T = M$, when the illumination beam has the diffraction limited opening. In this particular case, the search time is 5 or 30 ms, depending on whether or not simultaneous frequency acquisition is performed. The performance bound given by signal model (c) is 3.2 ms. The acquisition times for PE = 10^{-4}, for signal model (a) or (b) are bounded by:

$$T \leq 100 \left[\left(\frac{N_o}{P^s} \right)^2 \frac{W}{N^F N^T} + \frac{N_o}{P^s} + \frac{\alpha N^T}{2W_s} \right] \tag{23}$$

where $\alpha = 0$ for model b) and $\alpha = 1$ for model a). Signal models a) and b) give markedly different results when the third term is dominant in (23). The actual signal after the mixing process has only slight amplitude fluctuations for very coherent fields, so that the result for signal b) may be close to the actual performance. Unless otherwise stated, the signal model b) will be considered in the following discussions.

The short search times predicted above correspond to an order of magnitude of 100 received photons (T = 5 ms). However, these performances are obtained only if 10^4 heterodyne detectors are available. This hardware constraint may be difficult to meet in practice. We will therefore derive in the following section, expressions for the performance when the number of detectors $K < M$.

2.6 Extension to One-Way Serial Acquisition

When the number of sensors K_A in the receiver is smaller than the desired resolution improvement M_A, the M_A cells in the uncertainty zone Ω_B^u may be searched sequentially by the K_A sensors in a scan of N_A^s steps. The number of scan steps N_A^s must be M_A/K_A. The decision, made after the complete scan is performed, is identical to the parallel receiver decision. The acquisition time of the parallel receiver is therefore simply multiplied by M/K. Expression (17) becomes

$$PE \leq N^F N^T (M-1) \operatorname{erfc} \frac{P^s \sqrt{T/N^s}}{\sqrt{\frac{2N_o{}^2 W}{N^F N^T} + 2P^s N_o}} \tag{24}$$

Figures 2.6 and 2.7 show curves of sequential receiver acquisition times.

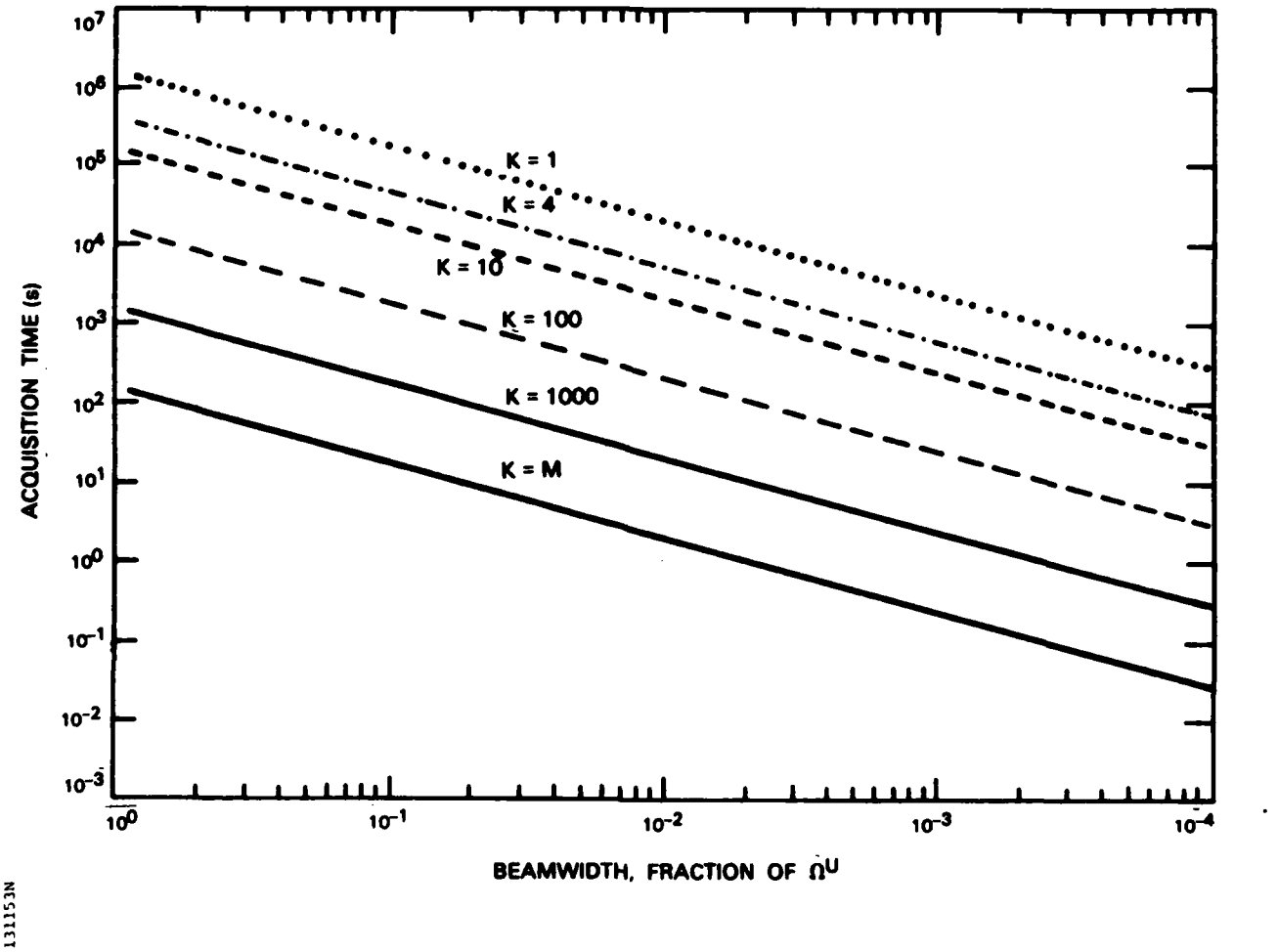

Fig. 2.6. Acquisition times for serial receiver operation: with no frequency processing.

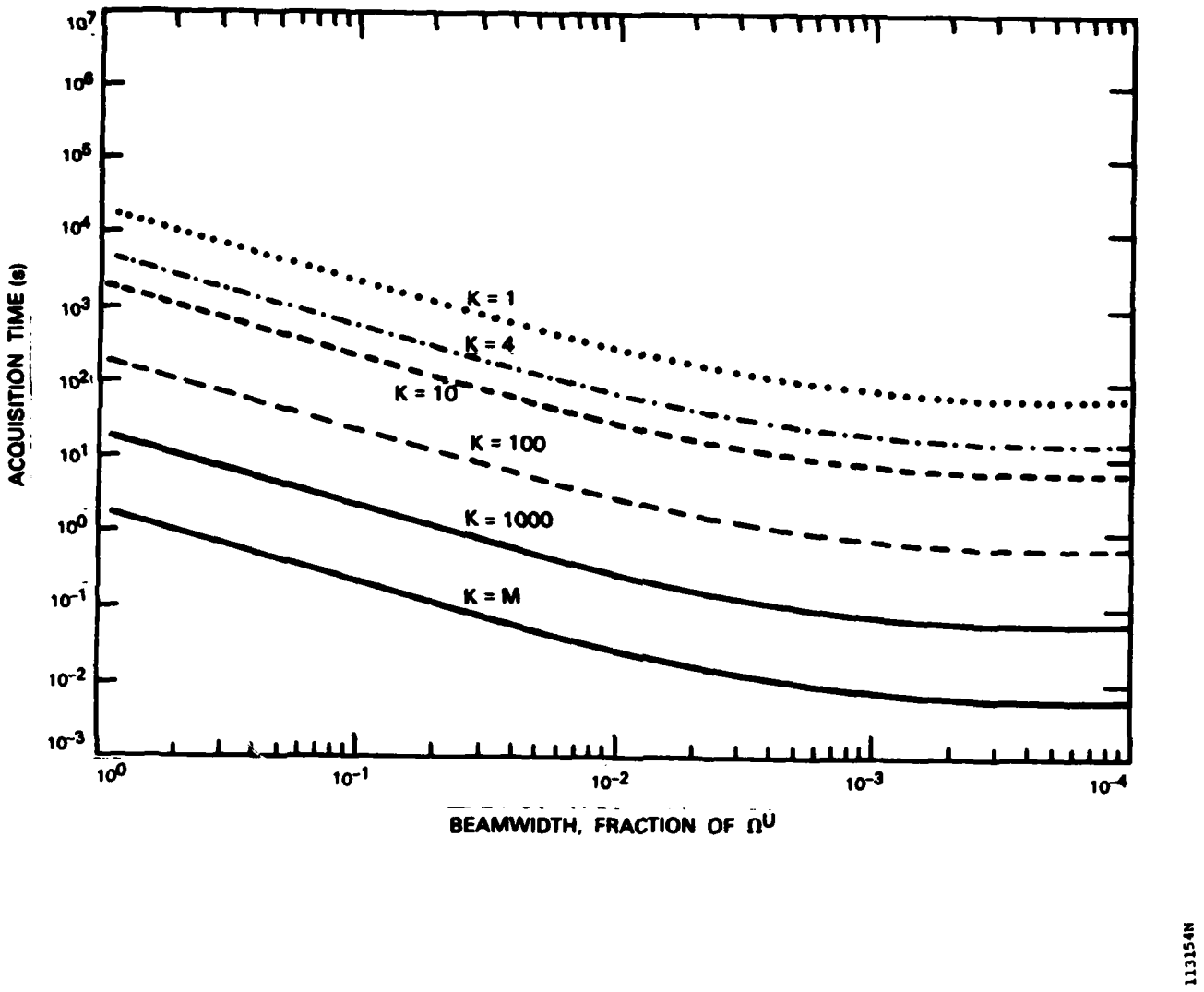

Fig. 2.7. Acquisition times for serial receiver operation: with simultaneous frequency acquisition.

3. SPATIAL ACQUISITION-DIRECT DETECTION ONE-WAY SEARCH

3.1 Organization of the Chapter

Some analysis of spatial acquisition with direct detection has been done. A good survey of the results may be found in Gagliardi [6]. We therefore limit ourselves in this report to list the expressions and derive numeric results which may be compared to those given in Chapter 2 for heterodyne detection. This chapter addresses parallel and serial receiver operations; zooming operation is left to Chapter 4. Section 2 handles the case where only background and quantum noise are present. Section 3 considers the effect of amplifier thermal noise. Section 4 addresses the issue of the excess noise produced by photo-detectors with multiplication. Sections 2 to 4 consider only a parallel receiver operation. Section 5 covers the extension to serial processing at the receiver.

3.2 Quantum and Background Noise Limited Performance

Let us first consider parallel illumination. The received continuous signal power P_s is given by Eq. 1.1. The mapping of the uncertainty zone Ω_B^U on the focal plane of the receiver on A is covered by M detectors, each covering an area of the size of the Airy disk of the optical system. The number of detected photons obeys Poisson statistics, with count rates $\lambda_b + \lambda_s$ for the sensor which receives the signal and λ_b for the other sensors. Assuming that we measure the exact number of detected photons, the optimal decision rule is to assign the signal to the detector with the highest count after the acquisition duration T. The probability of error PE is given by

$$PE = 1 - \sum_{k_1=1}^{\infty} \frac{e^{-(\lambda_b+\lambda_s)T}[(\lambda_b+\lambda_s)T]^{k_1}}{k_1!} \left[\sum_{k_2=0}^{k_1-1} \frac{e^{-\lambda_b T}(\lambda_b T)^{k_2}}{k_2!}\right]^{M-1} \quad (1)$$

assuming that the acquisition is erroneous when a noise count equals the signal count. Approximations to Poisson error probabilities are addressed in Appendix 4. The Union-Chernov bound is tight for large $\lambda_b T$ and easy to invert.

$$PE \leq (M-1)\, e^{-(\sqrt{\lambda_b + \lambda_s} - \sqrt{\lambda_b})^2 T} \quad (2)$$

where $\lambda_s = \eta P^s/h\nu$. Because each detector covers one spatial mode, we have $\lambda_b = \lambda_{bo}$ where λ_{bo}, the background noise count rate per spatial mode, is assumed constant over space. In a situation where a geostationary satellite tries to acquire the position of a low orbit satellite, the background field is the earth. A typical receiver optical bandwidth of 3 Å collects then a background count rate λ_{bo} on the order of $10^5\ s^{-1}$. When looking toward the high orbit satellite, the count rate λ_{bo} is much larger if the sun is in the field of view, and significantly lower otherwise. However, the star images introduce significant and unknown spatial fluctuations in the background noise. The numbers given in Sec. 2.5 and used for the examples above give $\lambda_s = 20{,}500\ s^{-1}$.

When sequential illumination is considered, the receiver splits the observation time T into N^T equal slots. The expected signal count in the signal slot is unchanged but the background count is reduced by the factor N^T.

$$PE \leq N^T(M-1)\, e^{-(\sqrt{\lambda_b+\lambda_s} - \sqrt{\lambda_b})^2 T} \tag{3}$$

where λ_b and λ_s are given by

$$\lambda_s = \frac{\eta P^s}{h\nu} \qquad \lambda_b = \frac{\lambda_{bo}}{N^T} \tag{4}$$

The bound in (3) may be inverted as

$$T \leq \frac{1}{(\sqrt{\lambda_b+\lambda_s} - \sqrt{\lambda_b})^2} \ln \frac{N^T(M-1)}{PE} \tag{5}$$

Curves of the time required to perform the acquisition with an error probability smaller than 10^{-4} according to Eq. (5) are shown in Fig. 3.1. The slight upward slope in the curves corresponding to low noise counts in an artifact of the union bound. The union bound overestimates the PE for a dark background by a factor of N^TM as is seen from the exact result for $\lambda_b = 0$.

$$PE = e^{-\lambda_s T} \quad \text{for } \lambda_b = 0. \tag{6}$$

For large background counts, the Gaussian approximation

$$PE \approx (M-1)\, N^T \operatorname{erfc}\left[\frac{\lambda_s\sqrt{T}}{\sqrt{2\lambda_b + \lambda_s}}\right] \tag{7}$$

is very good as is seen from the comparison of Figs. 3.1 and 3.2.

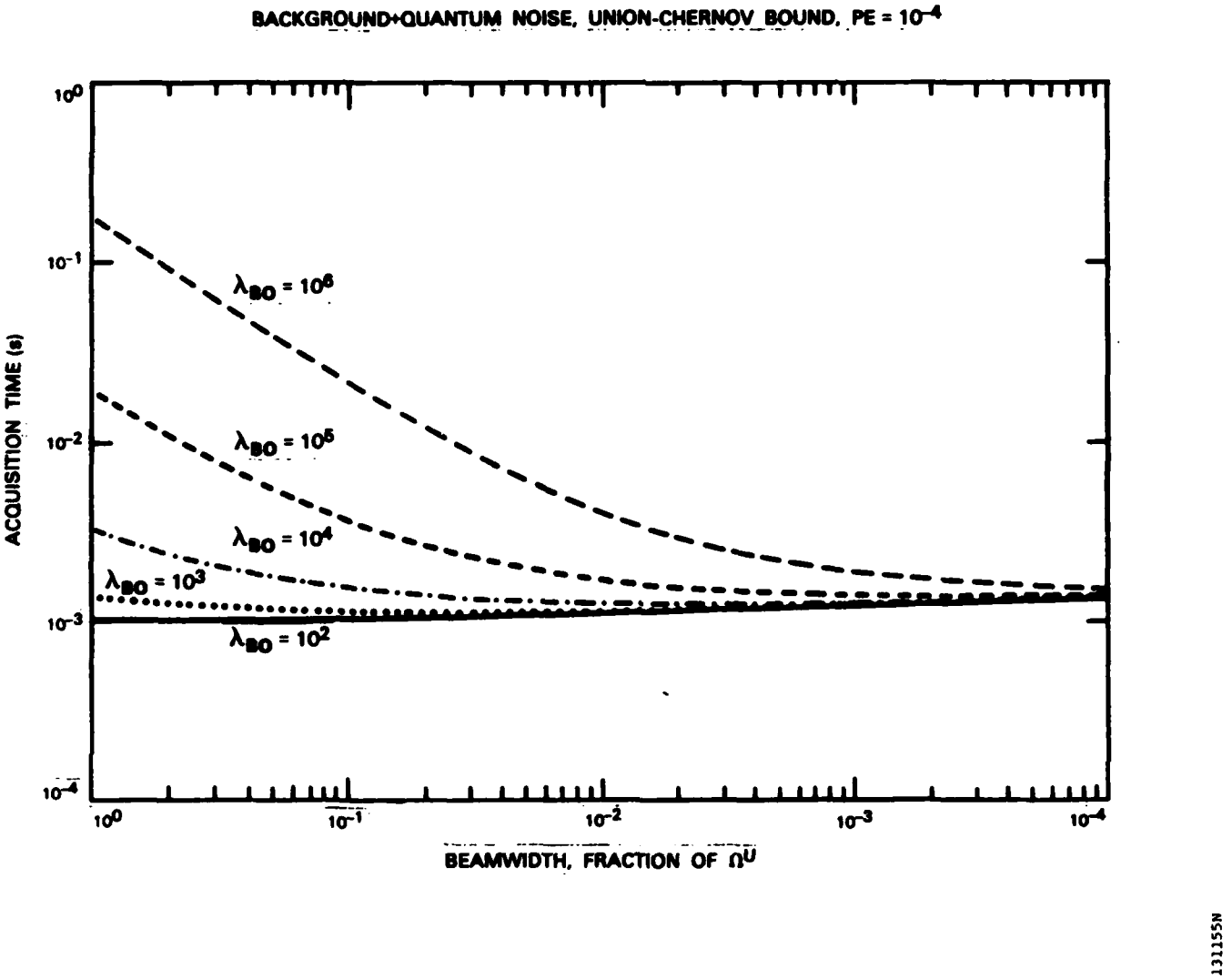

Fig. 3.1. Acquisition times for parallel receiver, background and quantum noise limited operation, Chernov bound.

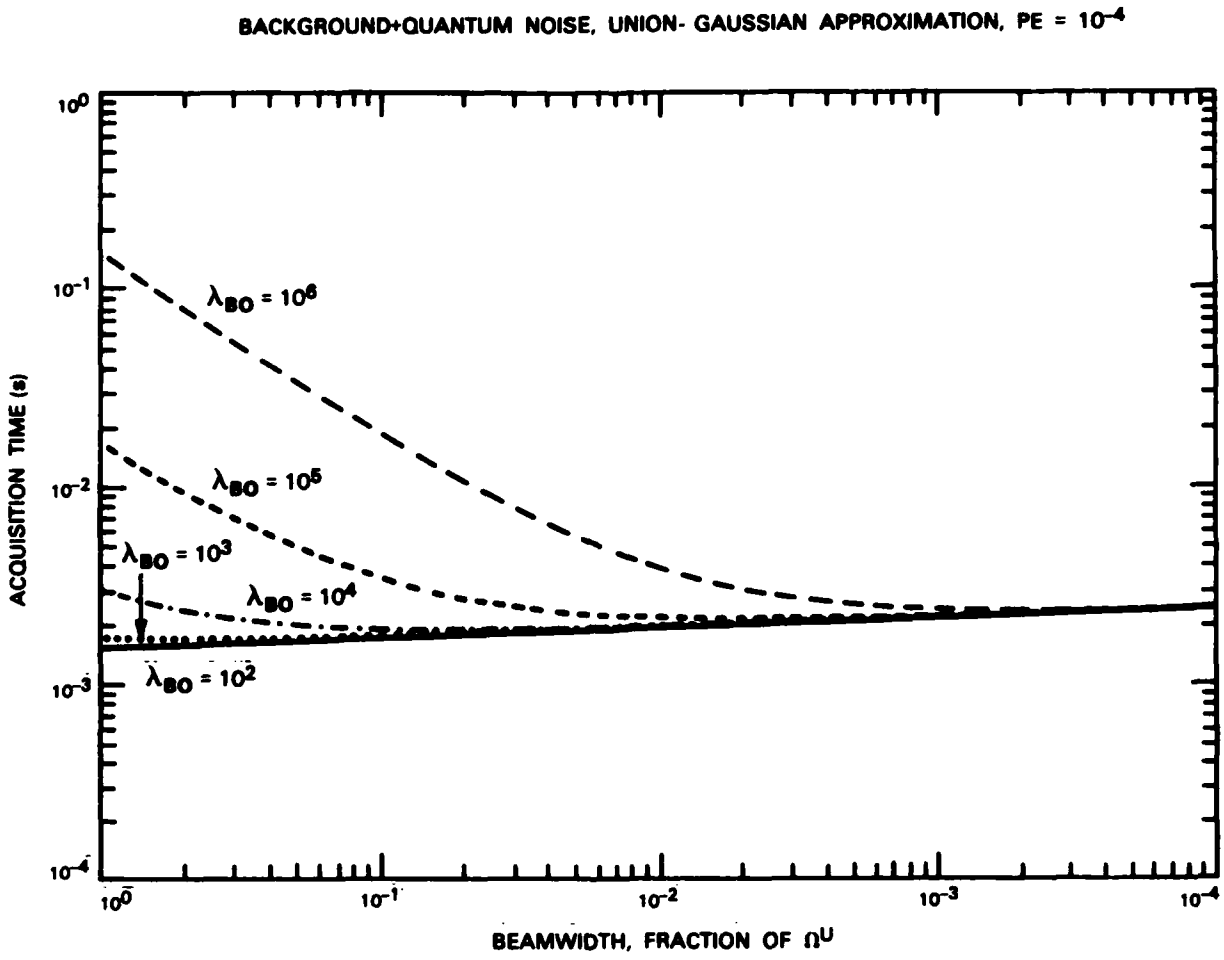

131156N

Fig. 3.2. Acquisition times for parallel receiver, background and quantum noise limited operation, Gaussian approximation.

3.3 Background and Amplifier Noise Limited Performance

We make here the a-posteriori verified assumption of large counts so that Poisson statistics are well approximated by Gaussian statistics. The received charge (integrated current) is modeled as $N(m_n, \sigma_n^2)$ when only noise is present and $N(m_s, \sigma_s^2)$ when the signal is present.

If we use an amplifier of input impedance Z, the thermal noise is an AWGN of double-sided spectral height $N_0/2 = k\tau/Z$ where τ is the amplifier noise temperature in K. We therefore have:

$$m_n = e\lambda_b T \qquad \sigma_n^2 = \frac{k\tau}{Z}\frac{T}{N^T} + e^2\lambda_b T$$

$$m_s = e(\lambda_b + \lambda_s)T \qquad \sigma_s^2 = \frac{k\tau}{Z}\frac{T}{N^T} + e^2(\lambda_s + \lambda_b)T \tag{8}$$

The error probability is bounded by

$$PE \leq (M-1)N^T \operatorname{erfc} \frac{\lambda_s \sqrt{T}}{\frac{2k\tau}{Ze^2N^T} + 2\lambda_b + \lambda_s} \tag{9}$$

Acquisition times derived from (9) for various values of Z are shown in Fig. 3.3 for $\lambda_{bo} = 10^6$. The acquisition time is almost independent of λ_{bo} in the range $Z = 1$ to 10^6.

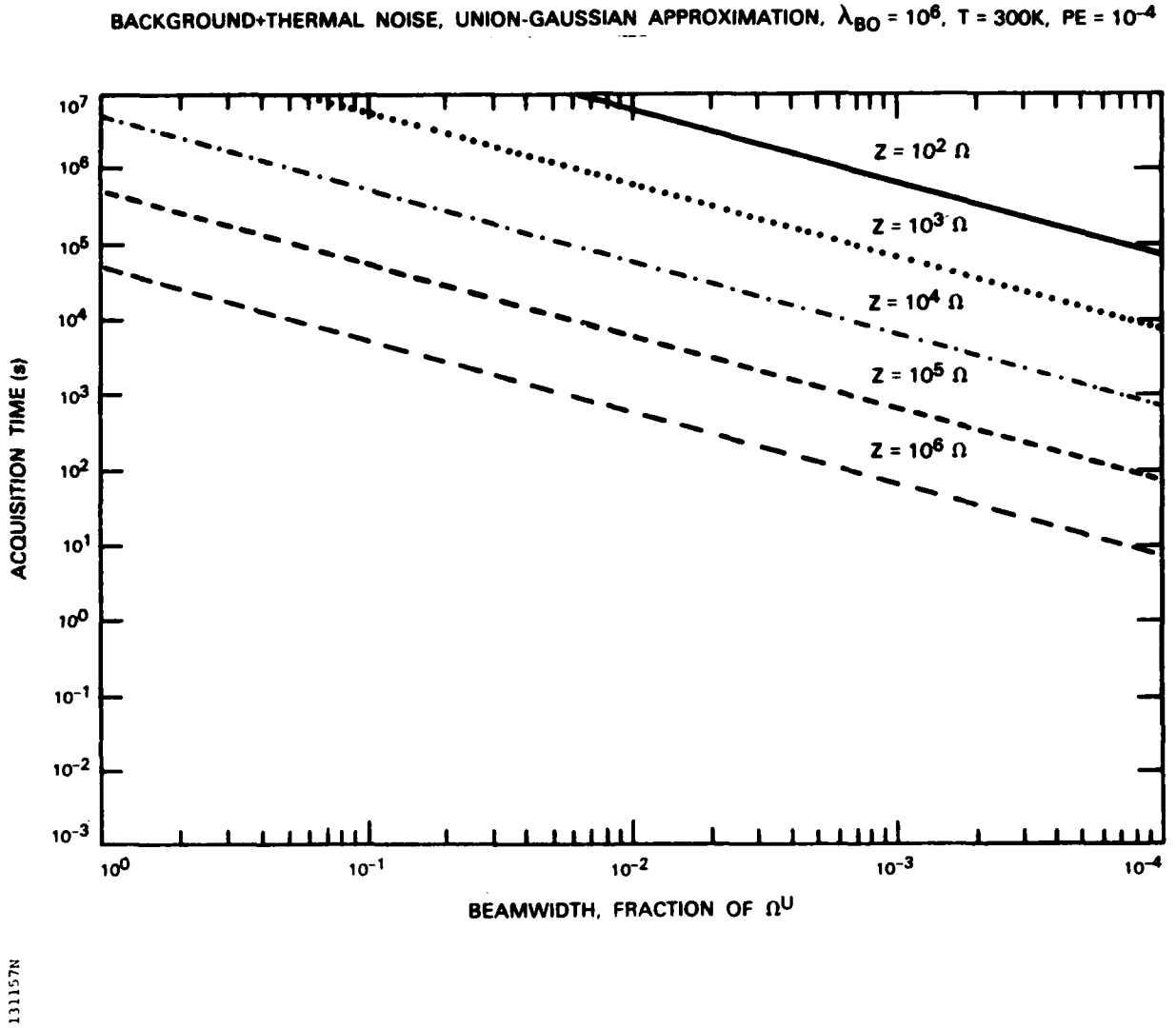

Fig. 3.3. Acquisition times for parallel receiver, thermal noise limited operation.

3.4 Background and Quantum-Limited with Excess Detector Noise

From the graph in Fig. 3.3, it is seen that photodiode detection is mostly corrupted by amplifier thermal noise. Improvement of performance versus thermal noise is obtained by photomultiplication. In a photomultiplier tube (PMT) or avalanche photo diode (APD), every detected photon produces G electrons. The multiplying factor G is random however, and this introduces what is called excess noise. The statistics of G are described by the mean gain $\overline{G}$ and the noise factor $F = \overline{G^2}/\overline{G}^2 = 1 + \text{var}(G)/(\overline{G})^2$. If the amplifier noise is dominated by background and excess noise, then the means and variances in (8) become

$$m_n = e\lambda_b \overline{G}\, T \qquad \sigma_n^2 = e^2 \lambda_b \overline{G}^2 F\, T \tag{10}$$

$$m_s = e(\lambda_b + \lambda_s)\, \overline{G}\, T \qquad \sigma_s^2 = e^2(\lambda_b + \lambda_s)\, \overline{G}^2 F$$

As a result,

$$PE \leq (M - 1)\, N^T \operatorname{erfc}\left[\frac{\lambda_s}{\sqrt{2\lambda_b + \lambda_s}} \sqrt{\frac{T}{F}}\right] \tag{11}$$

The acquisition times derived from (11) are therefore just the times derived from (6) multiplied by F. The noise factor F is on the order of 2 for a PMT and 10 for an APD.

3.5 Sequential Receiver Operation

When the number of available sensors K is smaller than the number of spatial modes in the uncertainty zone M, the M spatial slots may be investigated sequentially by the K sensors in a number of steps given by M/K. The decision rule is the same as for a parallel receiver operation and the required acquisition time for a defined probability of error is the parallel receiver acquisition time multiplied by M/K. Figs. 3.4 and 3.5 show typical curves for sequential acquisition.

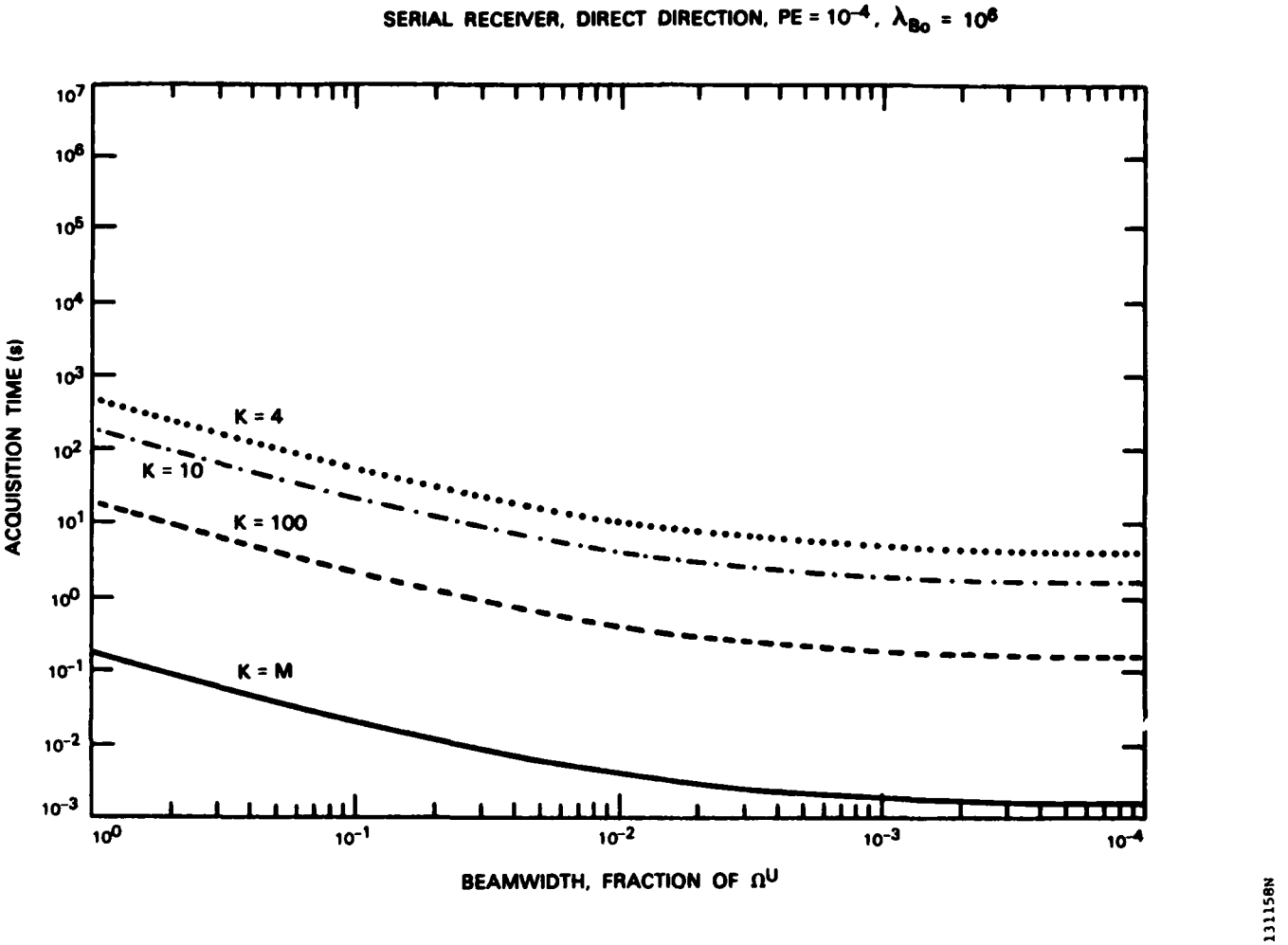

Fig. 3.4. Acquisition times for serial receiver, background and quantum noise limited operation, Chernov bound.

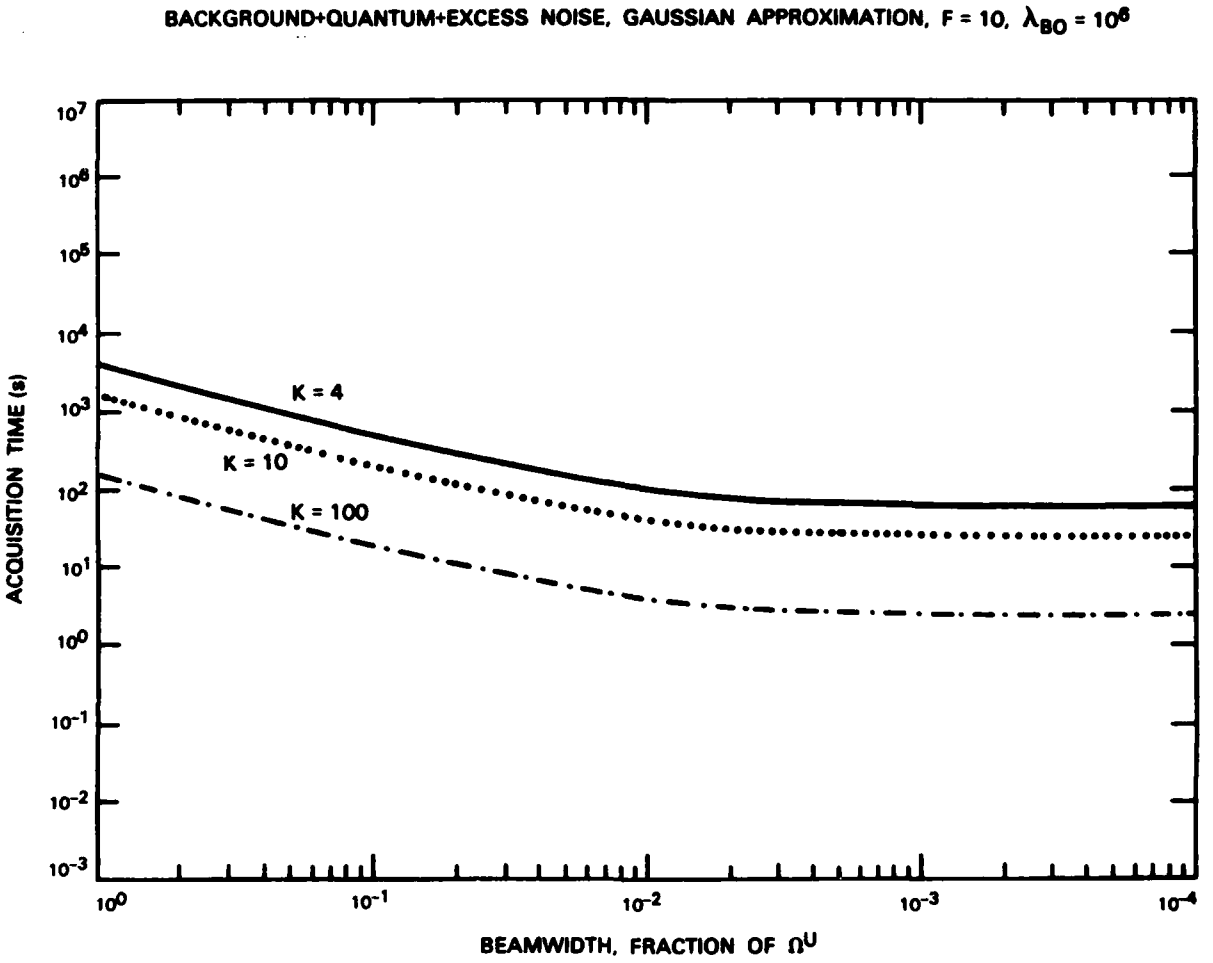

Fig. 3.5. Acquisition times for serial receiver, background, quantum and excess noise limited operation, Chernov bound.

4. ZOOMING SPATIAL ACQUISITION

4.1 Preliminaries

In the preceding chapters, the spatial acquisition consisted of a data collecting part followed by a unique decision. We discuss in this chapter a different acquisition strategy where the decision is taken in several stages. At each stage, a residual uncertainty zone is investigated and a partial decision reduces the estimated range of the parameter. The residual range is then more finely investigated during the next stage. The process is repeated until the desired accuracy is obtained. We present in Sec. 4.2 the notations used for this chapter. We address in Sec. 4.3 the optimal partition of both the total search time and the allowed probability of error at each stage. We apply these results with heterodyne detection in Sec. 4.4 and direct detection in Sec. 4.5.

4.2 Notation and Framework

Each stage i, $i = 0, 1, \ldots, I-1$ of the zooming consists of a spatial acquisition by itself. The number of required stages is given by

$$I = \log_K M \tag{1}$$

where M is the desired resolution gain or, otherwise stated, the number of spatial modes in the initial uncertainty zone when diffraction limited resolution is desired.

At each stage, the residual spatial uncertainty zone $\Omega^U(i)$ is mapped onto the K-sensor receiver array and, after collecting the received signal during the partial acquisition time T(i), the receiver decides which sensor receives the signal. This decision is taken with an error probability PE(i).

The noise statistics vary between the stages because the number of spatial modes covered by each detector, M/K^{i+1} is not constant. For heterodyne detection, the multimode mixing efficiency is lower than for monomode operation and the signal to noise ratio is therefore decreased. This phenomenon is modeled by multiplying the noise level by the number of spatial modes covered by the detector

$$\frac{N_o(i)}{2} = M \cdot K^{-(i+1)} \frac{h\nu}{2\eta} \tag{2}$$

For direct detection, the background noise count rate is the product of the background noise count rate per spatial mode, which is a constant, by the number of spatial modes covered by each detector

$$\lambda_b(i) = M \cdot K^{-(i+1)} \lambda_{bo} \tag{3}$$

The remaining noise contributions, i.e., amplifier, quantum and excess noise are unchanged for direct detection.

If one-way acquisition is considered, then each satellite illuminates the full initial uncertainty zone $\Omega^U(0)$ during the whole acquisition. The incident signal power for parallel illumination P^S and the number of "time slots" N^T which is the ratio of the illuminated zone solid angle $\Omega^U(i)$ to the illuminating beam solid angle $\Omega^B(i)$, are constant throughout the search

$$P^s(i) = P^s(0)$$
$$N^T(i) = N^T(0) \qquad (4)$$

In a cooperative two-way acquisition, only the residual uncertainty zone $\Omega^U(i)$ is illuminated at each step. The parallel illumination incident signal power at each stage is therefore increased as

$$P^s(i) = P^s(0)\, K^i \qquad (5)$$

Several strategies may be followed for serial illumination, to narrow the illumination beamwidth from the initial opening $\Omega^B(0) = \Omega^U(0)N^T(0)$ down to the diffraction limit Ω^R. Two strategies are investigated here. The "wide beam" strategy (A) corresponds to maintaining the initial illumination beamwidth $\Omega^B(0)$ until it fills the entire residual uncertainty zone $\Omega^U(i)$, then using parallel illumination.

$$\Omega^B(i) = \min\,[\Omega^B(0),\ \Omega^U(i)]$$
$$N^T = \max\,[N^T(0)\ K^{-i},\ 1] \qquad \text{Strategy A} \qquad (6)$$

The "narrow beam" strategy (B) corresponds to maintaining the same ratio between the illumination beam $\Omega^B(i)$ and the residual uncertainty zone $\Omega^U(i)$ until the diffraction limited beamwidth Ω^R is attained; see Fig. 4.1.

$$\Omega^B(i) = \max\,[\Omega^B(0)\ K^{-i},\ \Omega^R]$$
$$N^T(i) = \min\,[N^T(0),\ MK^{-i}] \qquad \text{Strategy B} \qquad (7)$$

We consider that the receiver operation is parallel at each stage. The performance expressions derived in Chapters 2 and 3 therefore apply with the

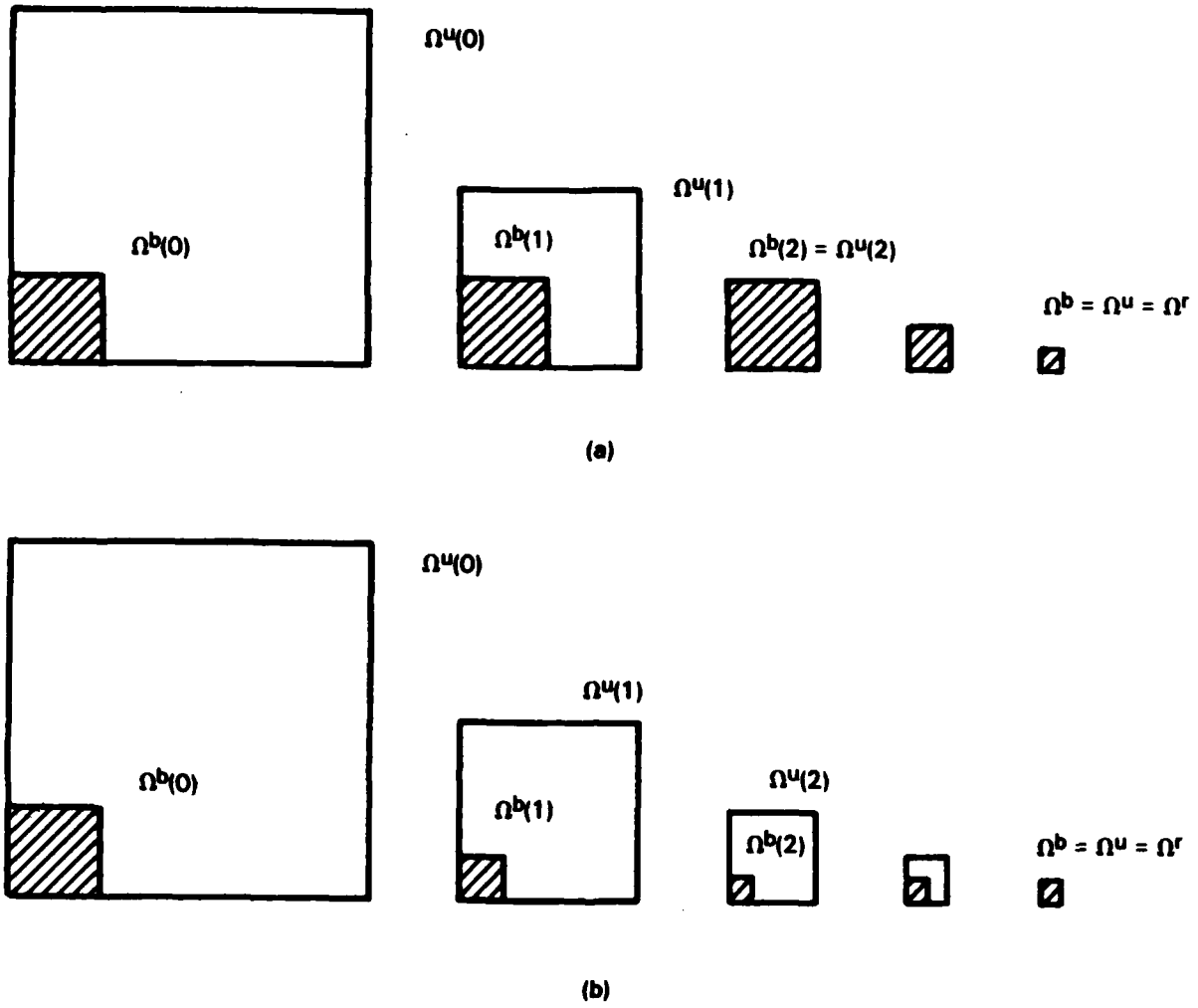

Fig. 4.1. Two-way zooming illumination strategies.

above modifications. For a two-way acquisition, the light travel time from A to B must be added between the stages. This fixed additional time will not be considered in the analysis presented in this chapter.

4.3 Optimization of the Zooming Schedule

The problem to solve is the minimization of the total acquisition time

$$T = \sum_{i=0}^{I-1} T(i) \tag{8}$$

with the constraint that the total probability of error be no more than a prescribed value PE. This inequality constraint is clearly met with equality at the optimum

$$PE = 1 - \prod_{i=0}^{I-1} (1 - PE(i)) \tag{9}$$

We approximate the above expression by

$$PE = \sum_{i=0}^{I-1} PE(i) \tag{10}$$

which is a good approximation for small PE. Our analyses in Chapters 2 and 3 give the performance expressions for each stage as

$$PE(i) = f_i(T(i)) \tag{11}$$

The optimum is attained when

$$\frac{\partial f_i(T(i))}{\partial T(i)} = \lambda \qquad \text{for all } i \tag{12}$$

where λ is a Lagrange multiplier. We consider particular expressions of the function $f_1(\cdot)$ in Secs. 4 and 5. We give here two general expressions for $f_1(\cdot)$ and derive the corresponding optimality relationships.

$$\text{a)} \quad f_1(T(i)) = A(i) \operatorname{erfc} [B(i) \sqrt{T(i)}\,] \tag{13}$$

where A(i) and B(i) are parameters which may differ for the various stages i but are independent of T(i). For small PE, the optimal partition is

$$PE(i) = \frac{\lambda}{[B(i)]^2} \tag{14}$$

$$\text{b)} \quad f_1(T(i)) = A(i) \exp [-B(i)\, T(i)] \tag{15}$$

The optimal partition of PE is

$$PE(i) = \frac{\lambda}{B(i)} \tag{16}$$

The problem is solved by first computing PE(i) from Eqs. (10) and (14) or (16). The partial acquisition times are obtained by inverting (13) or (15).

4.4 Heterodyne Detection

Expression (2.17) gives the error probability for heterodyne detection, and a signal with no amplitude fluctuations. If we consider that frequency acquisition, if any, is performed only at the first stage, we have

$$PE(i) = N^T(i)N^F(i)\,(K-1)\operatorname{erfc}\left[\frac{\sqrt{T(i)}}{\sqrt{\frac{2N_o^2(i)}{P^{s2}(i)}\,\frac{W}{N^T(i)N^F(i)} + 2\,\frac{N_o(i)}{P^s(i)}}}\right] \tag{17}$$

where $N^F(i) = 1$ for $i \neq 0$ and $N^T(i)$, $P^s(i)$, $N_o(i)$ are defined in Eqs. (2), (5), (6), and (7). The expression of $f_i(\cdot)$ is in the form of (13). The optimal partition of PE is therefore given by (14). Figure 4.2(a-f) shows the optimal partial error probabilities and acquisition times, as well as the total acquisition time in the case $K = 4$, $N^F = 1$. Figure 4.3(a-f) shows the same graphs for $N^F = 100$. One-way illumination, two-way "wide beam" illumination and two-way "narrow beam" illumination are addressed in each figure. It is seen from these figures that the first stage of the acquisition is predominant in all cases. Since this stage is not affected by the zooming strategy, the total acquisition times are comparable for the three strategies as is seen in Fig. 4.4.

4.5 Direct Detection

In the case of direct detection, the expression for $f_i(\cdot)$ depends on the noise statistics, which may in turn depend on the hardware implementation.

4.5.1 Background and Quantum Noise Limited Operation

The performance is approximated in Fig. 3.3 as

$$PE(i) \leq N^T(i)\,(K-1)\exp\left\{-\left[\sqrt{\lambda_b(i) + \lambda_s(i)} - \sqrt{\lambda_b(i)}\,\right]^2 T(i)\right\} \qquad (18)$$

where

$$\lambda_b(i) = \frac{\lambda_{bo} M}{N^T(i)\,K^{i+1}}\,, \quad \lambda_s(i) = \eta\,\frac{P^s(i)}{h\nu}$$

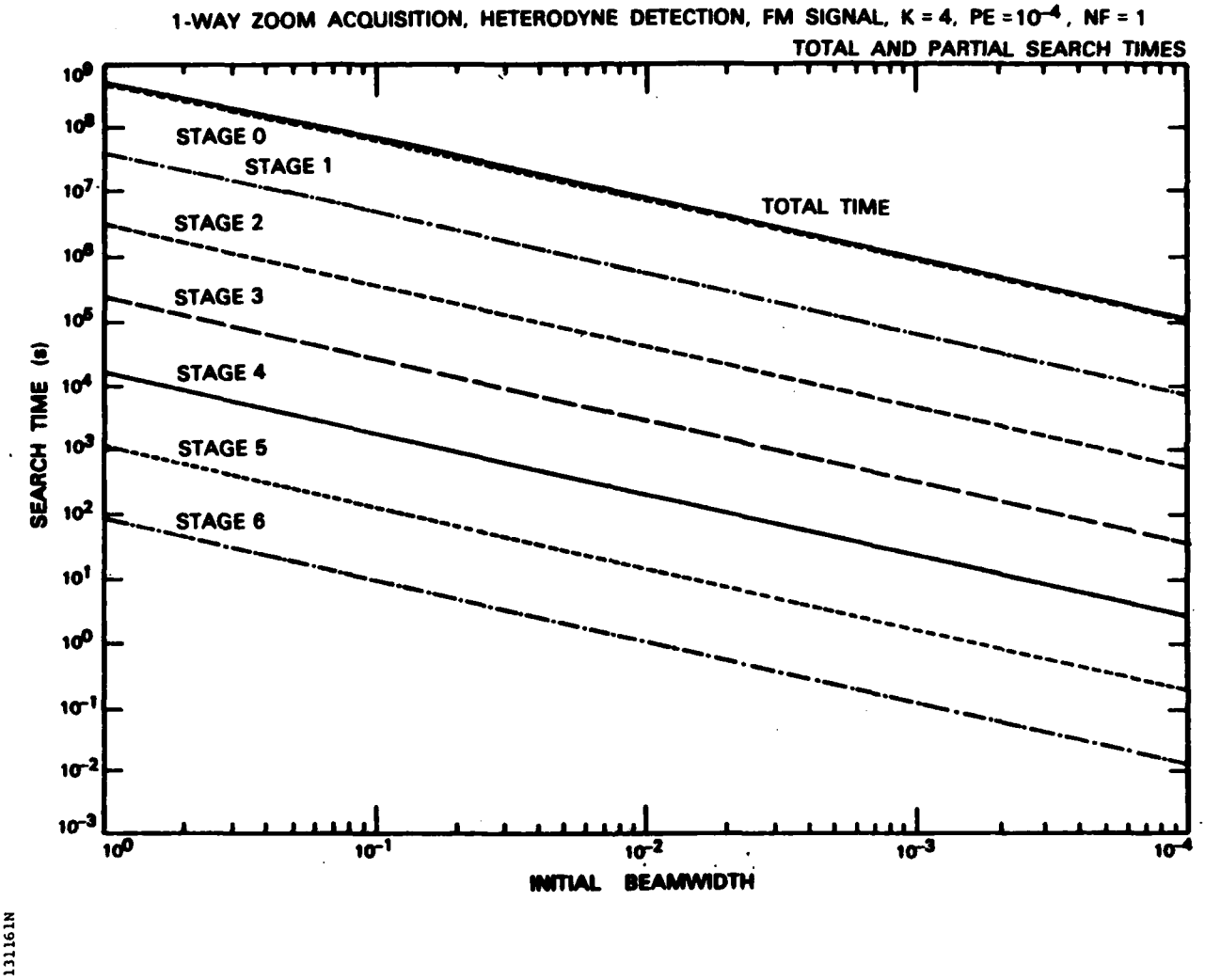

Fig. 4.2. Acquisition with zooming receiver, heterodyne detection, no frequency processing: (a) Optimal partition of T, 1-way zooming strategy.

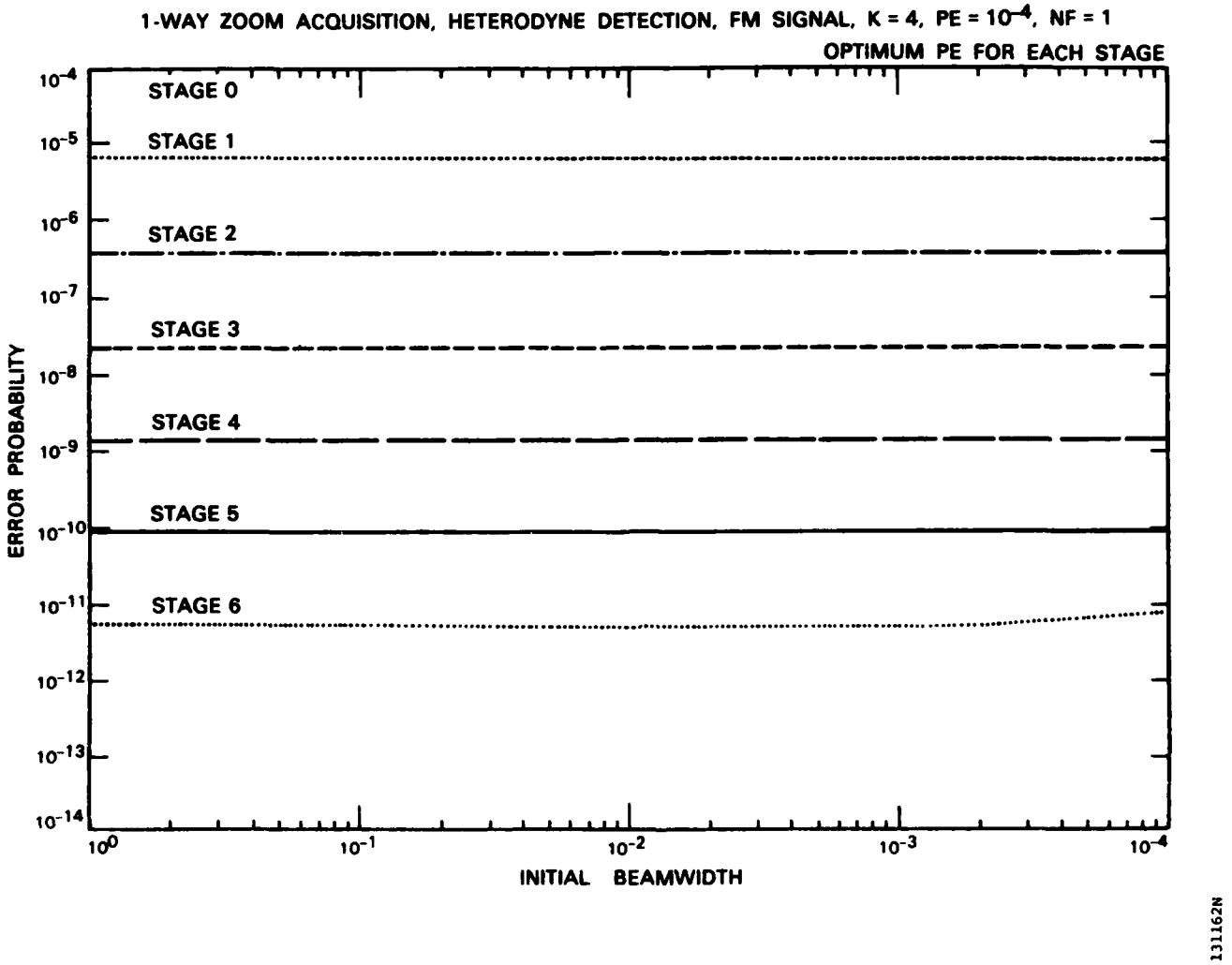

Fig. 4.2. Acquisition with zooming receiver, heterodyne detection, no frequency processing: (b) optimal partition of PE, 1-way zooming strategy.

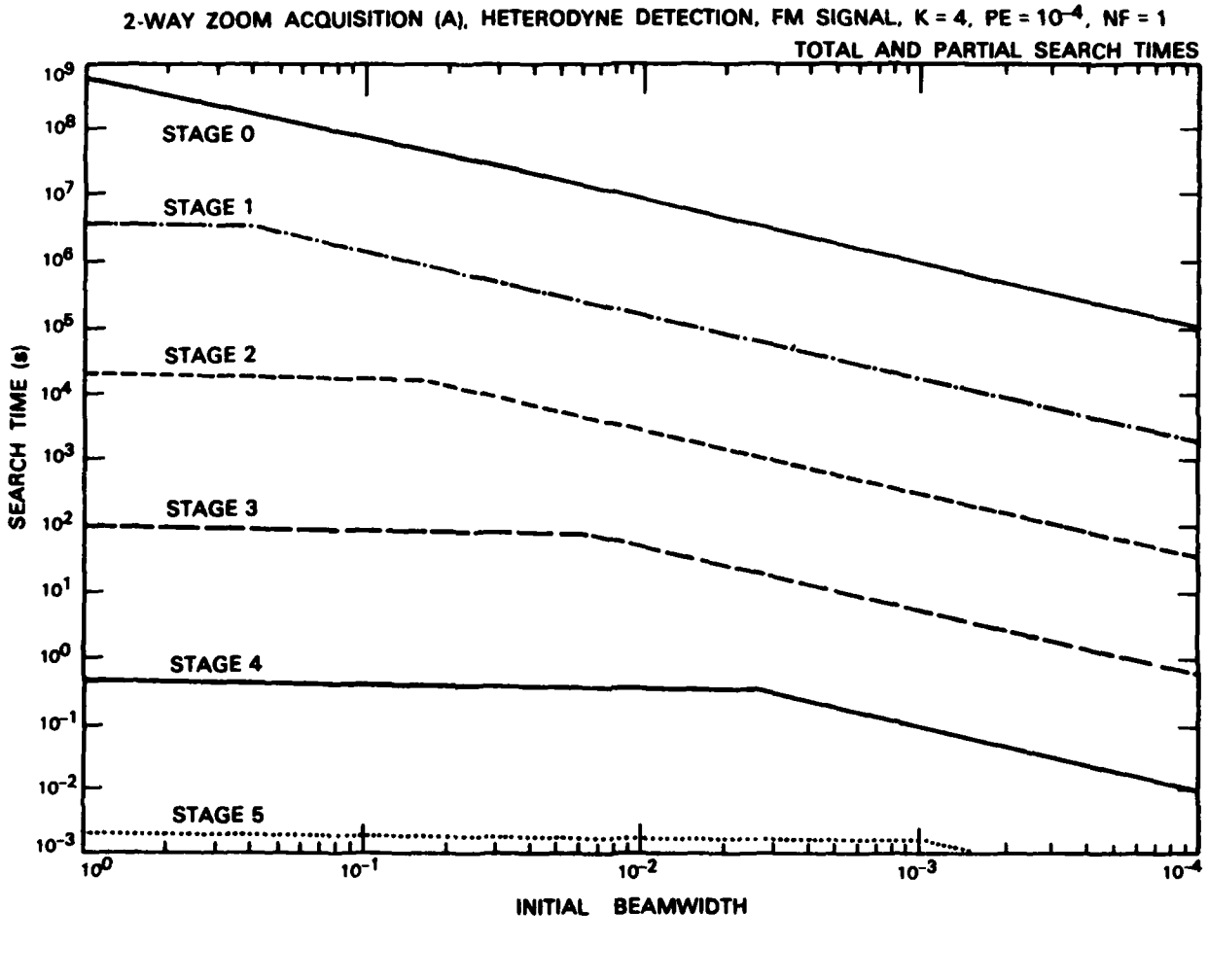

Fig. 4.2. Acquisition with zooming receiver, heterodyne detection, no frequency processing: (c) optimal partition of T, 2-way zooming strategy (A).

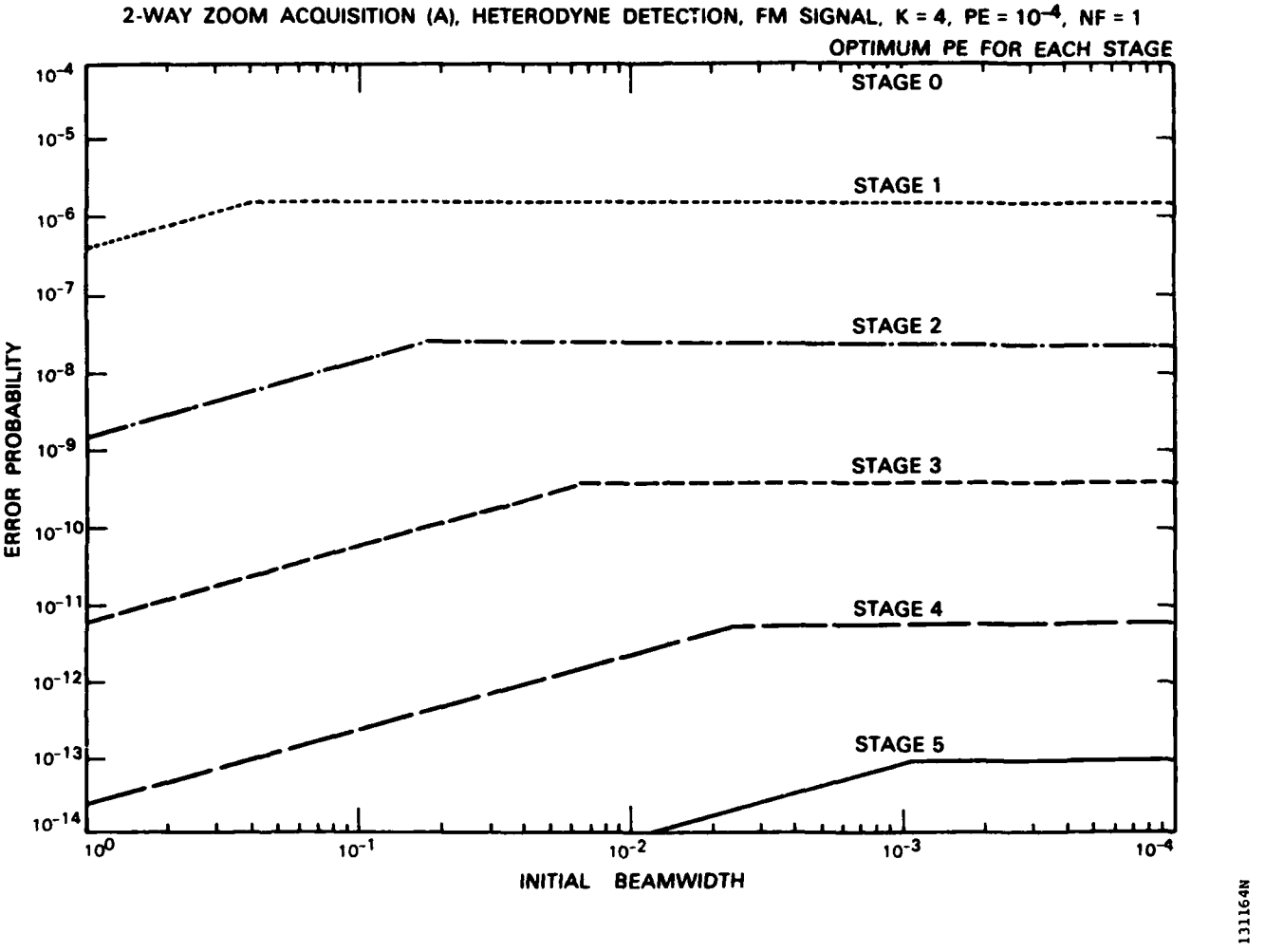

Fig. 4.2. Acquisition with zooming receiver, heterodyne detection, no frequency processing: (d) optimal partition of PE, 2-way zooming strategy (A).

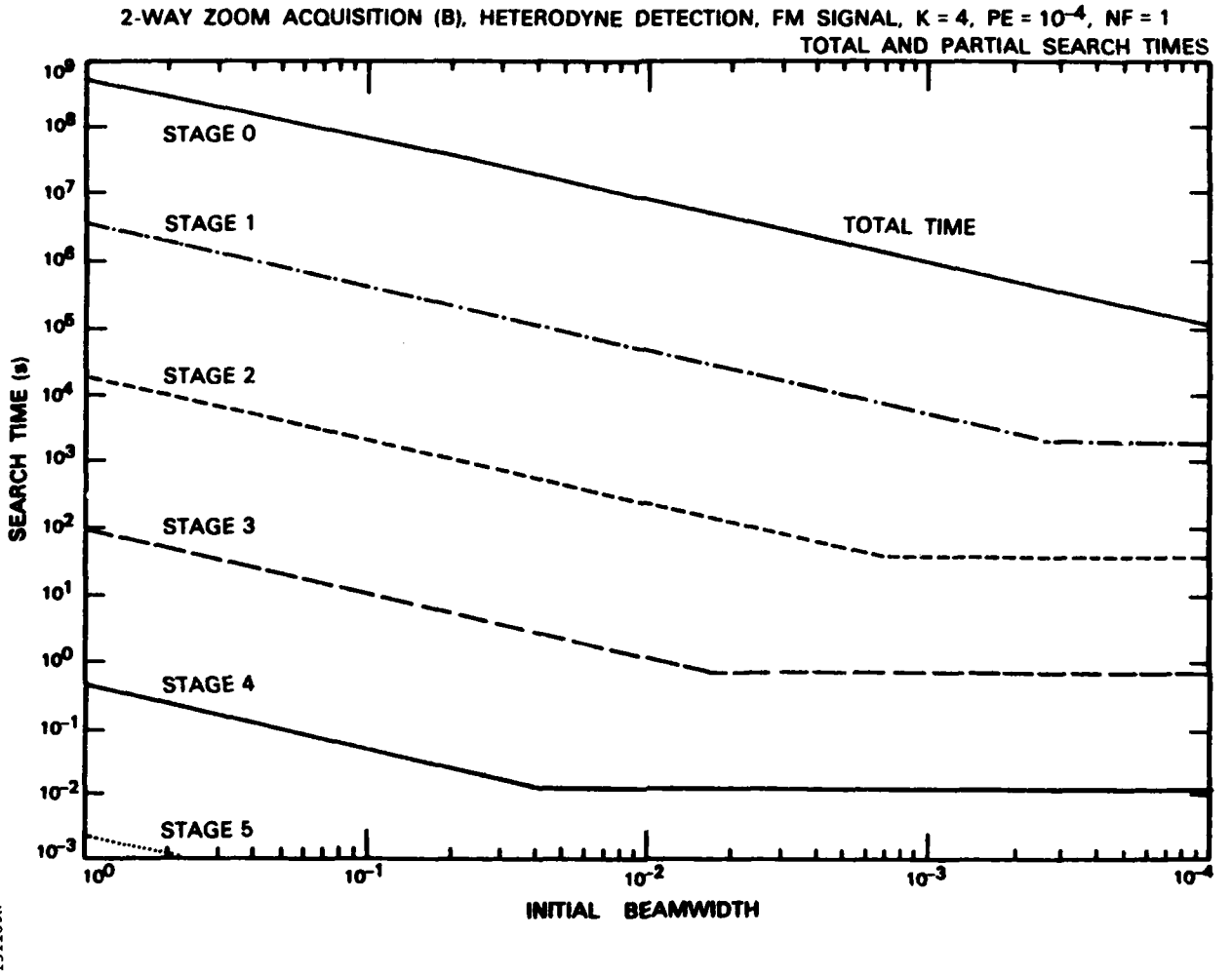

Fig. 4.2. Acquisition with zooming receiver, heterodyne detection, no frequency processing: (e) optimal partition of T, 2-way zooming strategy (B).

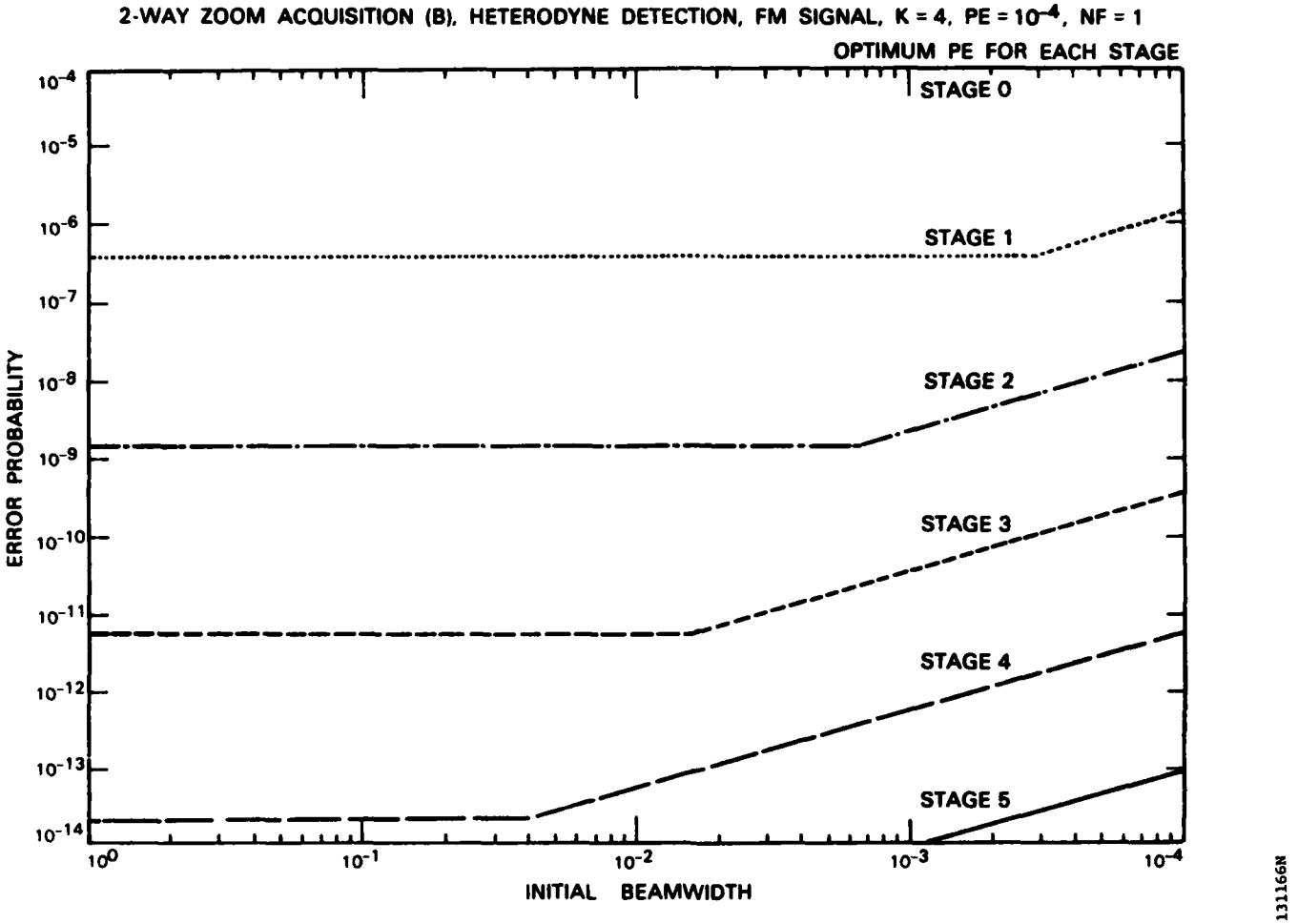

Fig. 4.2. Acquisition with zooming receiver, heterodyne detection, no frequency processing: (f) optimal partition of PE, 2-way zooming strategy (B).

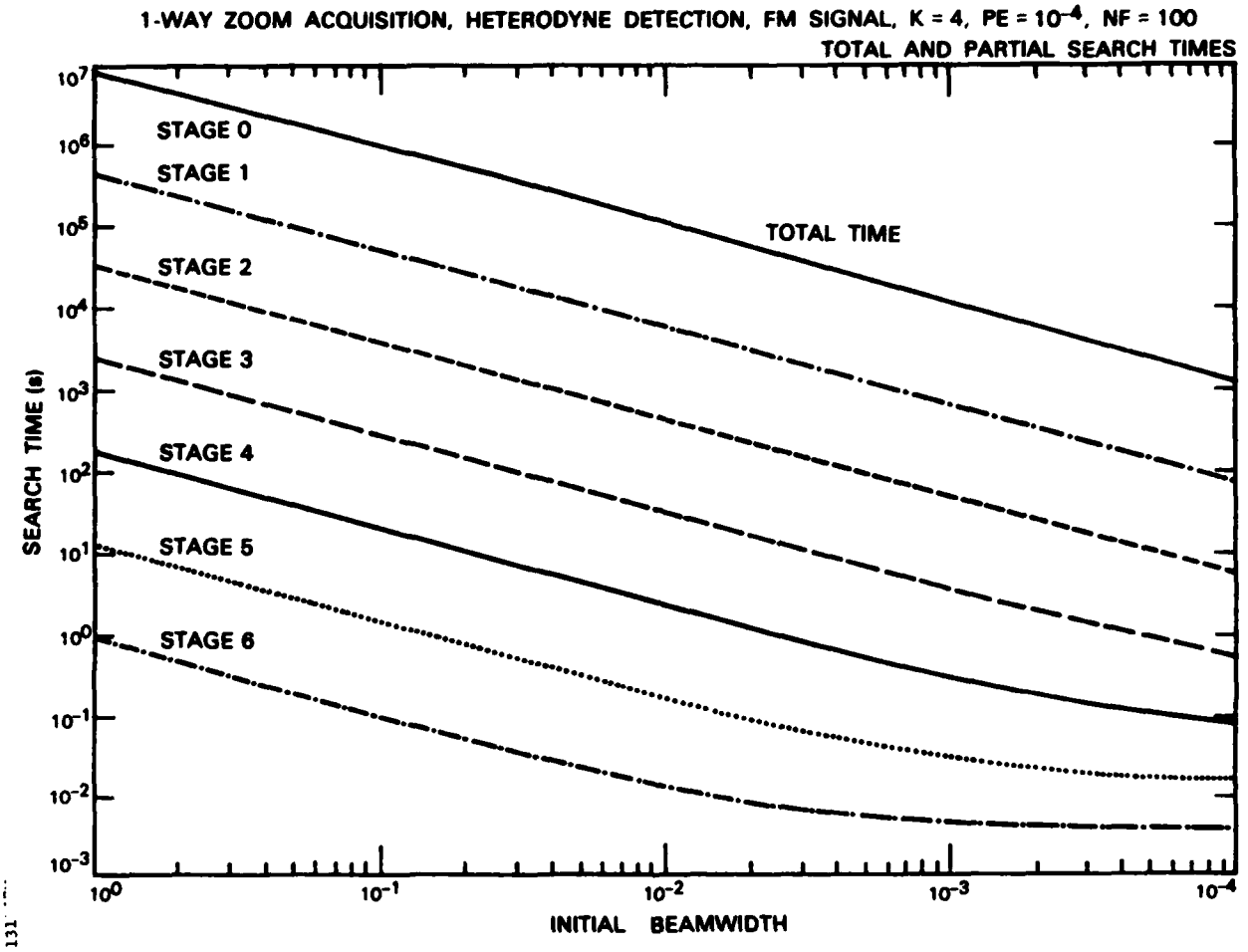

Fig. 4.3. Acquisition with zooming receiver, heterodyne detection, simultaneous frequency acquisition: (a) optimal partition of T, 1-way zooming strategy.

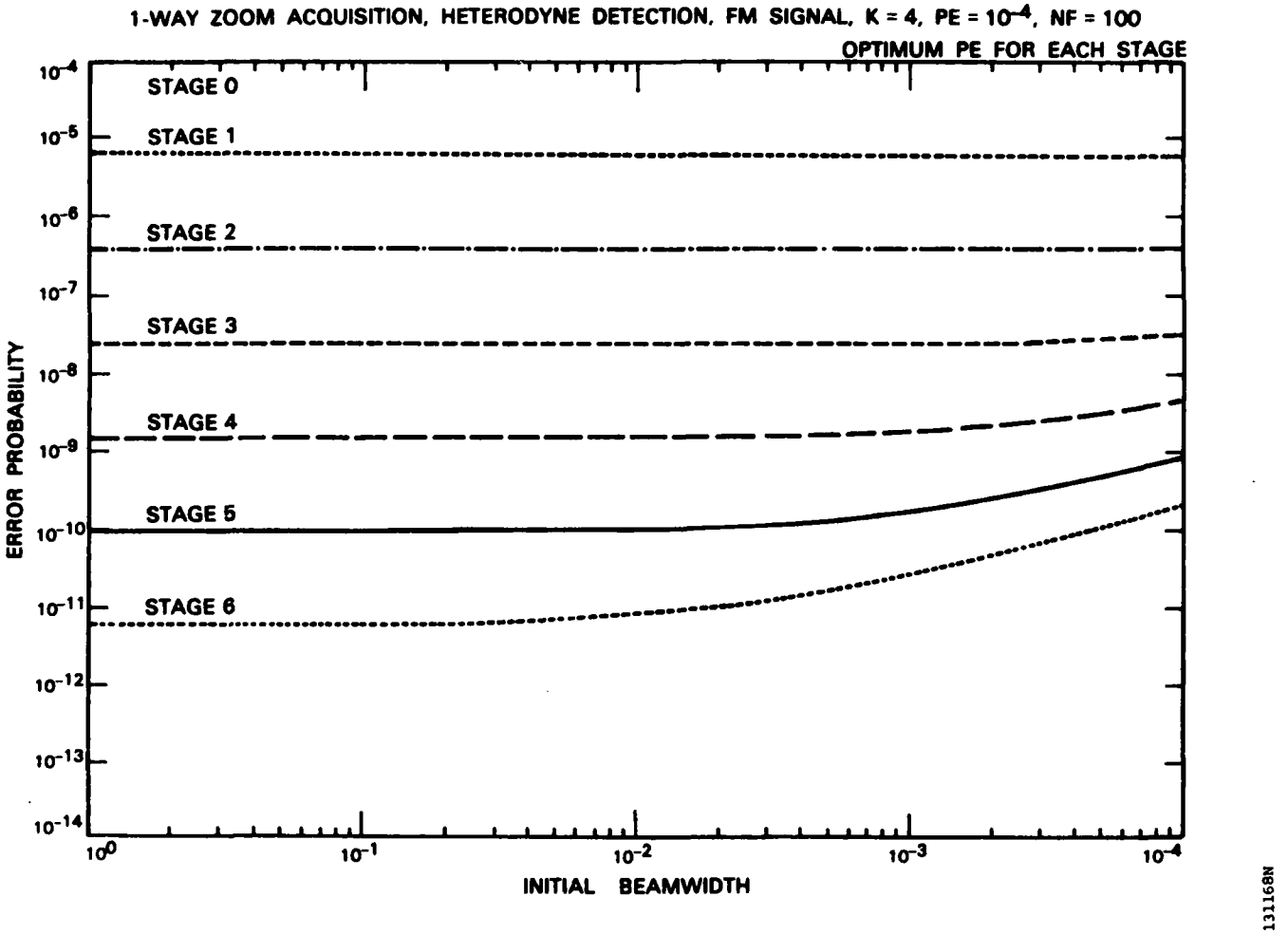

Fig. 4.3. Acquisition with zooming receiver, heterodyne detection, simultaneous frequency acquisition: (b) optimal parition of PE, 1-way zooming strategy.

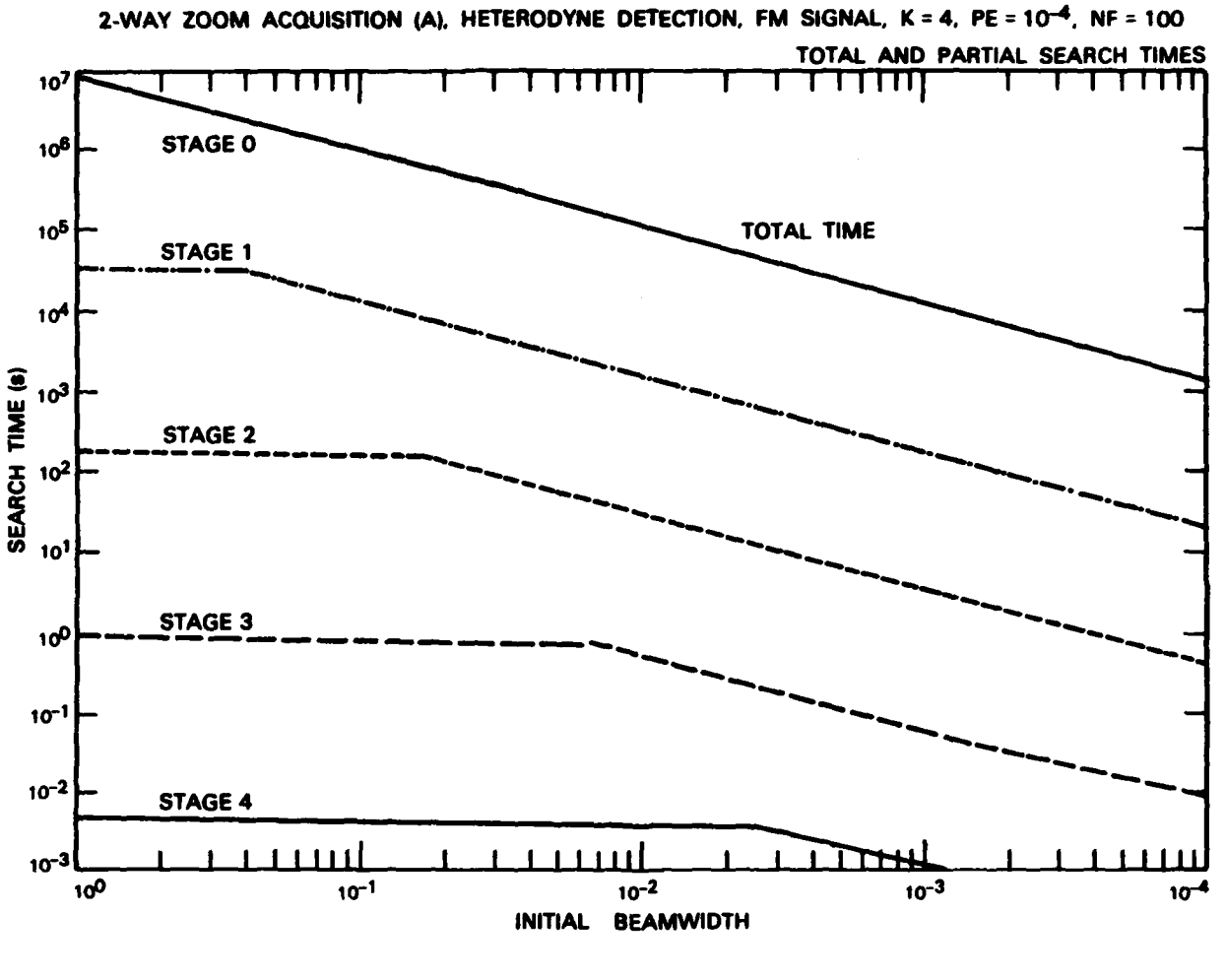

Fig. 4.3. Acquisition with zooming receiver, heterodyne detection, simultaneous frequency acquisition: (c) optimal partition of T, 2-way zooming strategy (A).

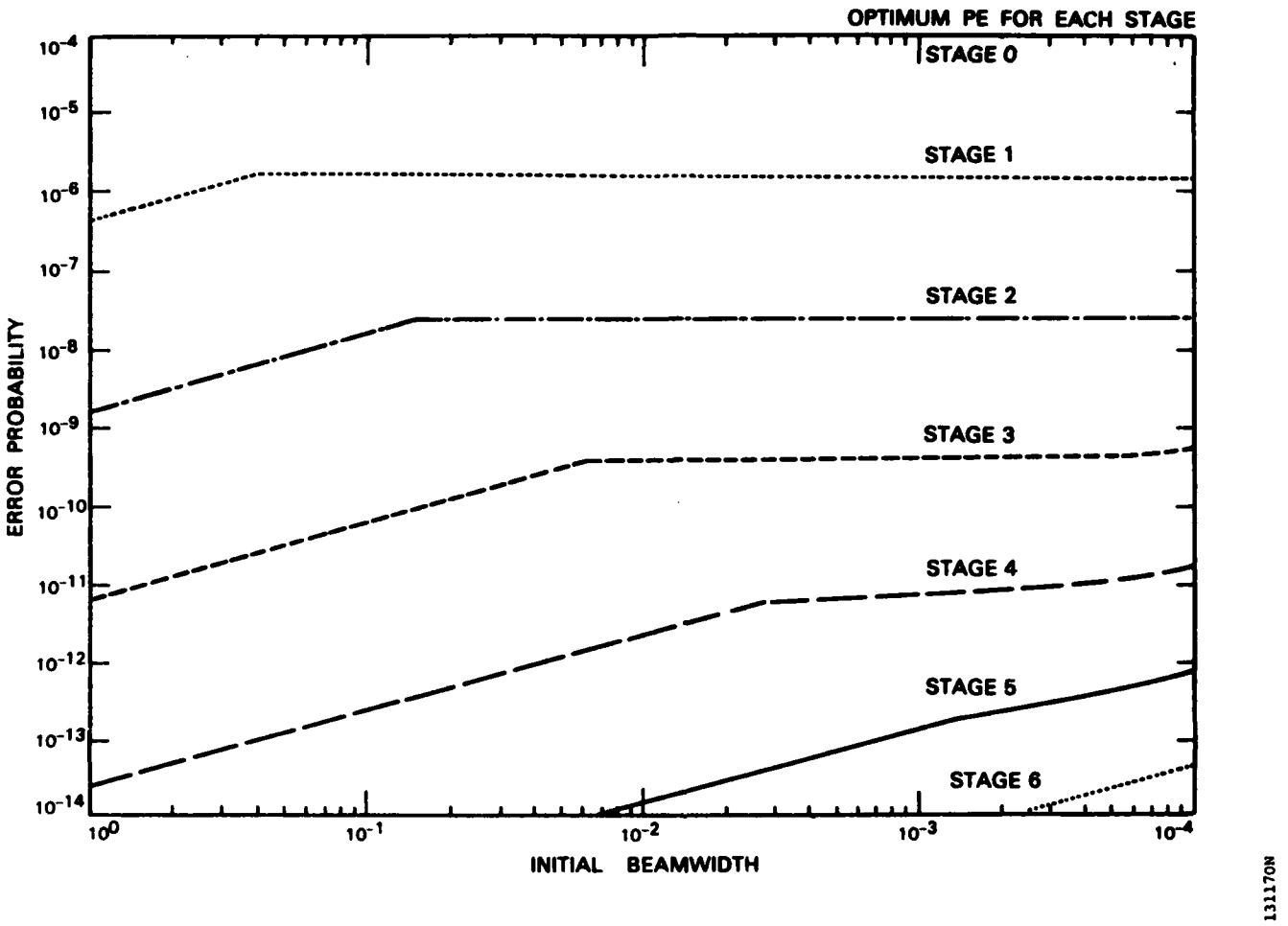

Fig. 4.3. Acquisition with zooming receiver, heterodyne detection, simultaneous frequency acquisition: (d) optimal partition of PE, 2-way zooming strategy (A).

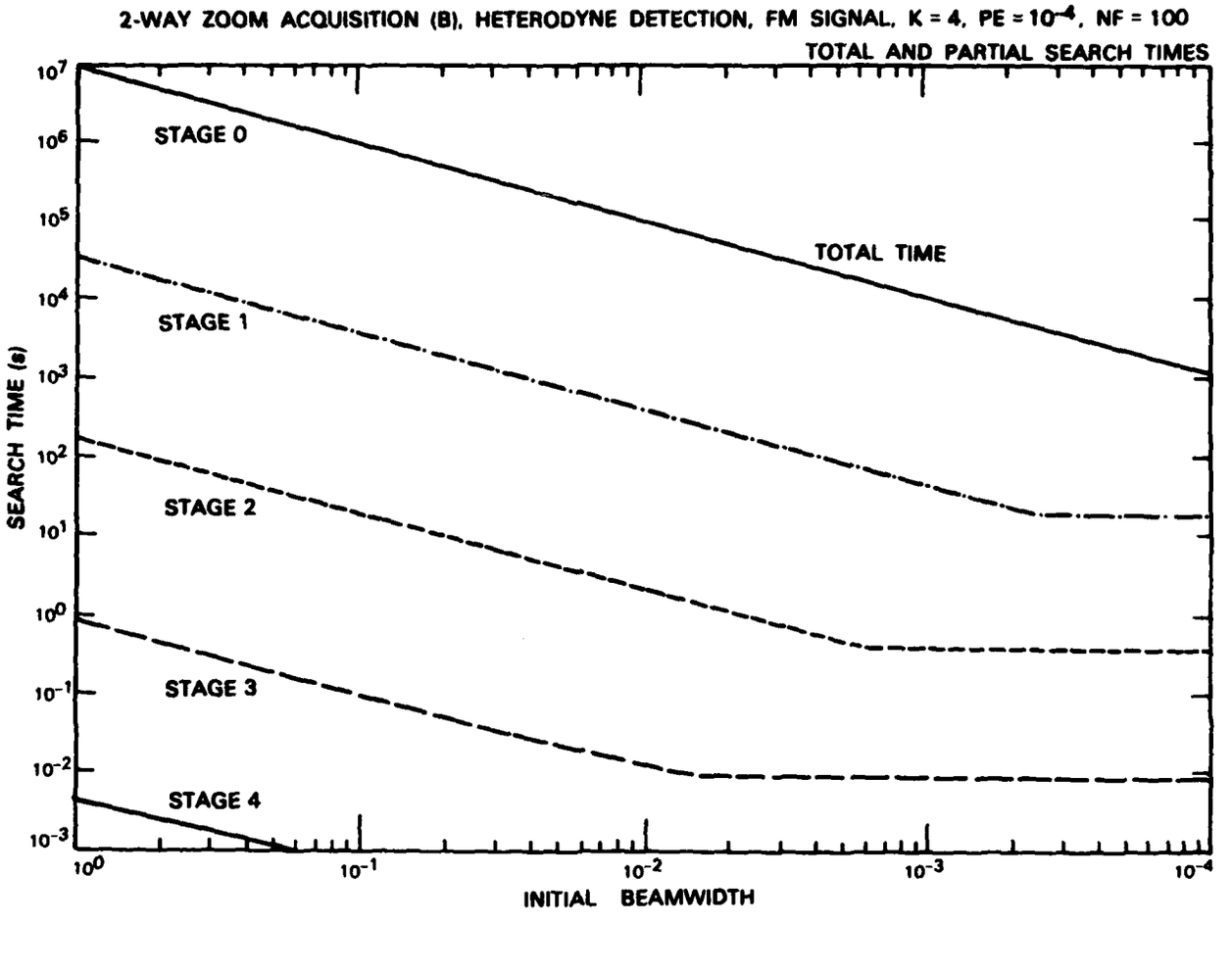

Fig. 4.3. Acquisition with zooming receiver, heterodyne detection, simultaneous frequency acquisition: (e) optimal partition of T, 2-way zooming strategy (B).

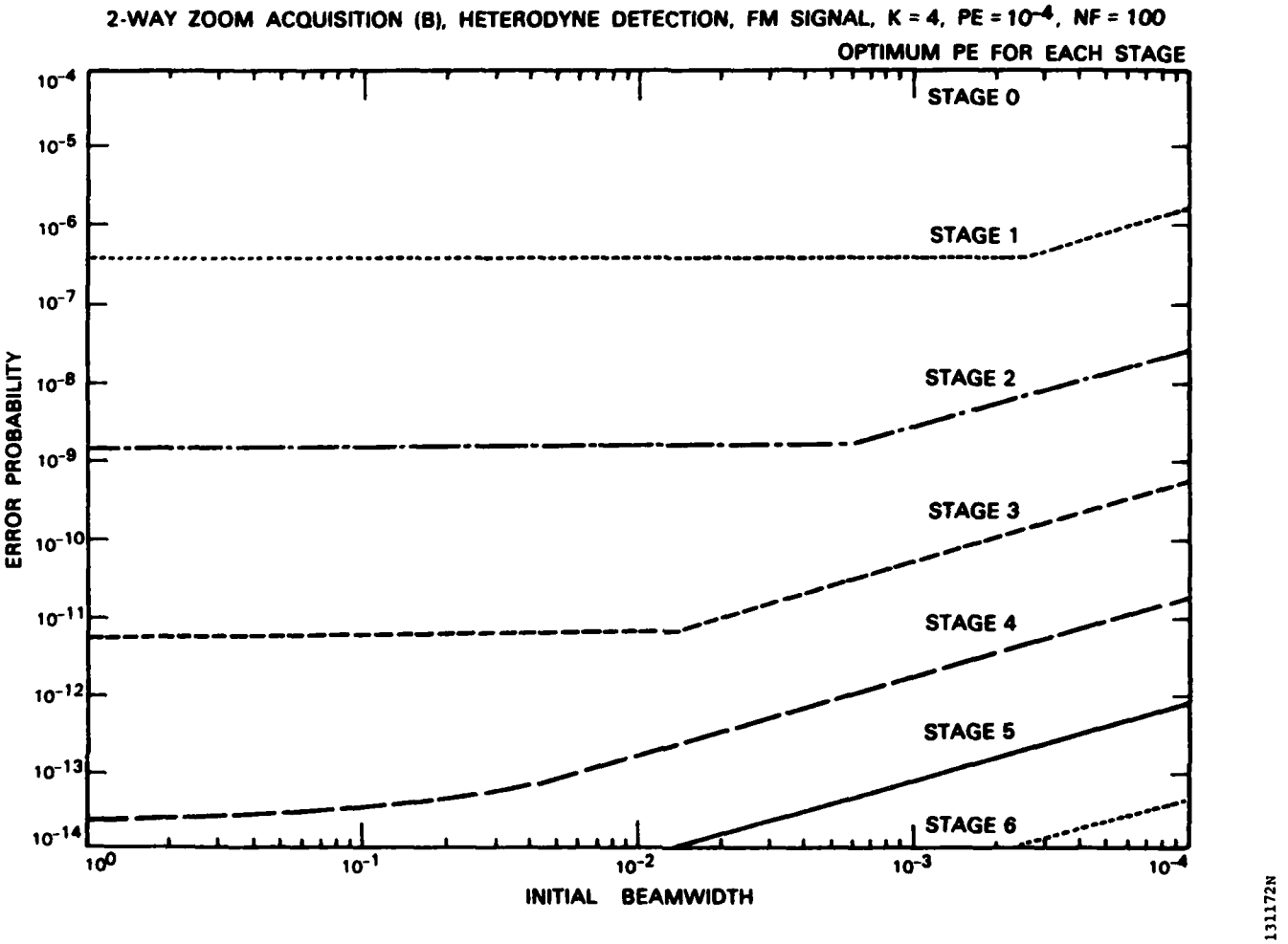

Fig. 4.3. Acquisition with zooming receiver, heterodyne detection, simultaneous frequency acquisition: (f) optimal partition of PE, 2-way zooming strategy (B).

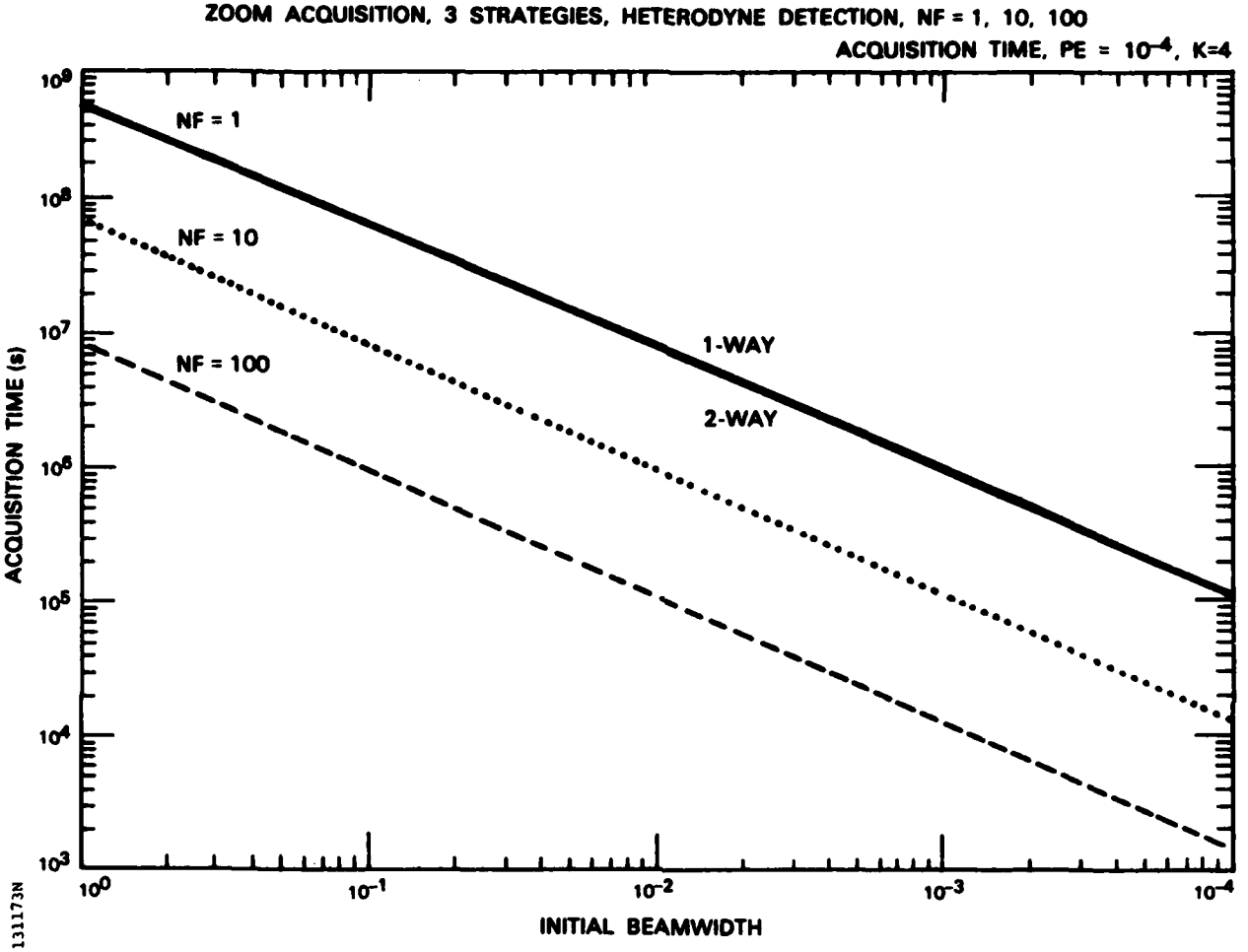

Fig. 4.4. Acquisition times with zooming receiver, heterodyne detection, comparison between the three zooming strategies. Processing in 1, 10, 100 frequency bands.

The expression of $f_1(\cdot)$ in (18) is in the form of (15) so that the optimum is given by (16). The optimal partition of PE and T, as well as the resulting total T are shown for the case K = 4, $\lambda_{bo} = 10^3$ in Fig. 4.5(a-f) and $\lambda_{bo} = 10^6$ in Fig. 4.6(a-f), for the three acquisition strategies. For large noise count rates, $(\lambda_{bo}/N^T > \lambda_s)$, the first stage of the search is dominant so that the three strategies are equivalent. For small noise counts, the first stage is also dominant for a two-way acquisition. The optimal strategy for a one-way acquisition in low background noise however is to spend approximately the same time at each stage of the zooming. The two-way acquisition is therefore faster in this case by a factor equal to the number of required zooming stages; see Fig. 4.7.

The background and shot noise limited operation is difficult to reach in practice without photomultiplication. The photomultiplier devices introduce excess noise so that the acquisition times need approximately to be multiplied by the noise factor of the detector.

4.5.2 Thermal Noise Limited Operation

The expression for $f_1(\cdot)$ is derived from Fig. 3.9 as

$$PE(i) \leq N^T(i)(K-1)\ \mathrm{erfc}\left[\frac{\lambda_s(i)\sqrt{T(i)}}{\sqrt{\frac{2k\tau}{e^2 N^T(i)}}}\right]$$

considering that the thermal noise is dominant. This expression is in the form of (13) so that the optimality relationship is (14). Optimal partition of PE

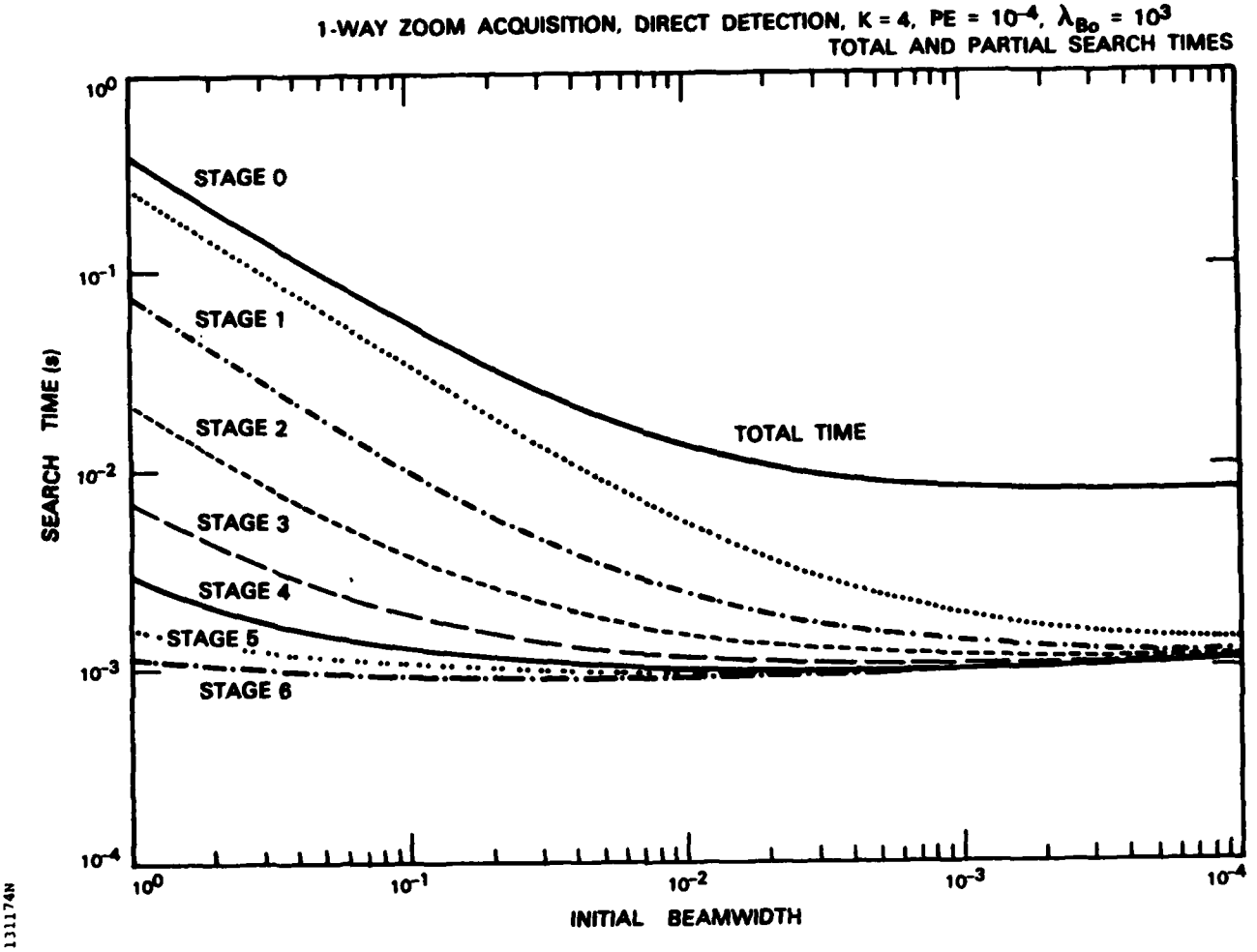

Fig. 4.5. Acquisition with zooming receiver, background and quantum noise limited direct detection, $\lambda_{Bo} = 10^3$: (a) optimal partition of T, 1-way zooming strategy.

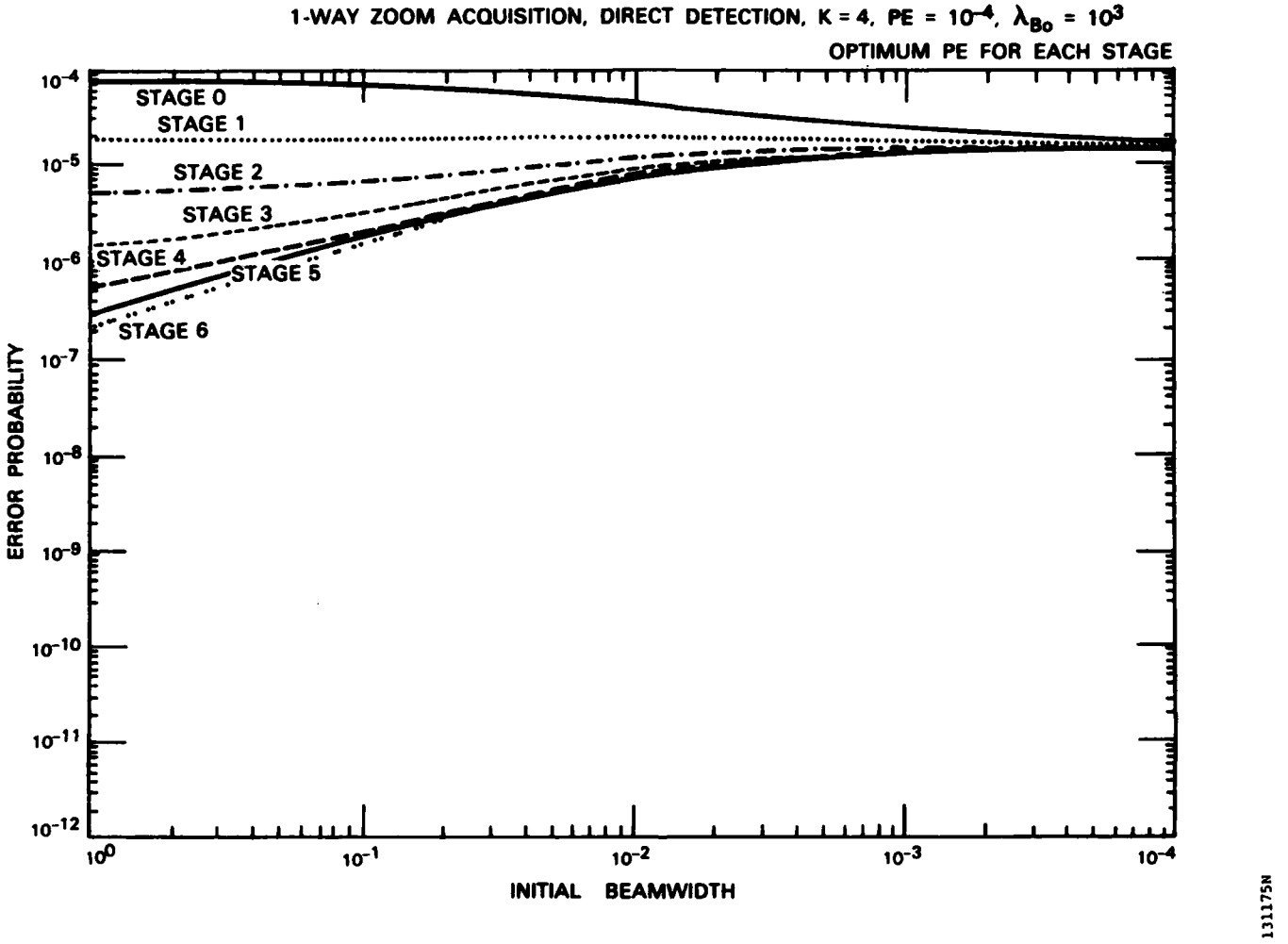

Fig. 4.5. Acquisition with zooming receiver, background and quantum noise limited direct detection, $\lambda_{Bo} = 10^3$: (b) optimal partition of PE, 1-way zooming strategy.

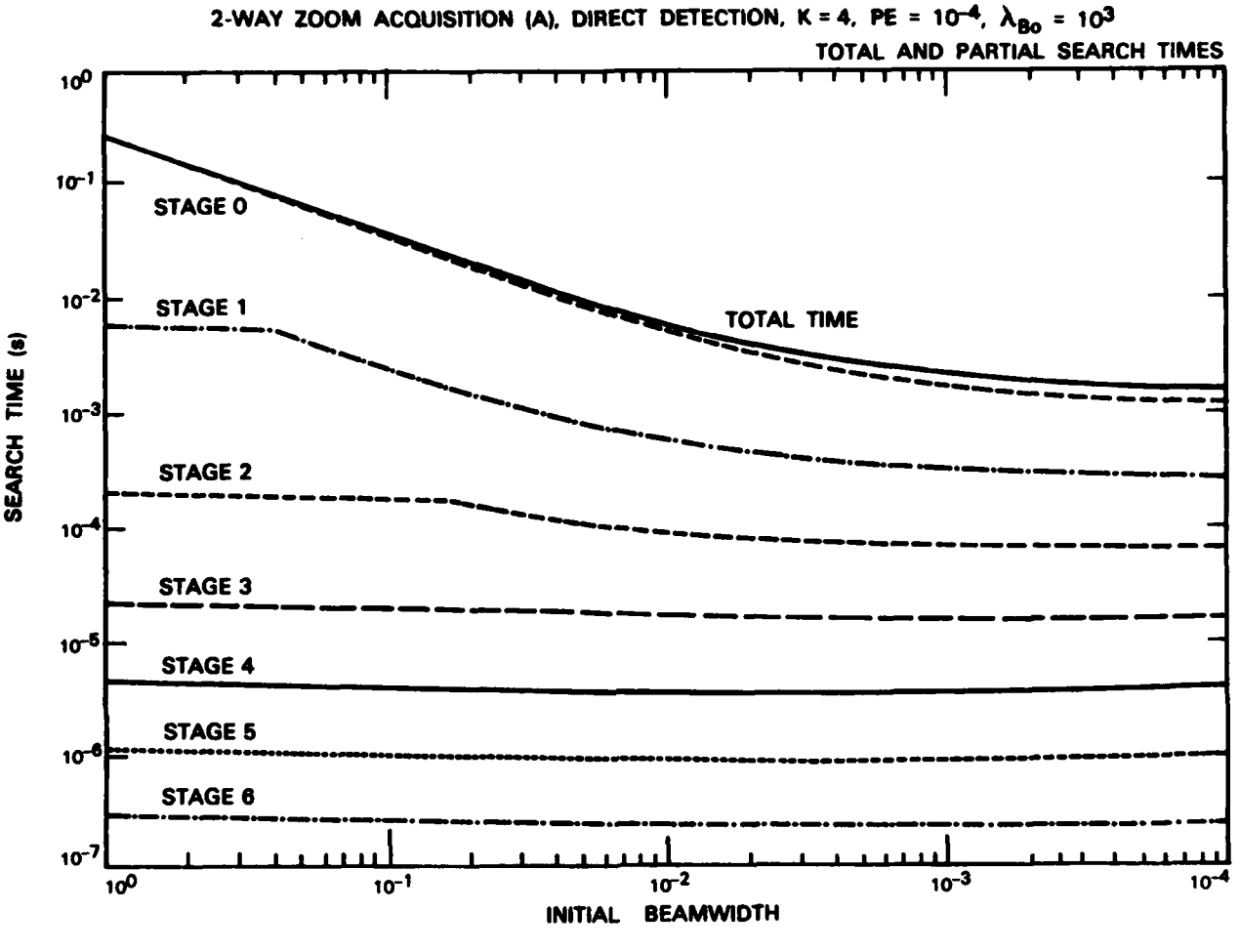

Fig. 4.5. Acquisition with zooming receiver, background and quantum noise limited direct detection, $\lambda_{Bo} = 10^3$: (c) optimal partition of T, 2-Way zooming strategy (A).

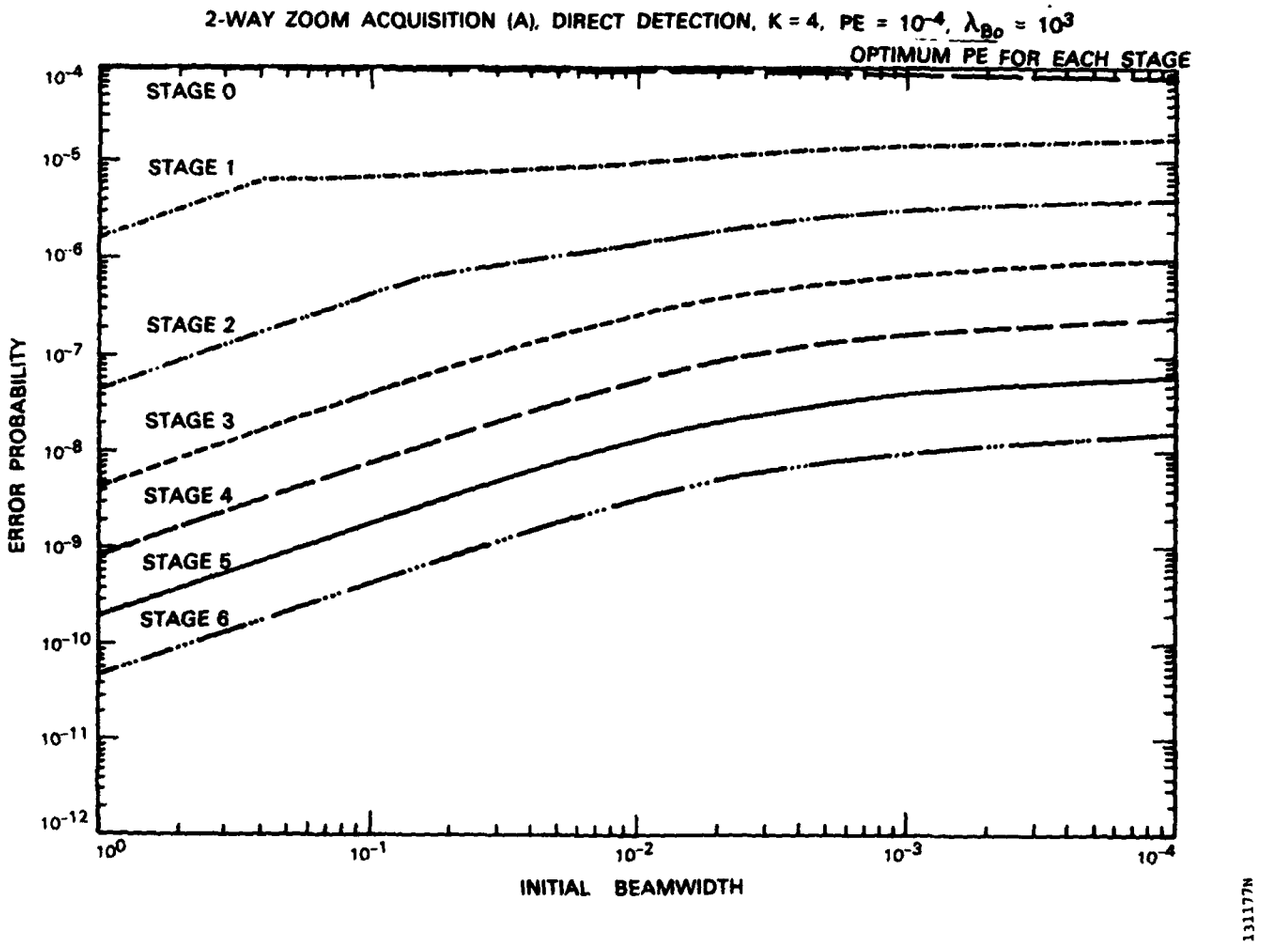

Fig. 4.5. Acquisition with zooming receiver, background and quantum noise limited direct detection, $\lambda_{Bo} = 10^3$: (d) optimal partition of PE, 2-way zooming strategy (A).

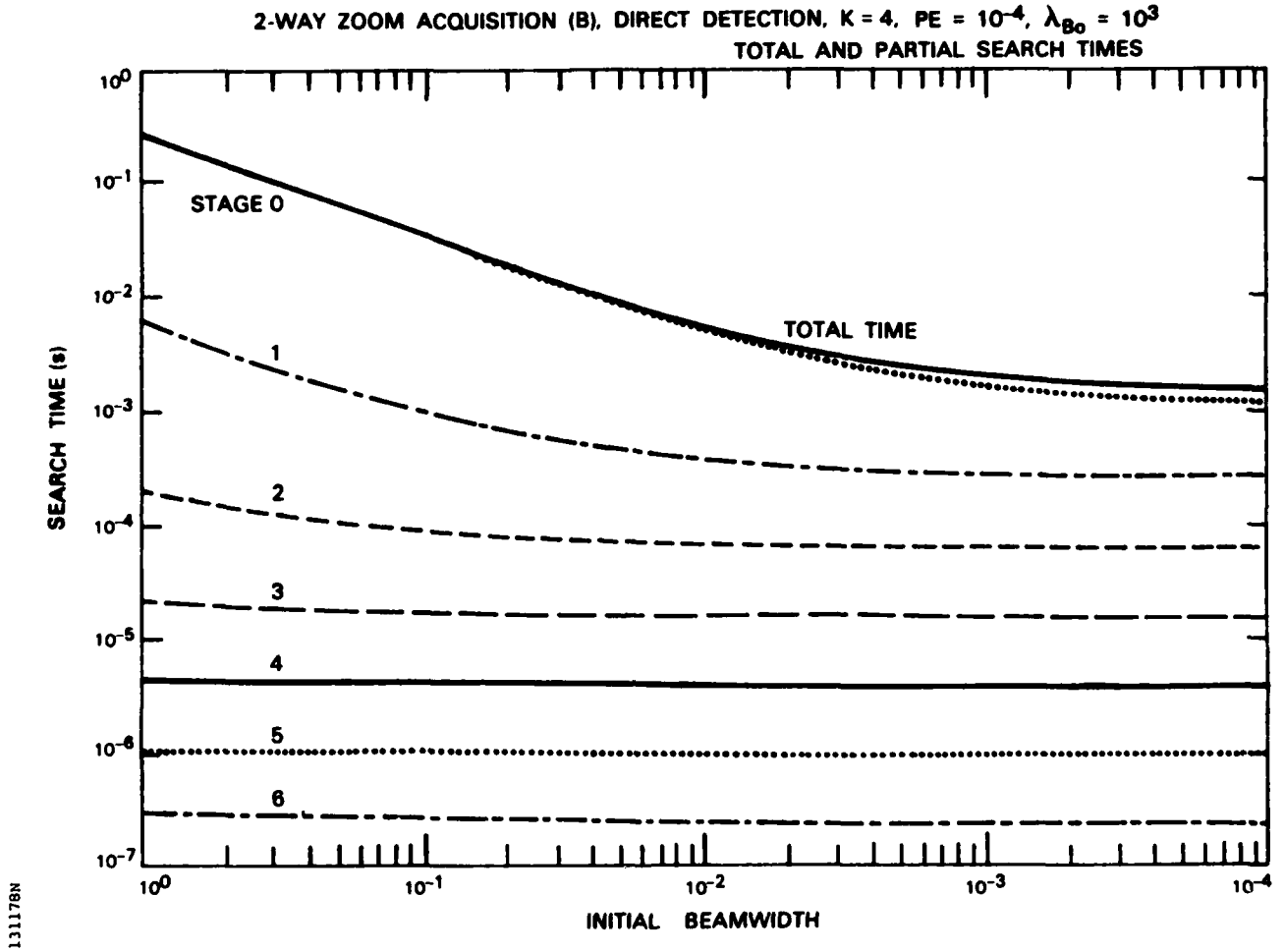

Fig. 4.5. Acquisition with zooming receiver, background and quantum noise limited direct detection, $\lambda_{Bo} = 10^3$: (e) optimal partition of T, 2-way zooming strategy (B).

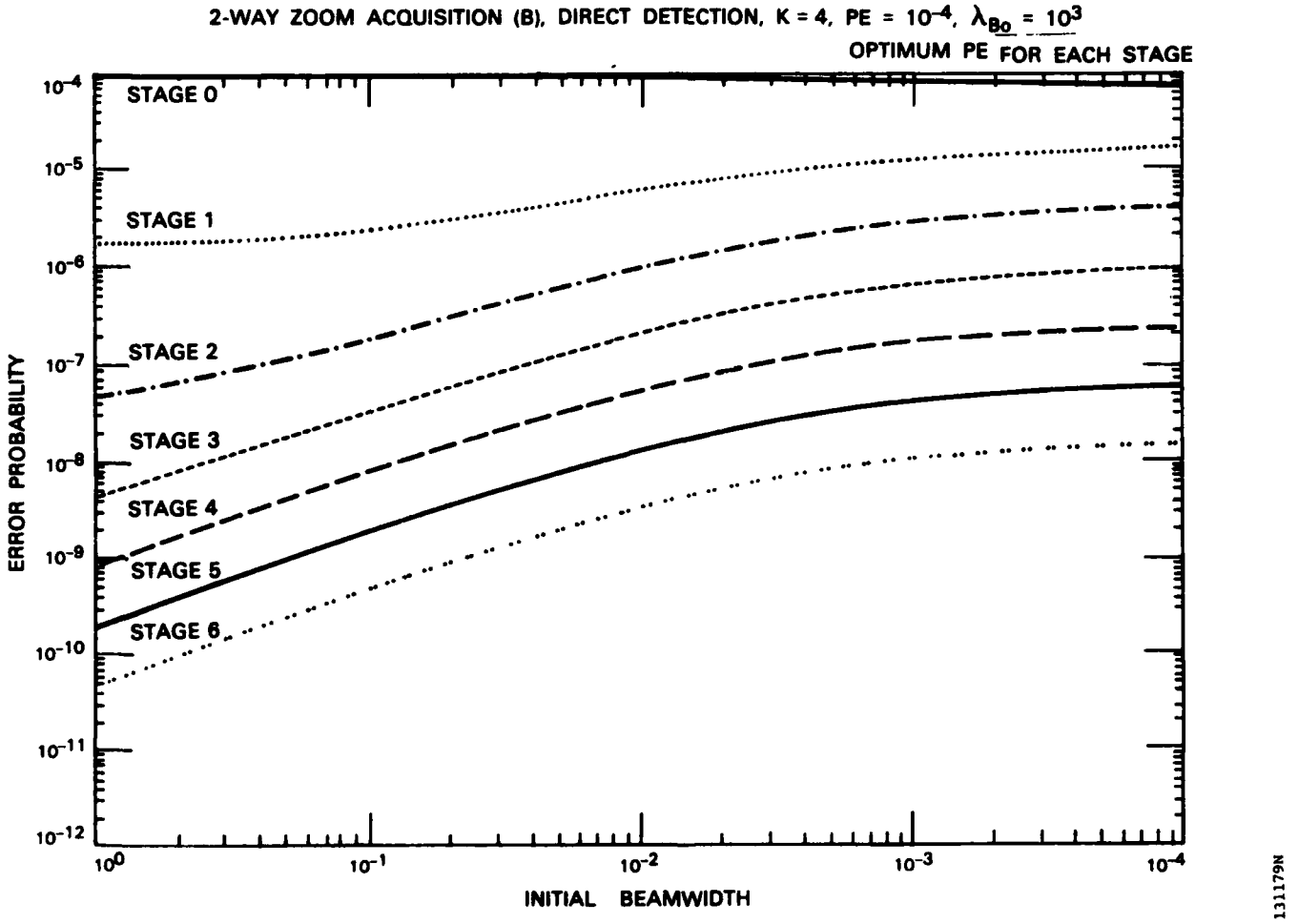

Fig. 4.5. Acquisition with zooming receiver, background and quantum noise limited direct detection, $\lambda_{Bo} = 10^3$: (f) optimal partition of PE, 2-way zooming strategy (B).

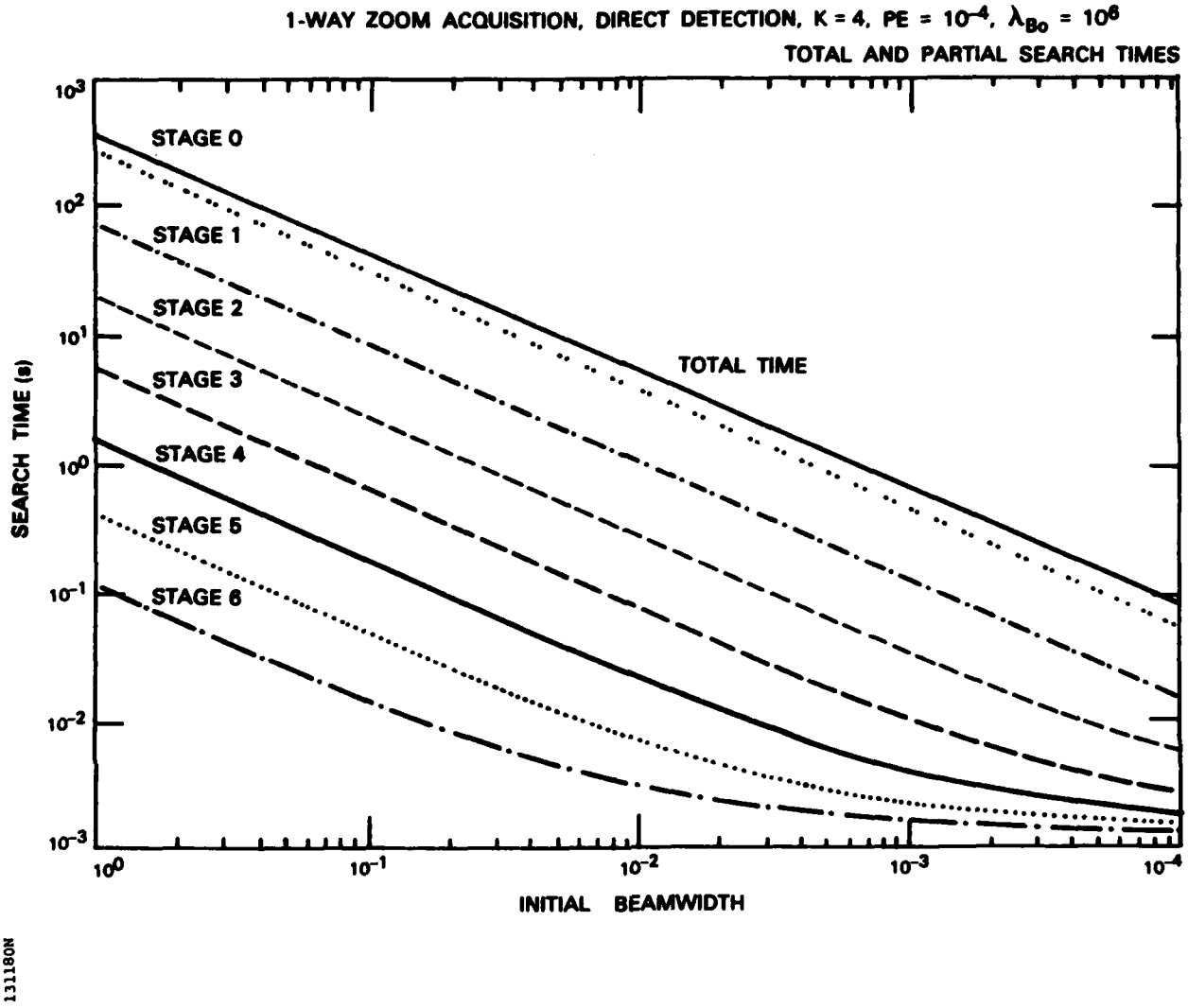

Fig. 4.6. Acquisition with zooming receiver, background and quantum noise limited direct detection, $\lambda_{Bo} = 10^6$: (a) optimal partition of T, 1-way zooming strategy.

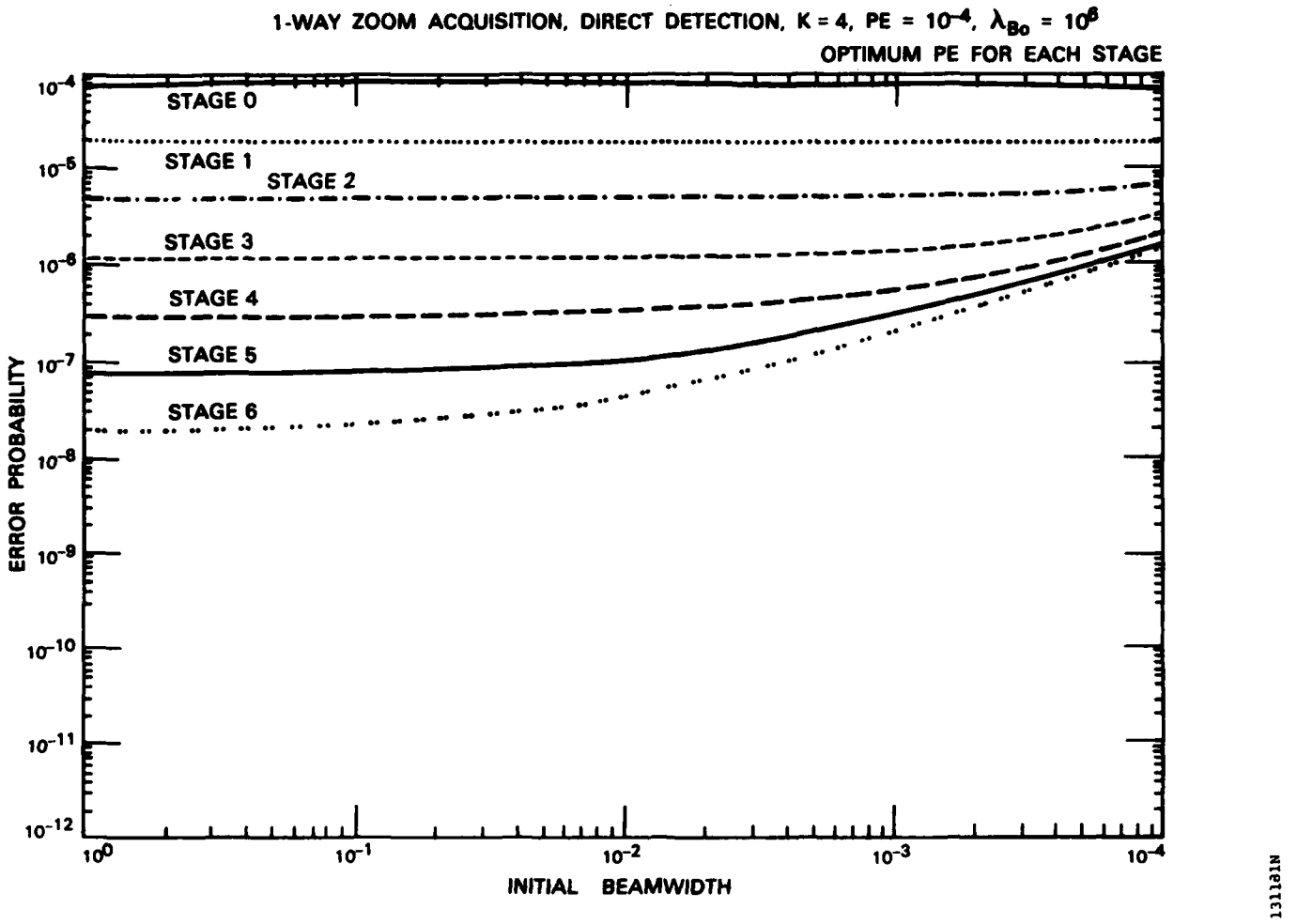

Fig. 4.6. Acquisition with zooming receiver, background and quantum noise limited direct detection, $\lambda_{Bo} = 10^6$: (b) optimal partition of PE, 1-way zooming strategy.

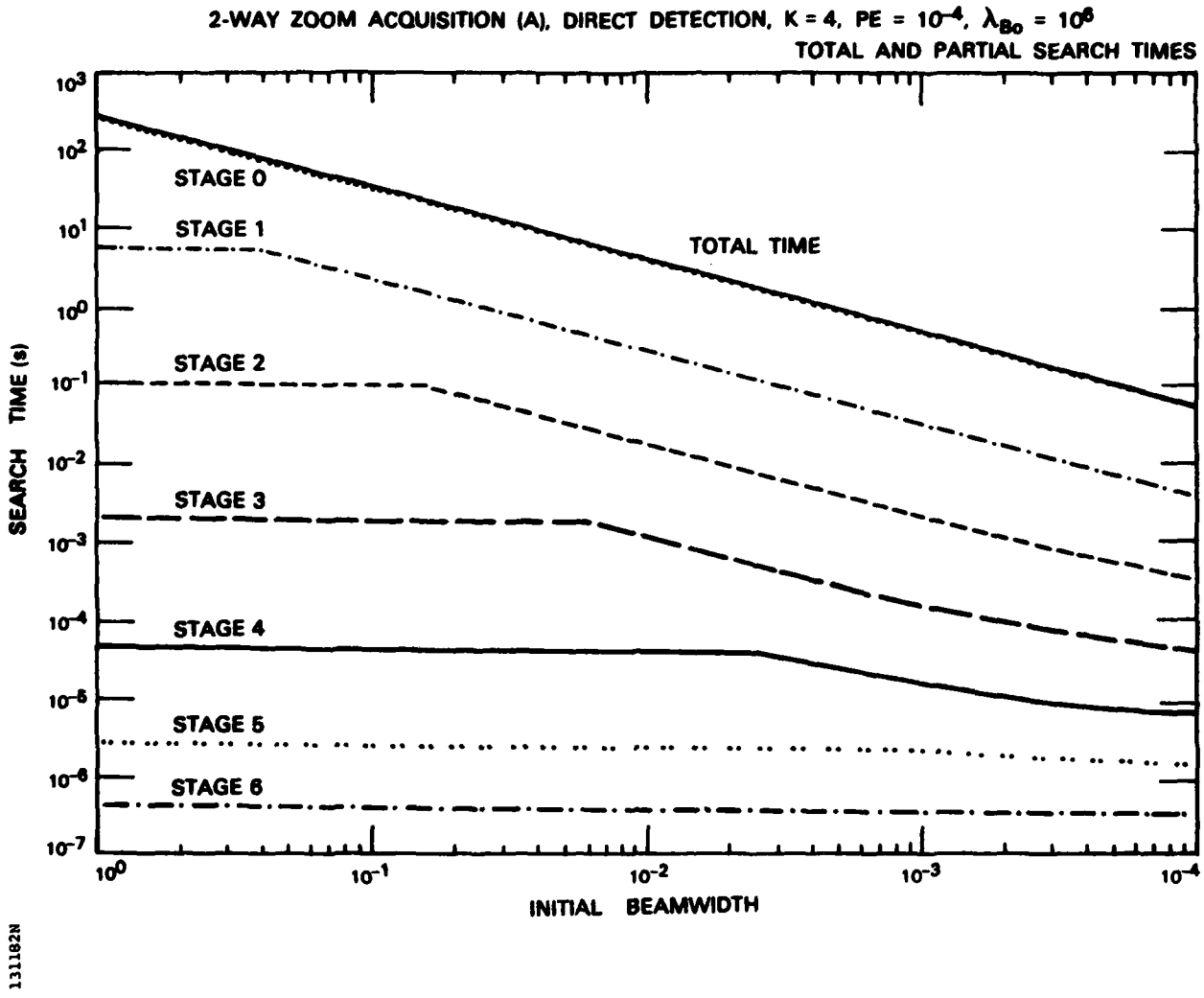

Fig. 4.6. Acquisition with zooming receiver, background and quantum noise limited direct detection, $\lambda_{Bo} = 10^6$: (c) optimal partition of T, 2-way zooming strategy (A).

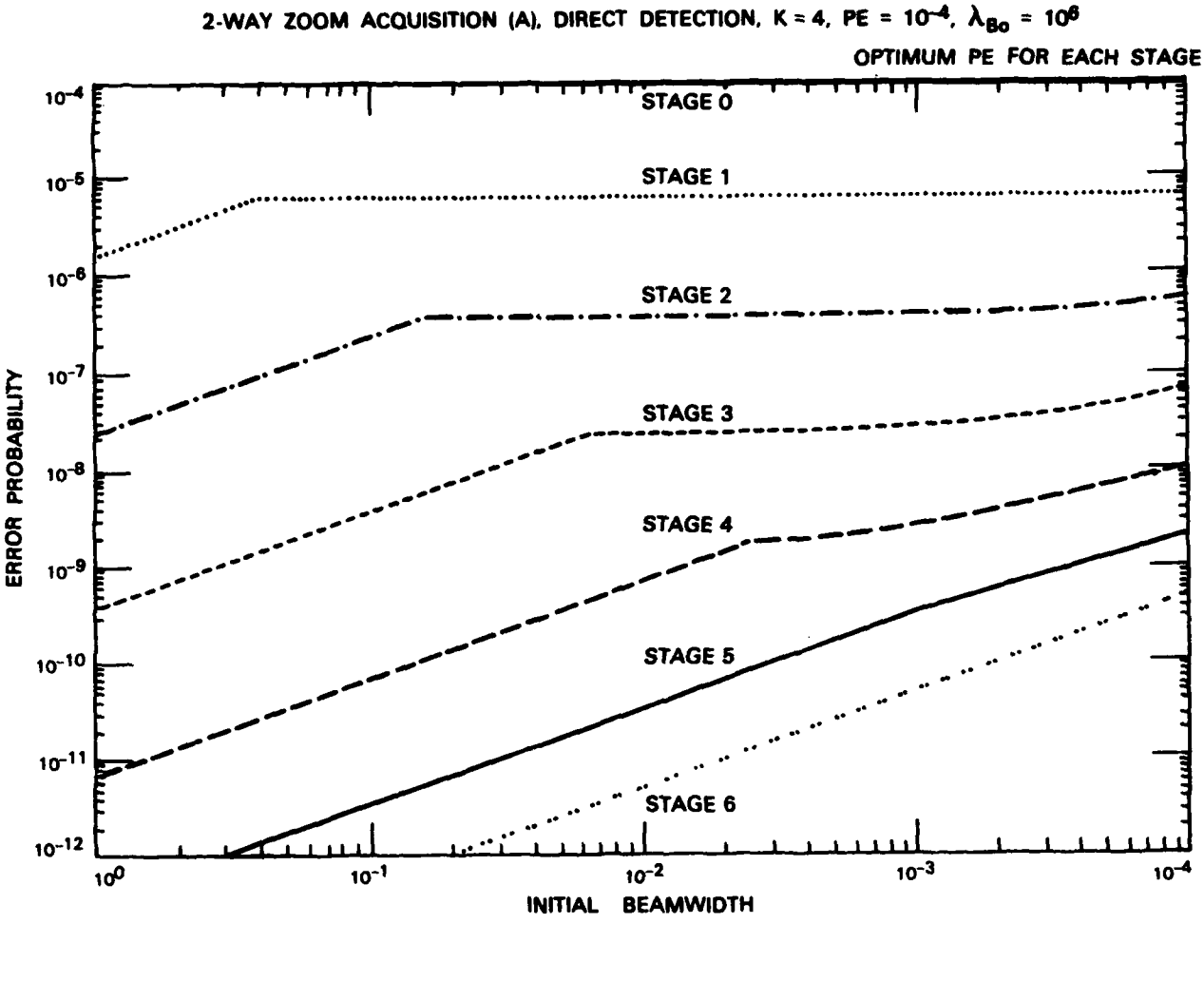

Fig. 4.6. Acquisition with zooming receiver, background and quantum noise limited direct detection, $\lambda_{Bo} = 10^6$: (d) optimal partition of PE, 2-way zooming strategy (A).

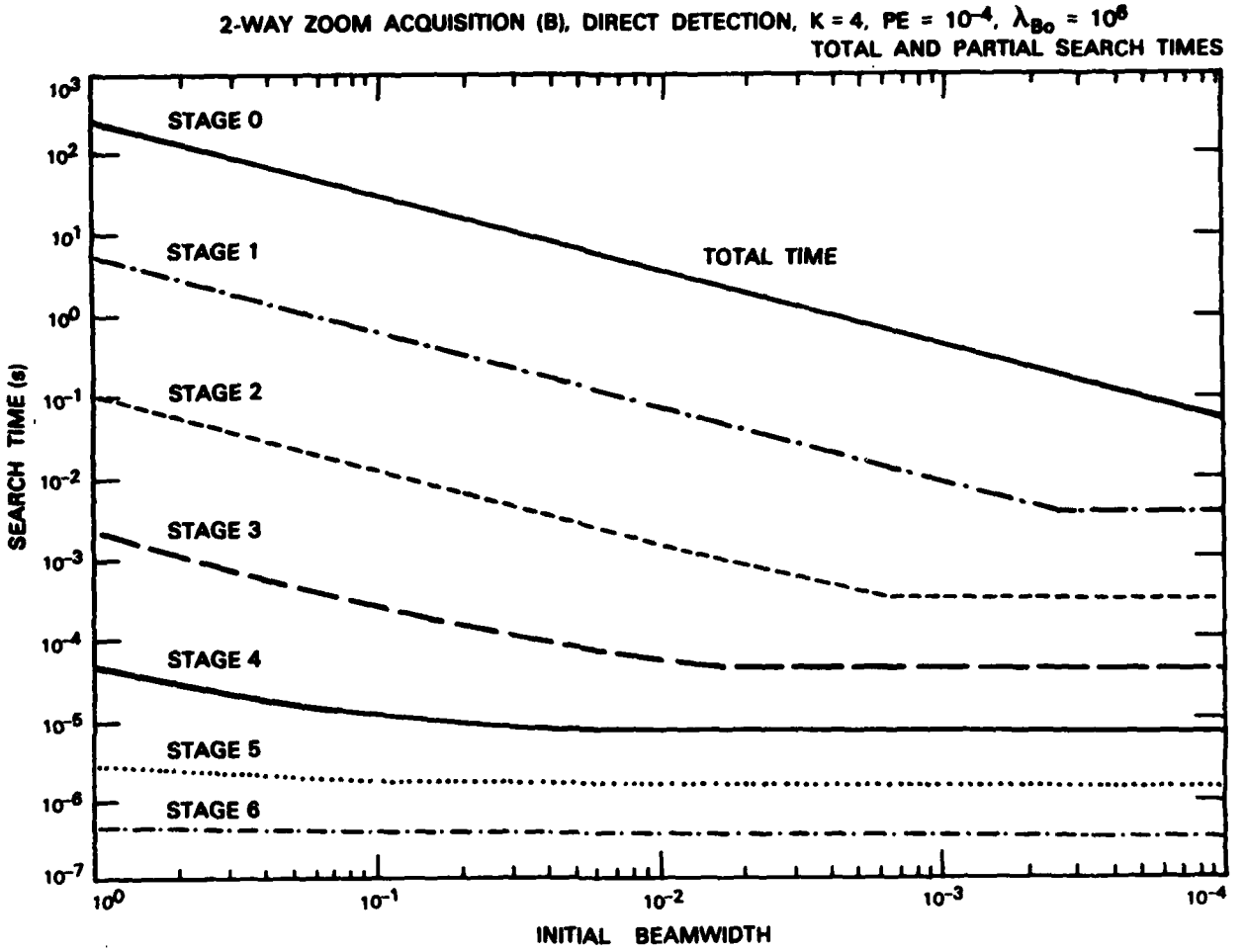

Fig. 4.6. Acquisition with zooming receiver, background and quantum noise limited direct detection, $\lambda_{Bo} = 10^6$: (e) optimal partition of T, 2-way zooming strategy (B).

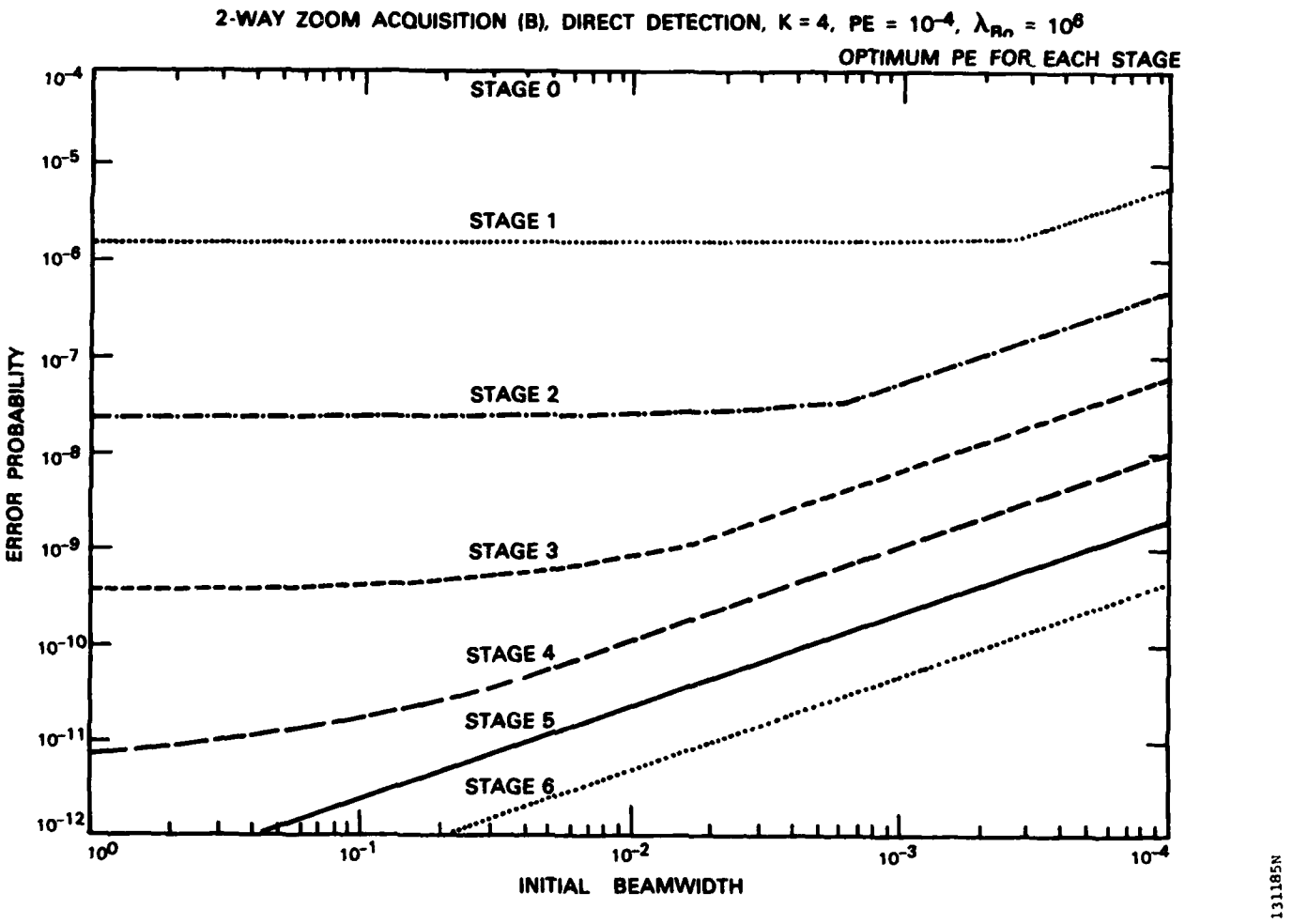

Fig. 4.6. Acquisition with zooming receiver, background and quantum noise limited direct detection, $\lambda_{Bo} = 10^6$: (f) optimal partition of PE, 2-way zooming strategy (B).

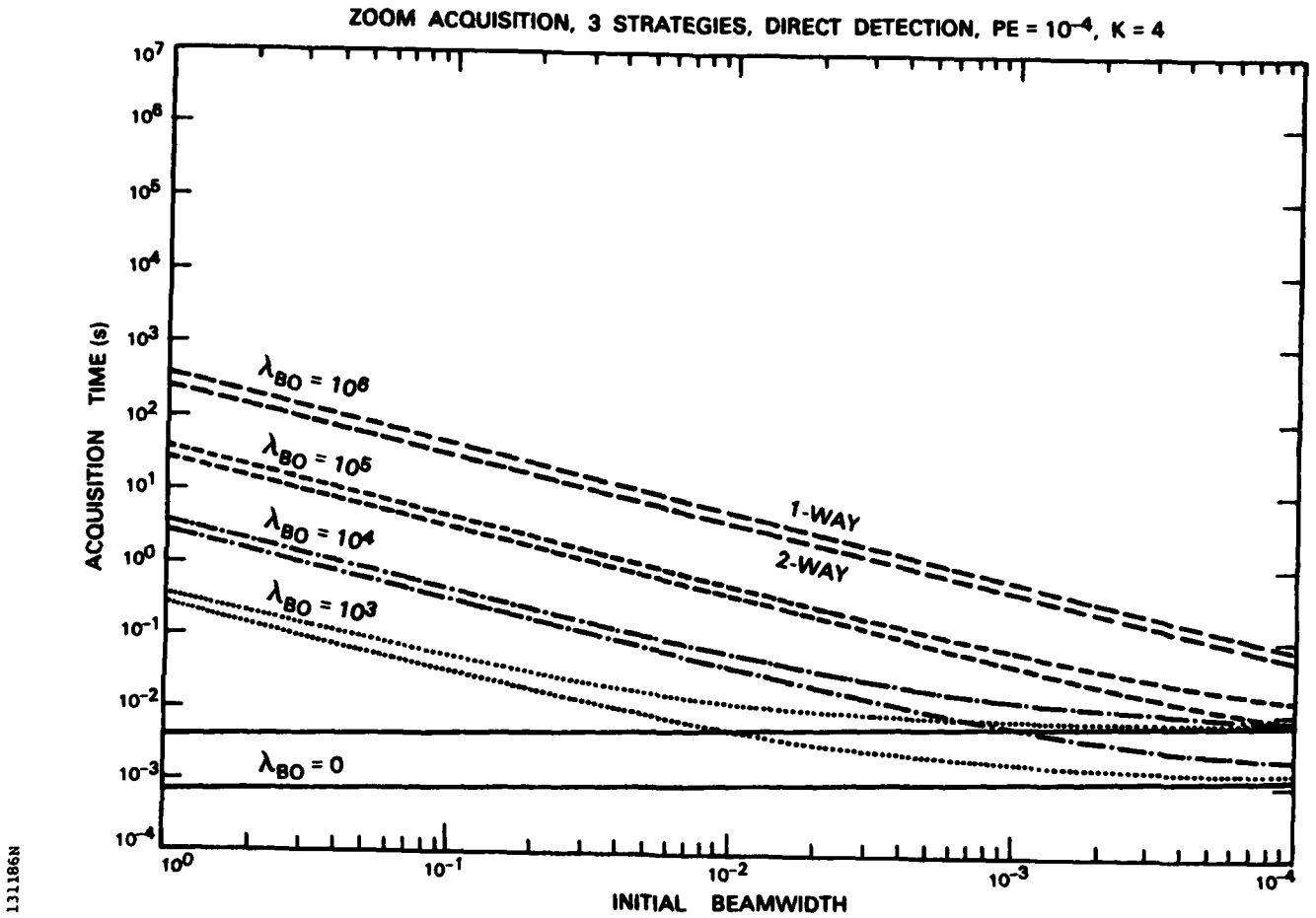

Fig. 4.7. Acquisition times for zooming receiver, background and quantum noise limited direct detection. Comparison between the three zooming strategies for different background noise count rates.

and T are given in Fig. 4.8(a-f) for the case K = 4, Z = 10^6 for the three acquisition strategies. The first stage of the zooming is dominant for a two-way acquisition whereas all the stages have the same importance for a one-way acquisition. The one-way acquisition times are therefore longer by a factor equal to the number of zooming stages as is shown on Fig. 4.9.

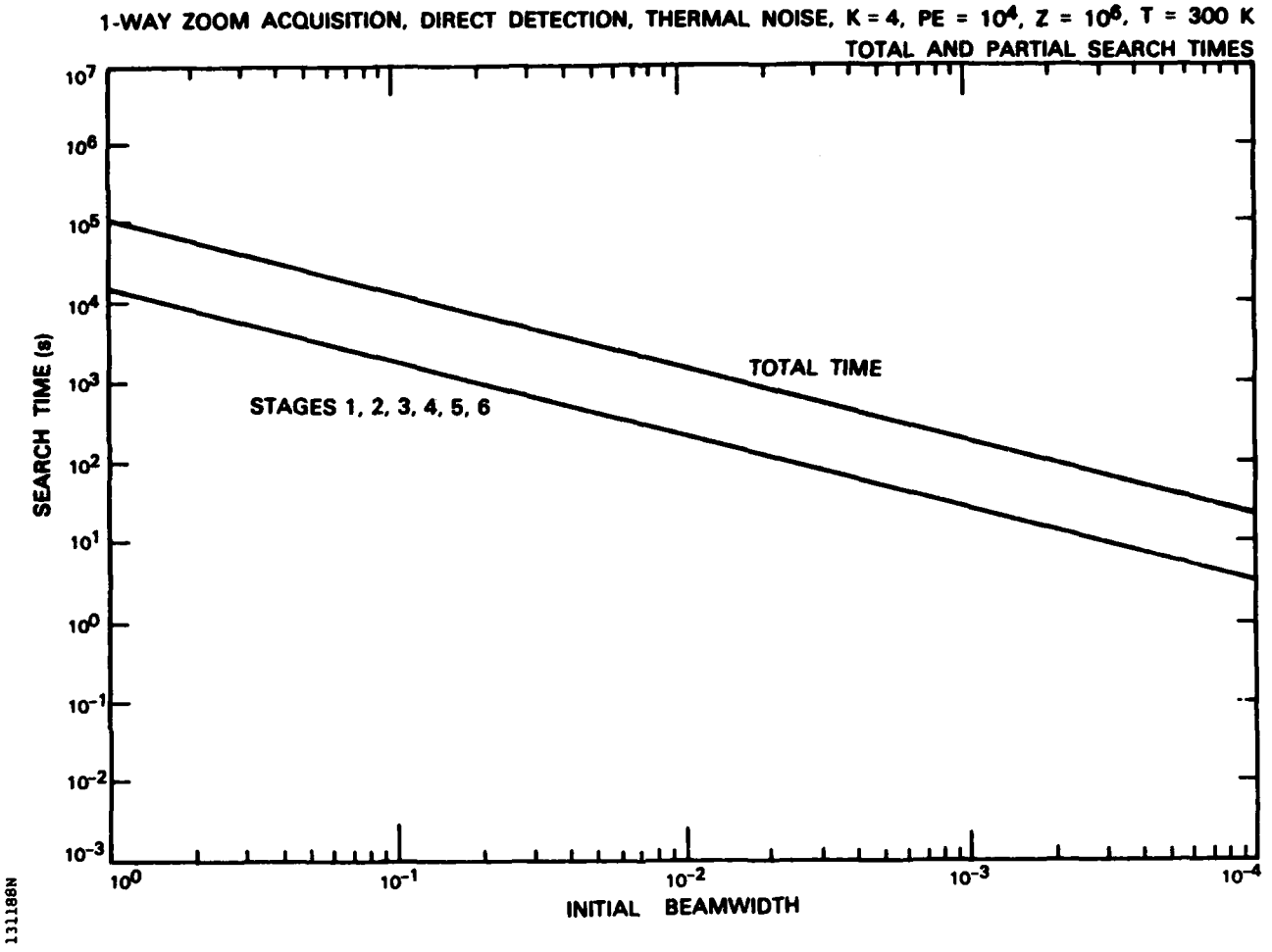

Fig. 4.8. Acquisition with zooming receiver, thermal noise limited direct detection, input impedance = 10^6 Ω: (a) optimal partition of T, 1-way zooming strategy.

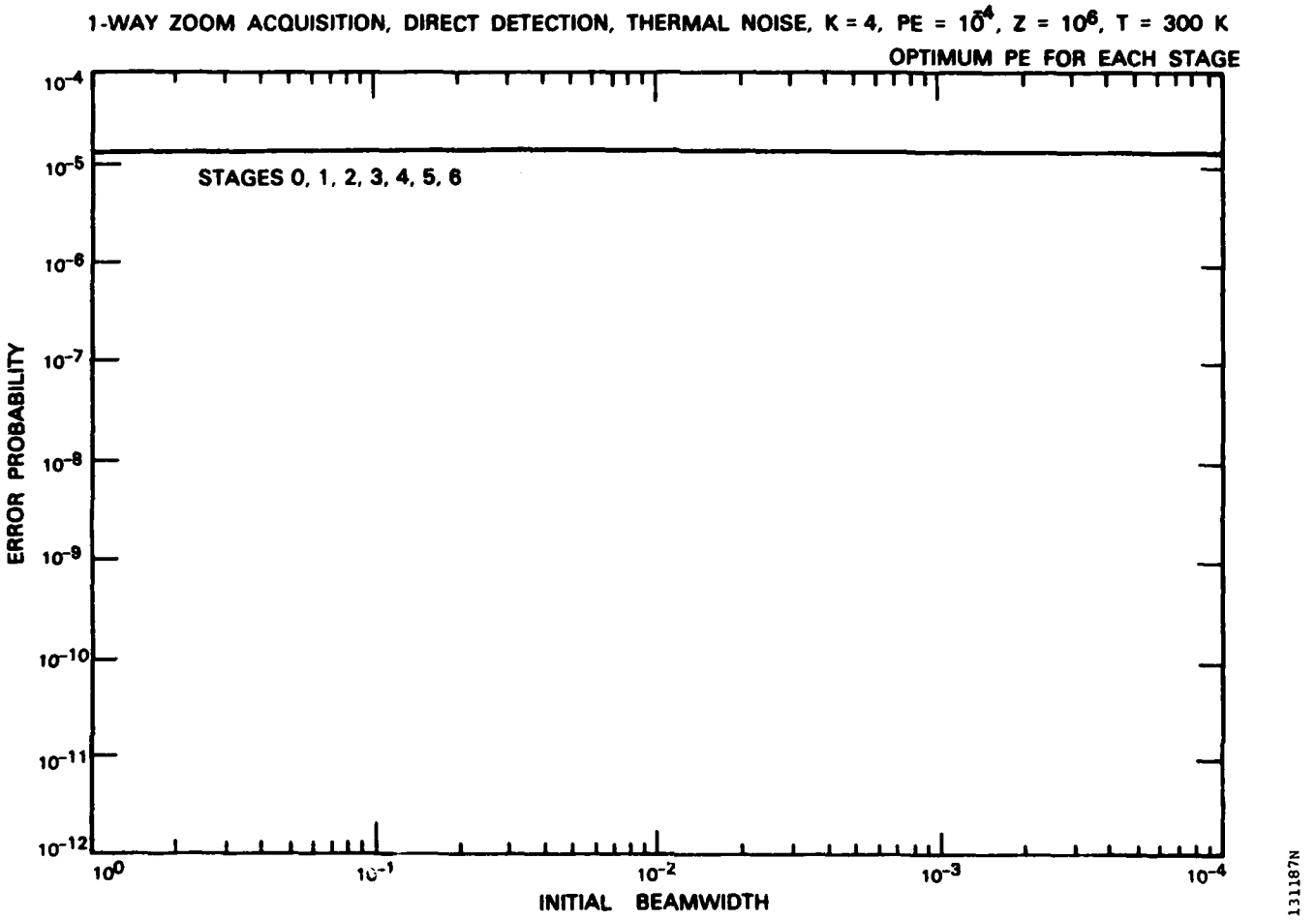

Fig. 4.8. Acquisition with zooming receiver, thermal noise limited direct detection, input impedance = 10^6 Ω: (b) optimal partition of PE, 1-way zooming strategy.

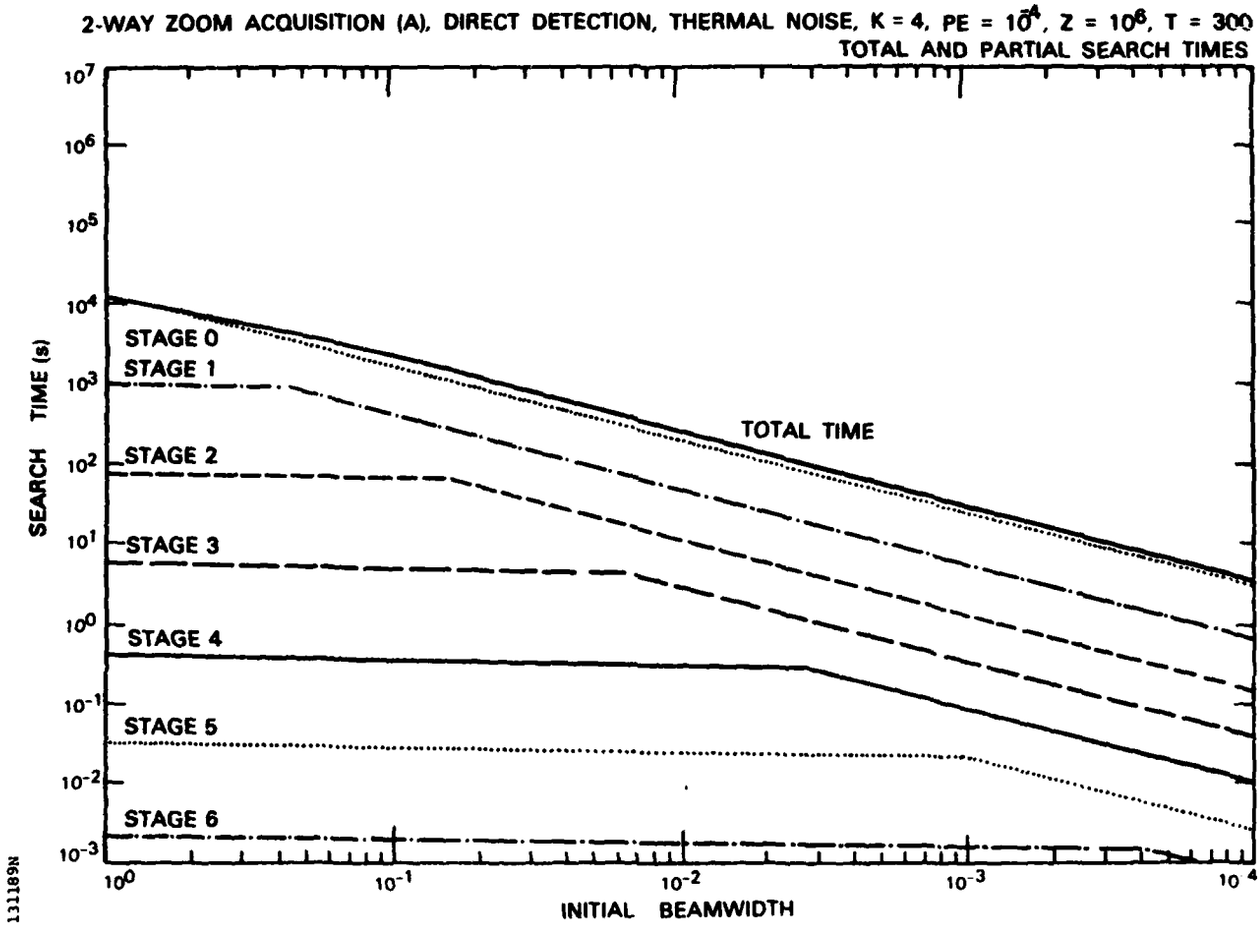

Fig. 4.8. Acquisition with zooming receiver, thermal noise limited direct detection, input impedance = 10^6 Ω: (c) optimal partition of T, 2-way zooming strategy (A).

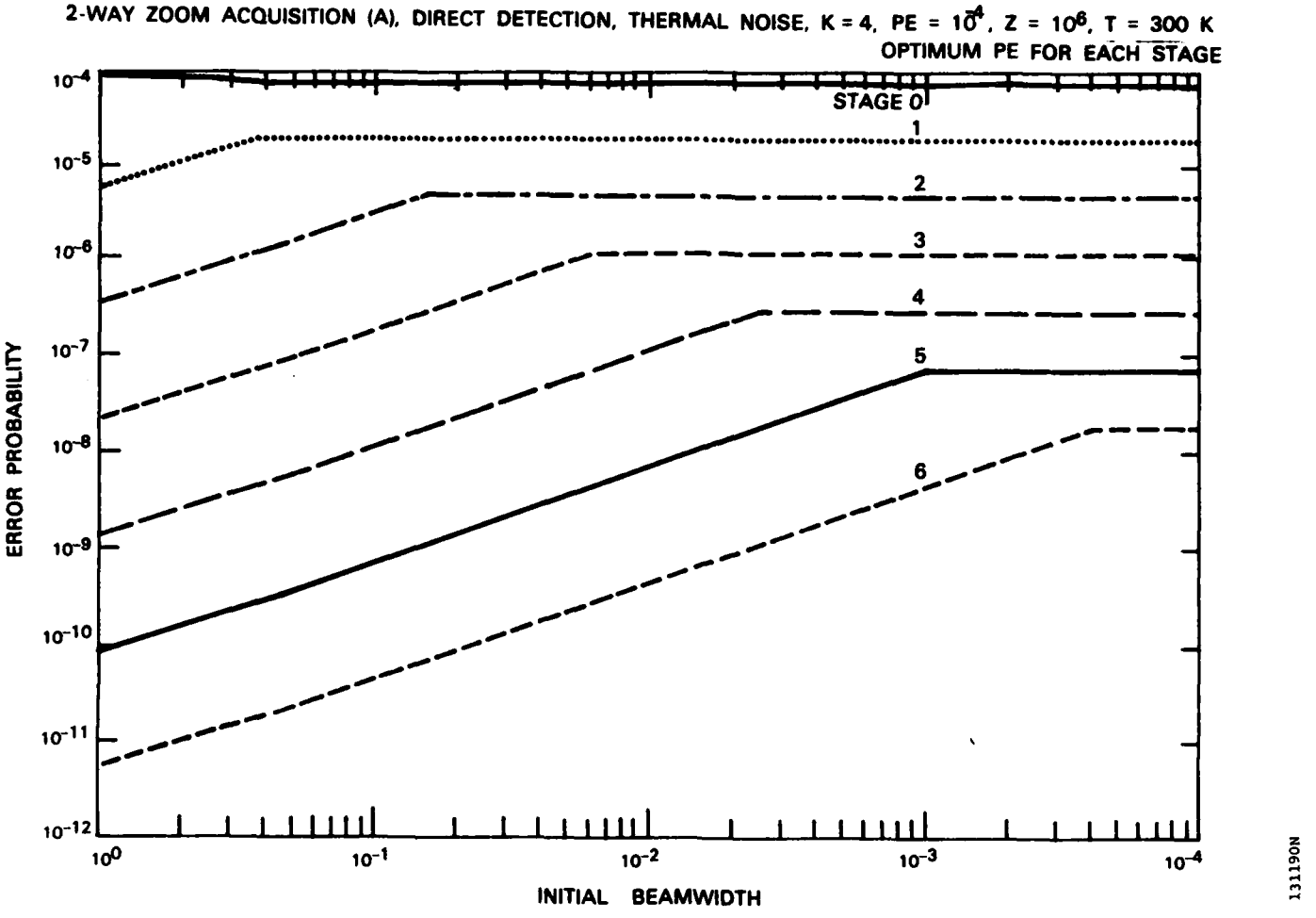

Fig. 4.8. Acquisition with zooming receiver, thermal noise limited direct detection, input impedance = 10^6 Ω: (d) optimal partition of PE, 2-way zooming strategy (A).

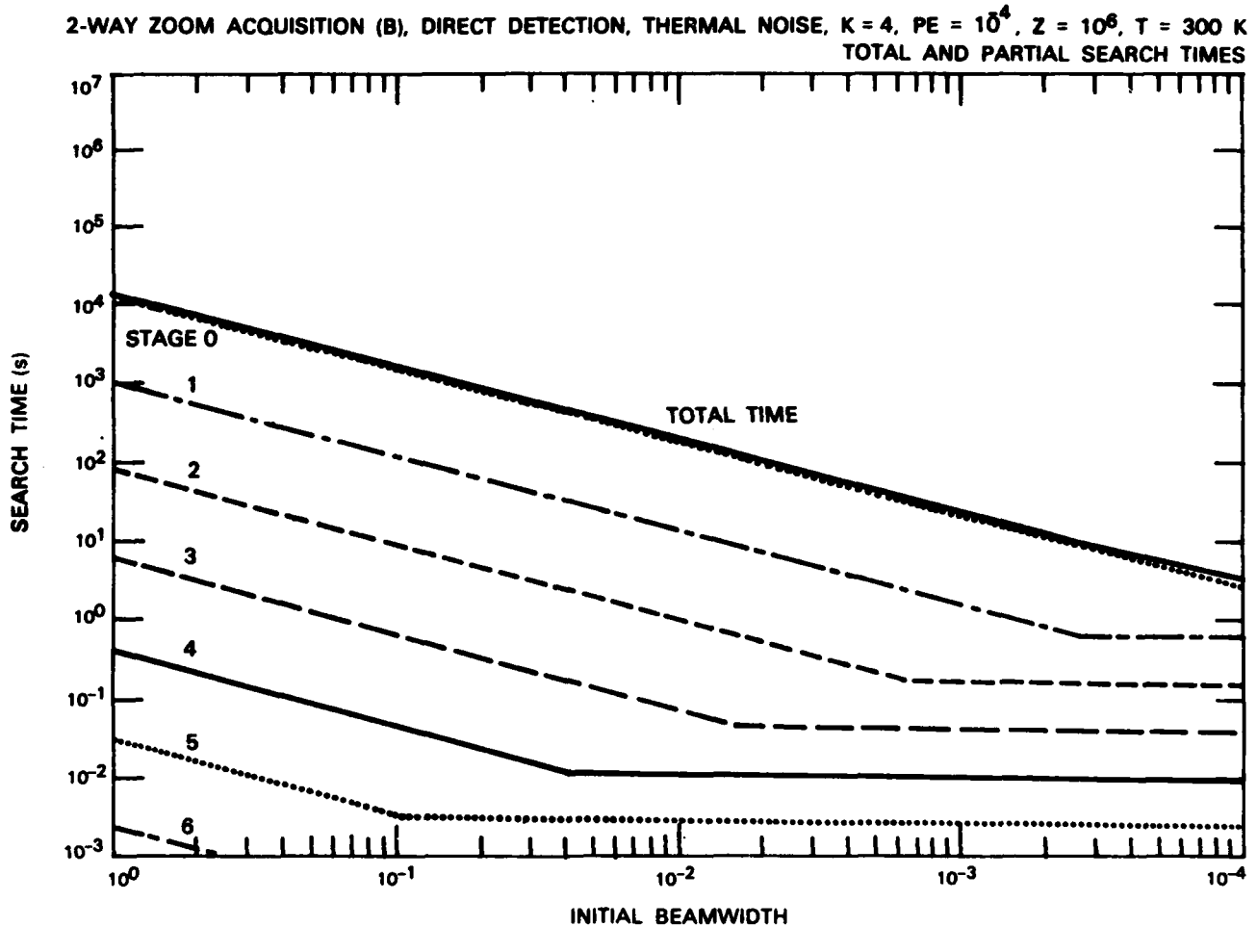

Fig. 4.8. Acquisition with zooming receiver, thermal noise limited direct detection, input impedance = 10^6 Ω: (e) optimal partition of T, 2-way zooming strategy (B).

AD-A150 794 SPATIAL ACQUISITION ALGORITHMS AND SYSTEMS FOR INTERSATELLITE OPTICAL COM..(U) MASSACHUSETTS INST OF TECH LEXINGTON LINCOLN LAB P VAN HOVE ET AL. 27 NOV 84 2/2

UNCLASSIFIED TR-667 ESD-TR-84-016 F19628-85-C-0002 F/G 17/2 NL

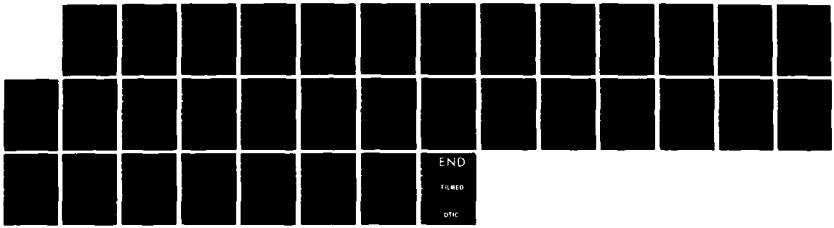

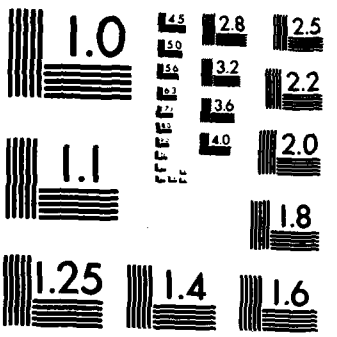

MICROCOPY RESOLUTION TEST CHART
NATIONAL BUREAU OF STANDARDS-1963-A

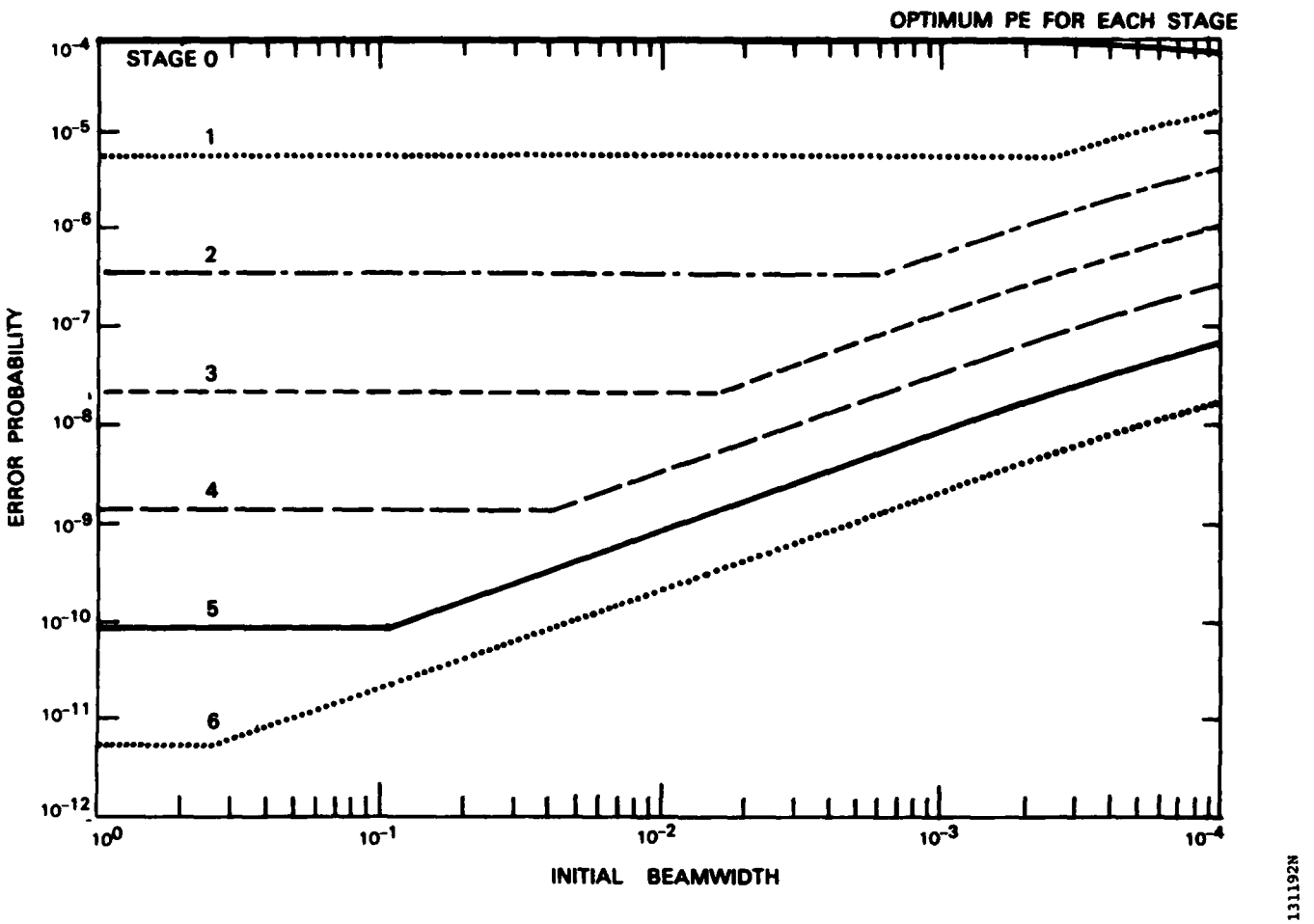

Fig. 4.8. Acquisition with zooming receiver, thermal noise limited direct detection, input impedance = 10^6 Ω: (f) optimal partition of PE, 2-way zooming strategy (B).

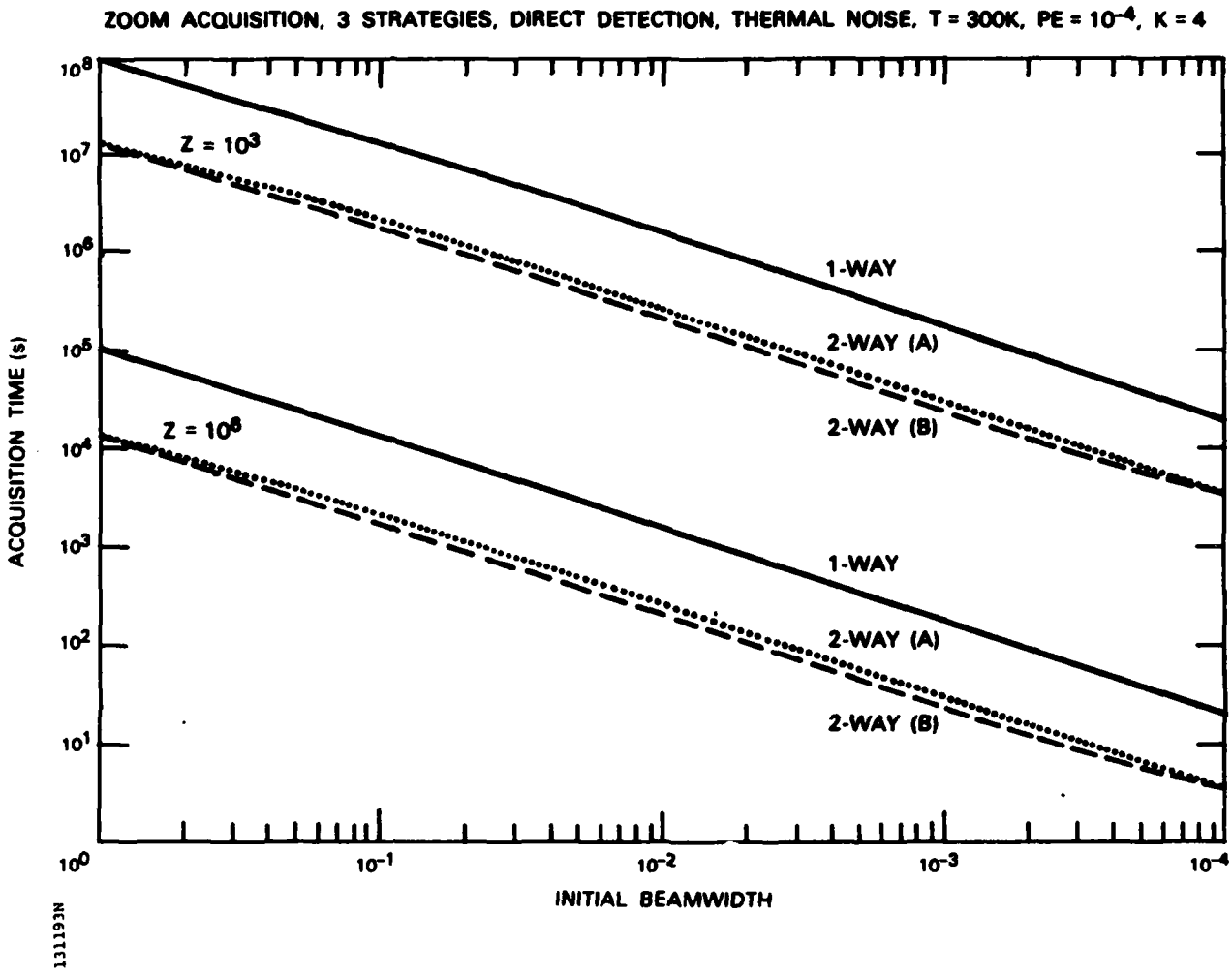

Fig. 4.9. Acquisition times for zooming receiver, thermal noise limited direct detection, comparison between three zooming strategies. Input impedance = 10^3, 10^6 Ω.

5. SUMMARY AND CONCLUSIONS

5.1 Introduction

We review in this chapter the results we have obtained for the spatial acquisition performance of a space optical communication link. Approximate expressions of the acquisition time for different transmitter and receiver strategies are given in Sec. 5.2. We suggest what the best receiver structure and acquisition strategy may be in Sec. 5.3.

5.2 Approximate Expressions for the Acquisition Time

We derive the approximate expressions in the following way. When the probability of erroneous acquisition is given by a Gaussian error function, we fix the argument of the function to 7. Because $\text{erfc}(7) \approx 10^{-12}$, this corresponds to the typical figure, $PE = 10^{-4}$, $M = 10^4$, $N^T = 10^4$. When the probability of error is given by an exponential, we use typical figures to derive a fixed value for the exponent.

The relevant signal parameter is the photon count rate for parallel illumination λ_s, derived from Eq. 1.2 as

$$\lambda_s = \frac{\eta_A P_B^L}{4h\nu} \left(\frac{D_A^R}{L\theta_A}\right)^2 \tag{1}$$

With the figures used in the examples of this report, $\lambda_s = 2 \times 10^4\ s^{-1}$.

5.2.1 Parallel Receiver Operation

For direct detection, Eq. (3.6) gives the performance for background noise and quantum noise limited operation and leads to the approximation

$$T \approx \frac{100}{N^T} \frac{\lambda_{bo}}{\lambda_s^2} + \frac{50}{\lambda_s} \tag{2}$$

Photomultiplication detectors usually need to be used to reach the above noise figures so that excess noise has to be taken into account.

$$T \approx F\left[\frac{100}{N^T} \frac{\lambda_{bo}}{\lambda_s^2} + \frac{50}{\lambda_s}\right] \tag{3}$$

Thermal noise limited operation results in an acquisition time given by inverting Eq. (3.9) and approximated by

$$T = \frac{100}{N^T} \frac{\lambda_{equ}}{\lambda_s^2} \tag{4}$$

where $\lambda_{equ} = k\tau/Ze^2 \approx 10^{17}/Z$ is a parameter which may be compared to λ_{bo} in Eq. (2). The quantum noise limit in Eq. (3.7) gives

$$T \approx \frac{10}{\lambda_s} \tag{5}$$

for an error probability of 10^{-4}.

For heterodyne detection, Eq. (2.17) corresponds to the performance of the acquisition when the signal has no amplitude fluctuations and is inverted as

$$T \simeq \frac{100}{N^T} \frac{W^F}{\lambda_s^2} + \frac{100}{\lambda_s} \tag{6}$$

The receiver filter bandwidth W^F has the same role as λ_{bo} in Eq. (2). Equation (2.21) corresponds to the unrealizable perfect frequency acquisition and gives

$$T \simeq \frac{60}{\lambda_s} \tag{7}$$

for a random frequency f_o and

$$T \simeq \frac{35}{\lambda_s} \tag{8}$$

for an a-priori known frequency f_o.

5.2.2 Serial Receiver Operation

In the case of a sequential search of the M spatial slots by K detectors at the receiver, the figures given above for parallel receiver operation are just increased by a factor of M/K.

5.2.3 Zooming Receiver Operation

We have seen in Chapter 4 that in most of the cases, the acquisition time is similar for one-way and two-way zooming and corresponds to the first stage of the search. The one-way zooming is much simpler to implement and should therefore be preferred. When we take into account that each detector covers M/K spatial modes at the first stage, we obtain the following approximations for the acquisition time T.

- Direct detection, background noise limited receiver

$$T \approx P\left[\frac{100}{N^T}\ \frac{M}{K}\ \frac{\lambda_{bo}}{\lambda_s^2} + \frac{50}{\lambda_s}\right] \tag{9}$$

- Direct detection, thermal noise limited/receiver

$$T \approx \frac{100}{N^T}\ \frac{\lambda_{equ}}{\lambda_s^2} \tag{10}$$

- Heterodyne detection, FM signal

$$T \approx \frac{100}{N^T}\ \frac{M}{K}^2\ \frac{W^F}{\lambda_s^2} + \frac{M}{K}\ \frac{100}{\lambda_s} \tag{11}$$

For background noise limited direct detection, i.e., when the first term is dominant in (3) and (9), the zooming performance in (9) is identical to the serial performance obtained by multiplying (3) by M/K. This may also be seen from the comparison of Figs. 3.4 and 4.7. For heterodyne detection, the zooming acquisition times given in Eq. (10) are worse than for the serial acquisition, due to the low efficiency of multimode mixing. This is obvious from the comparison of Figs. 2.7 and 4.4.

5.3 Discussion

The issue of choosing the right acquisition strategy for a specific situation depends on various factors such as performance, hardware complexity, weight, cost and device availability. The choice may therefore be dependent on

evolving factors such as technology state-of-the-art, so that no permanent answer exists. We will compare different strategies and point out the reasons why one should be preferred to the other. Among the various choices that have to be made, we will address the following. The illumination of the uncertainty zone may be parallel or serial, with the illumination beamwidth left as a parameter for serial illumination. The receiver is usually difficult to implement with a parallel structure, due to hardware complexity; the choice has therefore to be made between serial and zooming receiver structures. The detector technology may be heterodyne or direct detection, with or without photomultiplication.

5.3.1 Receiver Technology

The comparison between the different technologies may be simplified to the following comparison for low incident power. We approximate (3), (4), (6) by

$$T^a \simeq \frac{100}{N^T} \frac{\lambda_{equ}}{\lambda_s^2}$$

where $\lambda_{equ} \simeq \frac{10^{17}}{Z}$ for a PIN diode receiver and an amplifier of input impedance Z

$\lambda_{equ} \simeq \lambda_{bo} F$ for an APD or PMT receiver with noise factor F, in a background noise limited operation

$\lambda_{equ} = W^F$ for heterodyne detection with a filter bandwidth of W^F

It is clear that direct detection without photomultiplication has always the worst performance. If $\lambda_{bo} = 10^6$ counts per second and per spatial mode and F = 10, then with heterodyne detection, the receiver needs to filter in

bandwidths of 10 MHz to achieve a performance comparable to the performance for photomultiplied direct detection. This last technique has therefore the advantage for achieving the same performance with a much simpler implementation. If progress is done in laser stabilization and tuning however, heterodyne detection may gain the advantage over direct detection because it is almost insensitive to background noise.

For larger incident powers, i.e., when the second term is dominant in (3) and (6), the two technologies are comparable for F = 2. The optimal quantum limited performance given in (5) and (7) or (8) give the advantage to direct detection.

Although heterodyne detection can be superior to direct detection for signal demodulation with very large data rates, this advantage does not apply to spatial acquisition when there is frequency and phase randomness. Moreover, heterodyne receivers have twice the noise bandwidth of homodyne receivers but homodyning is not practical for spatial acquisition.

5.3.2 Receiver Strategy

The optimum receiver strategy is the parallel receiver in all cases, but receiver arrays of 10^4 elements and the accompanying electronics are unrealistic. For heterodyne detection, the sequential receiver operation outperforms the zooming operation. For direct detection, the zooming and serial operations give comparable performance for low signal to noise ratios, when the illumination beams are wide. Both receivers are then background noise limited. When the illumination beams are narrowed down, the serial receivers

reach the quantum limited performance earlier than the zooming receivers; see Fig. 5.1.

From expression (3), the serial receiver is background limited when

$$\frac{\lambda_{bo}}{N^T \lambda_s^2} > \frac{2}{\lambda_s} \quad \text{or} \quad N^T < \frac{\lambda_{bo}}{2\lambda_s}$$

From expression (9), the zooming receiver is background limited when

$$\frac{M}{K} \frac{\lambda_{bo}}{N^T \lambda_s^2} > \frac{2}{\lambda_s} \quad \text{or} \quad N^T < \frac{M}{K} \frac{\lambda_{bo}}{2\lambda_s}$$

Background noise limited operation is therefore obtained for larger values of N^T, for the zooming receiver.

The expressions derived here therefore give the advantage to the zooming receiver operation. Caution should be taken however because the background noise model includes no spatial variations. This assumption is not verified in practice and a quantum noise limited operation may prove much more robust than a background noise limited operation.

In all cases except for thermal noise limited direct detection, the first stage of a zooming strategy is predominant. Since the first stage is independent on the zooming strategy, the most simple strategy may be chosen. One-way zooming, which consists of illuminating the complete initial uncertainty zone during the total search time, is therefore the advisable zooming strategy. Moreover, the travel time of light from A to B needs to be added between the stages in a cooperative two-way zooming procedure. The one-way zooming strategy is therefore optimal for small T.

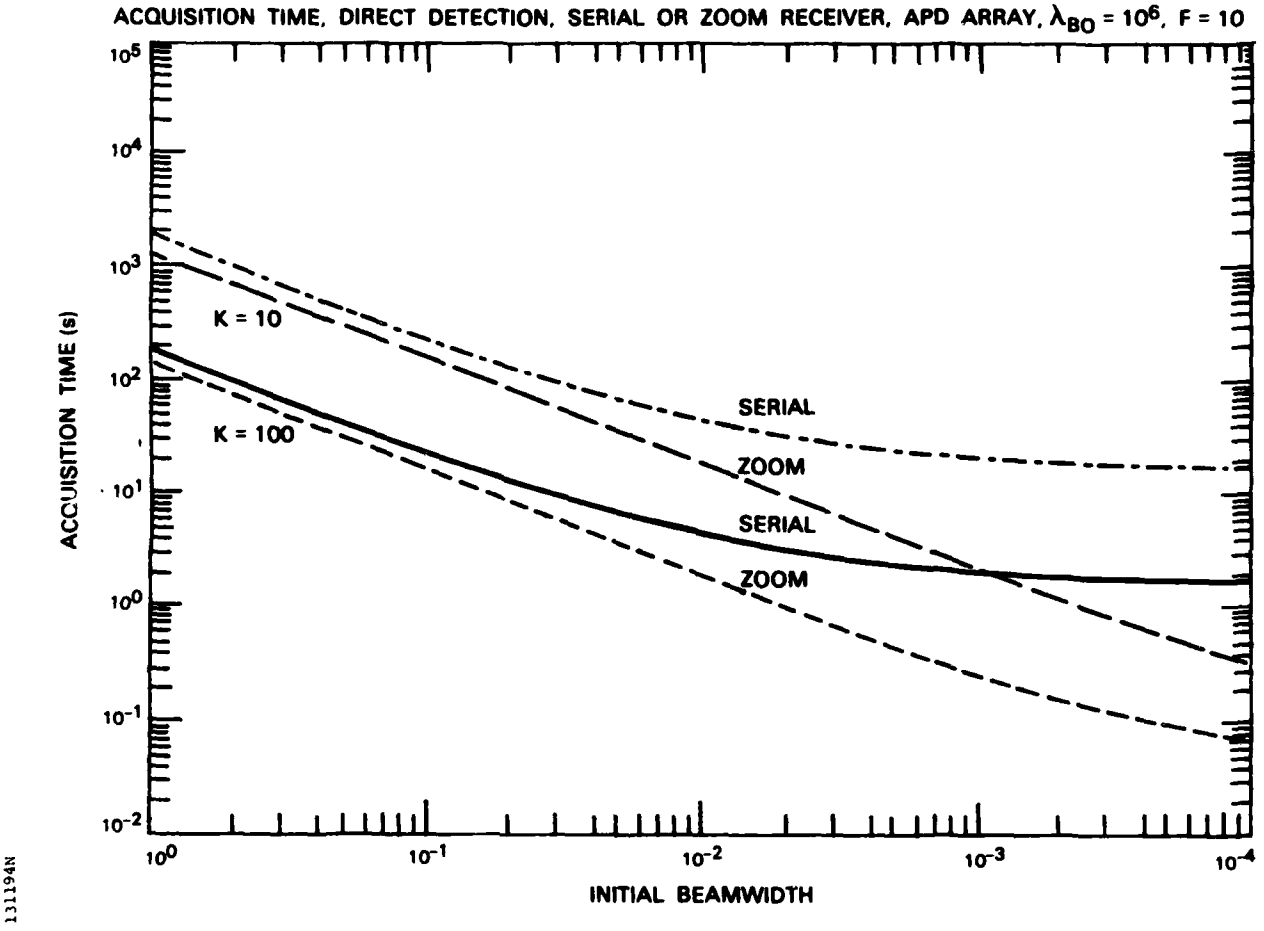

Fig. 5.1. Acquisition times with a receiver array of 10, 100 photomultiplied direct detectors, comparison between serial and zooming strategy.

5.3.3 Illumination Strategy

The performance is always improved by illuminating the uncertainty zone sequentially with a diffraction limited beam. The robustness of this strategy with respect to relative motion may not be adequate however. A performance close to optimal may be reached with a wider illumination beam for a sequential receiver if the two terms in expressions (3) or (6) have the same order of magnitude. This implies that increasing N^T above $5\lambda_{bo}/\lambda_s$ for direct detection and $2W^F/\lambda_s$ for heterodyne detection does not reduce the acquisition time significantly for a sequential receiver operation.

5.3.4 Conclusion

From the present analysis, it turns out that two acquisition strategies are advisable. They both use a receiver of photomultiplied direct detectors and a serial illumination scheme. The receiver operation may be a serial or a one-way zooming operation depending on robustness considerations, with the advantage to zooming over serial for the performance.

Arrays of APD are not yet realizable because of the large bias voltages involved. This issue may be circumvented by linking the optical system focal plane to a number of separated APD by an optical fiber bundle. A different photomultiplied receiver array may be obtained by combining a microchannel plate and a photodiode array.

Figure 5.1 shows curves of acquisition times for the two above mentioned strategies, for K = 10 and K = 100. The noise factor F is taken as 10 and the background noise count rate per spatial mode λ_{bo} as 10^6 s^{-1}.

The assumption that the spatial parameter is discrete valued is not verified in practice. If the incoming signal is centered on a corner of the detector array, the signal power is split to four detectors. The signal power has therefore to be increased by a factor of 4.

If shorter acquisition times are required, it is possible to improve the search by providing a beacon laser of power $P^{LA} \gg P^{L}$ on one of the satellites, say A. Satellite B will therefore acquire the position of A with a search time given by the above expressions, with P_A^L replaced by P_A^{LA}. The acquisition time decreases at least as fast as the inverse of the laser power P^{LA}. The acquisition of the position of B from A is afterwards improved because Ω_A^U is reduced to the diffraction limit, so that B may concentrate the smaller power of its laser into a smaller zone. An asymmetric spatial acquisition may therefore be dominated by the fastest search, if the two searches are done successively.

REFERENCES

1. V. W. S. Chan, "Coherent Optical Space Communications System Architecture and Technology Issues," Proc. SPIE Vol. 295: Control and Communications Technology in Laser Systems (Society of Photo-Optical Instrumentation Engineers, Bellingham, Washington, 1981), pp. 10-17, DTIC AD-A114499/7.

2. H. L. Van Trees, Detection, Estimation and Modulation Theory 1, Sec. 4.2.3 (Wiley, New York, 1968).

3. A. Wald, Sequential Analysis (Wiley, New York, 1947).

4. H. L. Van Trees, "Detection, Estimation and Modulation Theory III, Secs. 2.1.3, 4.1.1, (Wiley, New York, 1971).

5. A. J. Viterbi, Principles of Coherent Communication, Sec. 8.10, (McGraw-Hill, New York, 1966).

6. R. M. Gagliardi and S. Karp, Optical Communications, Sec. 11.2, (Wiley, New York, 1976).

7. R. M. Gagliardi and S. Karp, op. cit., Sec. 7.4.

APPENDIX 1

STATISTICS AFTER ENERGY DETECTION IN A BANDWIDTH W^F

The incoming signal is processed by the detector shown in Fig. A1.

Signal Model (a): GRP with rectangular PSD, power P^S

Bandwidth W^S one-sided included in W^F

AWGN of PSD $N_o/2$

Signal and noise statistically independent.

The spectral density of the signal x is shown on Fig. A2. The output y of the bandpass filter has a spectrum Syy(f) which is also shown on Fig. A2. Furthermore,

$$R_{yy}(0) = \int_{-\infty}^{+\infty} S_{yy}(f)\, df = P^S + N_o W^F = S^S W^S + N_o W^F \quad .$$

where $S^S/2 = P^S/2W^S$ is the signal double sided PSD height.

The signal y is squared and the resulting signal z is characterized by

$$m_z = R_{yy}(0)$$

$$R_{zz}(\tau) = R_{yy}^2(0) + 2\, R_{yy}^2(\tau)$$

$$S_{zz}(f) = R_{yy}^2(0)\, \delta(f) + 2\, S_{yy}(f) * S_{yy}(f)$$

The squared signal z is integrated during T seconds and the result R is characterized by

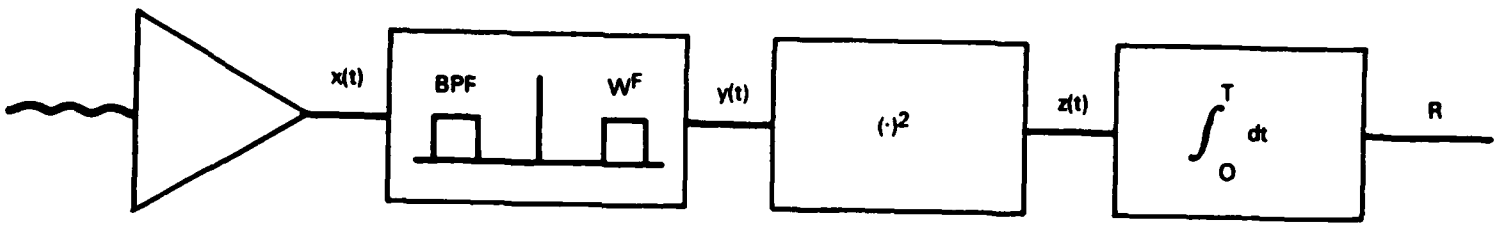

Fig. A1. Receiver front-end block diagram.

131195N

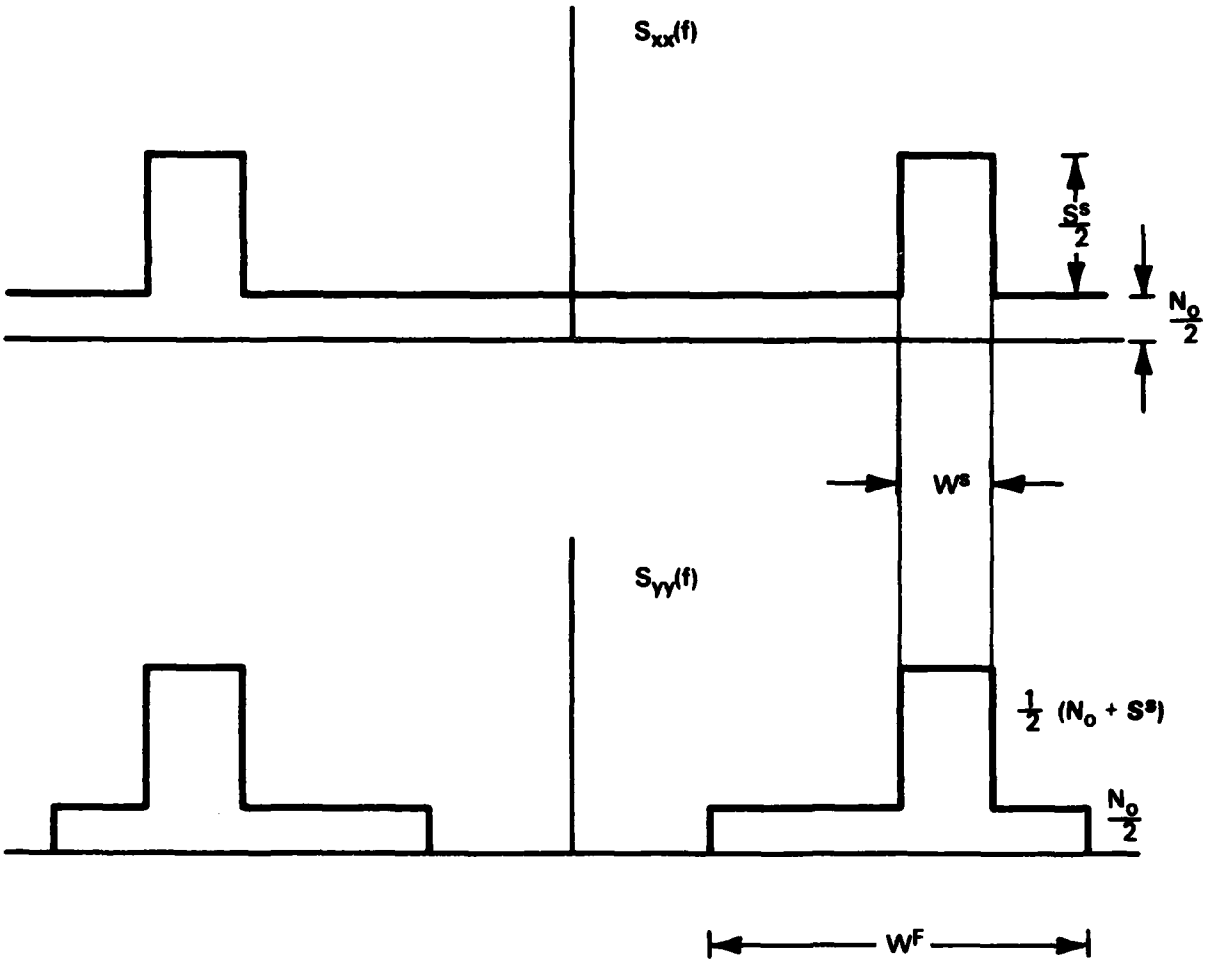

131196R

Fig. A2. Spectra of x(r), y(r).

$$E(R) = T\,m_z = T\,R_{yy}(0) = P^s T + N_o W^F T$$

$$E(R^2) = \int_{-\infty}^{+\infty} S_{zz}(f)\,T^2 \left(\frac{\sin \pi fT}{\pi fT}\right)^2 df$$

$$= R_{yy}^2(0)T^2 + 2\int_{-\infty}^{+\infty} [S_{yy}(f) * S_{yy}(f)]\,T^2 \left(\frac{\sin \pi fT}{\pi fT}\right)^2 df$$

If $S_{yy}(f)$ is smooth over frequency intervals of the order of magnitude of $1/T$, the convolution product may be taken out of the integral

$$E(R^2) = R_{yy}^2(0)\,T^2 + 2\,S_{yy}(f) * S_{yy}(f)\Big|_{f=0} \cdot \int_{-\infty}^{+\infty} T^2 \left(\frac{\sin \pi fT}{\pi fT}\right)^2 df$$

$$\text{Var}\,(R) = E(R^2) - E^2(R) = 2T \int_{-\infty}^{+\infty} \left[S_{yy}(f)\right]^2 df$$

$$= 2T \left(\frac{No}{2}\right)^2 (2W^F - 2W^s) + \left(\frac{N_o}{2} + \frac{S^s}{2}\right)^2 (2W^s)$$

$$= N_o^2\,W^F T + 2N_o P^s T + \frac{{P^s}^2}{W^s}\,T \quad .$$

The random variable R is a χ^2 variable of order approximately $2W^F T$. If the order is larger than 100, the statistics are accurately modeled by Gaussian statistics.

In the presence of the signal, we have therefore

$$R \approx N(m_s, \sigma_s^2)$$

$$m_s = N_o W^F T + P^S T$$

$$\sigma_s^2 = N_o^2 W^F T + 2 N_o P^S T + \frac{P^{S^2}}{W^S} T$$

When only noise is present, the statistics are obtained from the above by inserting $P^S = 0$:

$$R \sim N(m_n, \sigma_n^2)$$

$$m_n = N_o W^F T$$

$$\sigma_n^2 = N_o^2 W^F T$$

Signal Model (b): Signal with frequency noise but no amplitude noise

Bandwidth W^S one-sided included in W^F

AWGN of PSD $N_o/2$

Signal and noise statistically independent.

We conserve the notation used for signal model (a).

x - characterization

$$x(t) = s(t) + n(t) \qquad E[s^2(t)] = P^S$$

y - characterization

$$y(t) = s(t) + n_f(t)$$

where $n_f(t)$ is the filtered version of $n(t)$, and assuming the signal is completely in the filter bandwidth.

z - characterization

$$z(t) = s^2(t) + s(t)\, n_f(t) + n_f^2(t)$$

$$m_z = E\,[s^2(t)] + 2\, E[s(t)]\, E[n_f(t)] + E[n_f^2(t)]$$

$$= P^S + N_o W^F$$

R - characterization

$$m_R = \int_o^T m_z(t)\, dt = P^S T + N_o W^F T$$

$$\text{Var}\,(R) = \text{Var} \int_o^T 2s(t)\, n_f(t)\, dt + \text{Var} \int_o^T n_f^2(t)\, dt$$

The first term is the variance of a zero-mean variable and therefore equal to its mean square. An expression for the second term is given by σ_n^2 in model (a) above.

$$\text{Var}\,(R) = N_o^2 W^F T + 4 \int_o^T dt \int_o^T du\, E[s(t)s(u)]\, E[n_f(t)n_f(u)]$$

$$\simeq N_o^2 W^F T + 4 \int_o^T dt \int_o^T du\, R_{ss}(t-u)\, \frac{N_o}{2}\, \delta(t-u)$$

$$= N_o^2 W^F T + 2 N_o P^S T$$

In this case also, R is the sum of approximately $2W^FT$ independent random variables. If $W^FT > 100$, we have:

$$R \approx N(m_n, \sigma_n^2)$$

$$m_n = P^ST + N_oW^FT$$

$$\sigma_n^2 = N_o^2W^FT + 2N_oP^ST$$

Signal Model (c): Random phase sinusoid

AWGN of spectral height $N_o/2$

Signal and noise statistically independent.

We conserve the notation introduced for signal (a)

$$x(t) = \sqrt{2P^S} \cos 2\pi f_o T + n(t)$$

$$y(t) = \sqrt{2P^S} \cos 2\pi f_o t + n_f(t)$$

$$z(t) = y^2(t) = 2P^S \cos^2(2\pi f_o t) + 2\sqrt{2P^S} \cos(2\pi f_o t)\, n_f(t) + n_f^2(t)$$

$$m_R = \int_o^T m_z(t)\, dt = P^ST + N_oW^FT$$

$$\text{Var}[R] = \text{Var} \int_o^T 2\sqrt{2P^S} \cos(2\pi f_o t) n_f(t) dt + \text{Var} \int_o^T n_f^2(t) dt$$

From the projection of the flat spectral density noise on one coordinate of an orthogonal expansion, we know that

$$\text{Var} \int_0^T \sqrt{\frac{2}{T}} \cos(2\pi f_o t)\, n(t)dt = \frac{N_o}{2}$$

The first term in the expression of Var [R] is therefore $4P^S T\, N_o/2$. The second term is σ_n^2 from signal model (a) and therefore,

$$\sigma_R^2 = N_o^2 W^F T + 2N_o P^S T \quad .$$

APPENDIX 2

BINARY AND M-ARY ORTHOGONAL DETECTION, WITH UNEQUAL MEANS AND VARIANCES FOR SIGNAL AND NOISE

The problem is expressed as follows for binary detection:

$$\begin{aligned} H_1: \quad & R_1 \sim N(m_s, \sigma_s^2) \\ & R_o \sim N(m_n, \sigma_n^2) \\ H_o: \quad & R_1 \sim N(m_n, \sigma_n^2) \\ & R_o \sim N(m_s, \sigma_s^2) \end{aligned} \tag{A2-1}$$

with $\sigma_s^2 > \sigma_n^2$ and $m_s > m_n$.

The conditional probabilities are given by:

$$P_{\underline{R}|H_o}(R_o, R_1 | H_o) = \frac{1}{2\pi\sigma_s\sigma_n} e^{\frac{1}{2}\left[\frac{(R_o - m_s)^2}{\sigma_s^2} + \frac{(R_1 - m_n)^2}{\sigma_n^2}\right]}$$

$$P_{\underline{R}|H_o}(R_o, R_1 | H_1) = \frac{1}{2\pi\sigma_s\sigma_n} e^{\frac{1}{2}\left[\frac{(R_o - m_n)^2}{\sigma_n^2} + \frac{(R_1 - m_s)^2}{\sigma_s^2}\right]} \tag{A2-2}$$

The LRT is obtained as:

$$(R_1 - R_o)(R_1 + R_o - 2R_T) \underset{H_o}{\overset{H_1}{\gtrless}} 0 \qquad \text{(A2-3)}$$

or

$$|R_1 - R_T| \underset{H_o}{\overset{H_1}{\gtrless}} |R_o - R_T| \qquad \text{(A2-4)}$$

where

$$R_T = \frac{m_n \sigma_s^2 - m_s \sigma_n^2}{\sigma_s^2 - \sigma_n^2} \qquad \text{(A2-5)}$$

The resultant partition of the decision plane (R_o, R_1) into (Z_o, Z_1) is shown in Fig. A3.

The implementation of the optimal rule (A2-4) implies the knowledge of R_T, related to the signal parameters.

The intuitive decision rule

$$R_1 \underset{H_o}{\overset{H_1}{\gtrless}} R_o \qquad \text{(A2-6)}$$

is only suboptimal, but is close to (A2-4) when R_T is small. The range of R_T is from $-\infty$ when $\sigma_s = \sigma_n$ to m_n when $\sigma_s \gg \sigma_n$. The signals considered in Chapter 3 result in the following values. For Signal Model b), $R_T = m_n/2$. For Model a), $m_n/2 < R_T < m_n$. We see therefore that the optimal decision rule is also dependent on the signal model. We therefore consider only the suboptimal rule given in (A2-6).

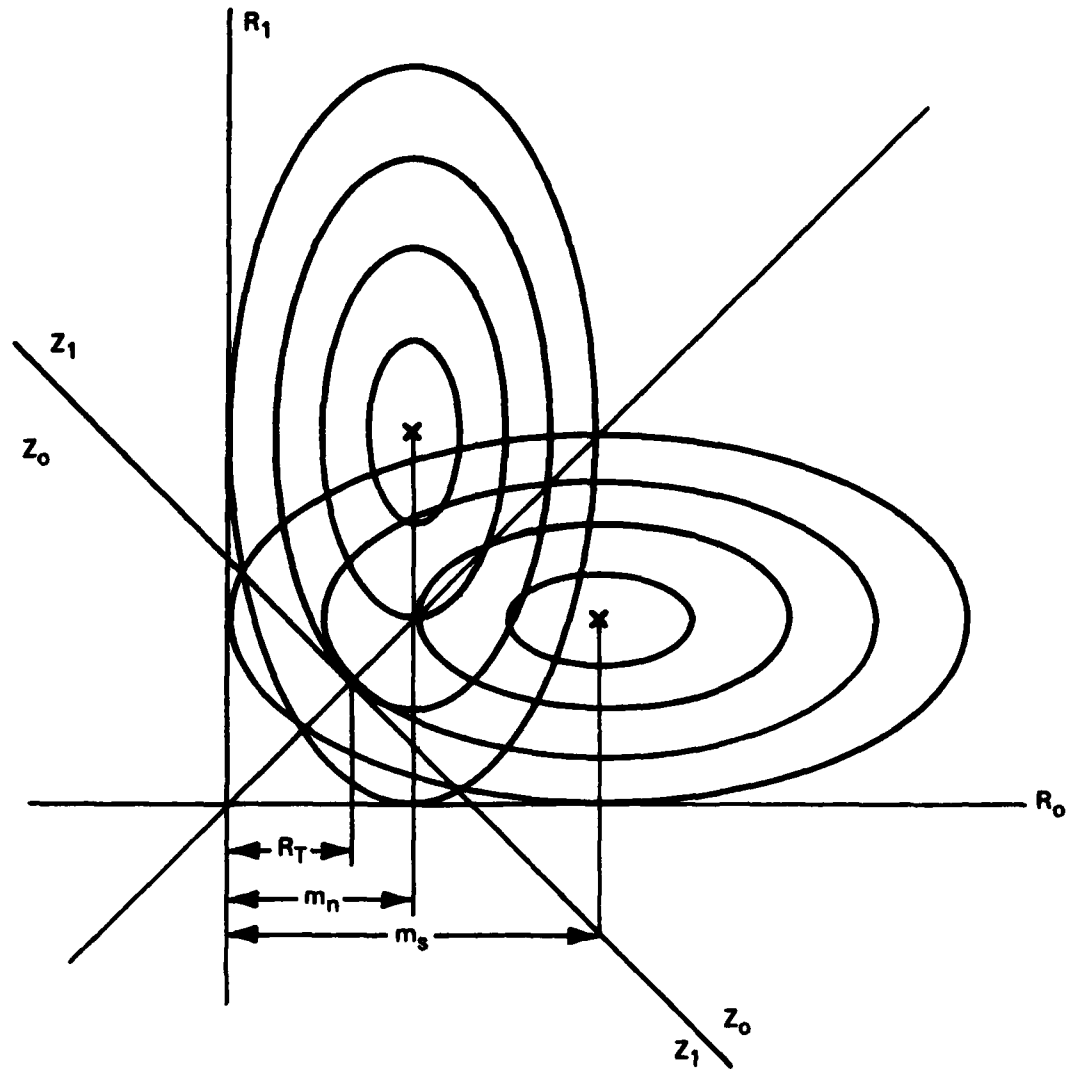

131197N

Fig. A3. Decision space for Gaussian binary detection, unequal means and variances.

The sufficient statistic for the suboptimal rule in (A2-6) is

$$\ell = R_1 - R_o \underset{H_o}{\overset{H_1}{\gtrless}} 0$$

$$\ell \approx N(m_s - m_n,\ \sigma_s^2 + \sigma_n^2) \,|H_1$$

$$\ell \approx N(-m_s + m_n,\ \sigma_s^2 + \sigma_n^2) \,|H_o$$

$$PE^{(2)} = \operatorname{erfc} \sqrt{\frac{m_s - m_n}{\sigma_s^2 + \sigma_n^2}}$$

M-ary Signaling The optimum decision rule is to find the largest $|R_1 - R_T|$ where R_T is given in (A2-5). The suboptimal rule of choosing the largest R_1 has an error probability which is upper bounded by

$$PE \leq (M - 1) \operatorname{erfc} \sqrt{\frac{m_s - m_n}{\sigma_s^2 + \sigma_n^2}}$$

APPENDIX 3

COMPOSITE M-ARY DETECTION WITH AN N-ARY UNWANTED PARAMETER APPLIED TO ORTHOGONAL RANDOM PHASE SINUSOIDS

One out of N x M orthogonal signals may be received with equal a priori probabilities. This set of possible signals is divided into M classes of N signals. The relevant problem is to detect the class of the received signal. The unwanted parameter specifies the particular signal in the class.

Mathematical formulation:

Under hypothesis H_{ij}, $\underline{r}(t) = \underline{S}_{ij}(t) + \underline{n}(t)$ (A3-1)

All $\underline{S}_{ij}(t)$ are orthogonal, $\underline{n}(t)$ is AWGN.

The index i specifies the relevant parameter and j the unwanted parameter. For our particular problem, i specifies the spatial position and j specifies the frequency and time of arrival of the signal. The analysis presented below is more general however. If C_{ij}^{kl} = cost of declaring hypothesis kl when signal ij is present, then the cost assignment

$$C_{ij}^{kl} = \delta_{ik} \tag{A3-2}$$

emphasizes no cost is incurred for $j \neq l$ as long as $i = k$. The optimal decision rule is to find

$$\max_{i} \sum_{j=1}^{N} P_{\underline{r}(t)|H_{ij}}(\underline{R}(t)|H_{ij}) \tag{A3-3}$$

and declare hypothesis H_p if the maximum is attained for i = p. In the particular case where $S_{ij}(t)$ are orthogonal random phase sinusoids, the observation is reduced to

$$X_{ij} = \left(R_{ijc}^2 + R_{ijs}^2\right)^{1/2} \tag{A3-4}$$

where R_{ijs} and R_{ijc} represent the sine and cosine integrated signal S_{ij}. The conditional statistics are

$$P_{\underline{x}|H_{ij}}(\underline{X}|H_{ij}) = \frac{2}{N_o}^{NXM} e^{-\frac{1}{N_o}\left(\sum_{k=1}^{M}\sum_{n=1}^{N} X_{kn}^2 + E\right)} I_o\left(\frac{2E}{N_o} X_{ij}\right) \prod_{k=1}^{M}\prod_{n=1}^{N} X_{kn} \tag{A3-5}$$

The optimal decision rule is to find:

$$\max_i \sum_{j=1}^{N} I_o\left(\frac{2\sqrt{E}}{N_o} X_{ij}\right) \tag{A3-6}$$

And declare hypothesis H_p if the maximum is attained for i = p. For large SNR, $I_o(x)$ has an exponential dependence on x. The suboptimal rule

$$\max_i \max_j X_{ij} \tag{A3-7}$$

is therefore close to optimal for large SNR. Furthermore, (A3-7) is independent of the signal parameters.

Exact error probability for the suboptimal receiver (A3-7)

$$PE = 1 - PAC = 1 - PAC|H_{11} \qquad \text{(symmetric problem)}$$

$$PAC\left|H_{11}\right. = \sum_{k=1}^{N} \Pr\left(X_{1k} \text{ is the largest of all } X_{ij}\left|H_{11}\right.\right)$$

$$= \Pr\left(X_{11} > \text{all } X_{ij} \text{ for } (ij) \neq (1,1)\left|H_{11}\right.\right)$$

$$+ (N-1)\Pr\left(X_{12} > \text{all } X_{ij} \text{ for } (i,j) \neq (1,2)\left|H_{11}\right.\right)$$

$$= P_a + (N-1)P_b$$

We now evaluate P_a and P_b.

$$P_a = \Pr\left[X_{11} > \text{all } X_{ij} \text{ for } (i,j) \neq (1,1)\left|H_{11}\right.\right]$$

$$= \frac{2}{N_o} e^{-\frac{E}{N_o}} \int_0^{\infty} dX_{11}\, e^{-\frac{X_{11}^2}{N_o}} I_o\left(\frac{2\sqrt{E}}{N_o} X_{11}\right) X_{11} \left[\frac{2}{N_o} \int_0^{X_{11}} dX_{ij}\, e^{-\frac{X_{ij}^2}{N_o}} X_{ij}\right]^{NM-1}$$

$$= \sum_{i=0}^{NM-1} \binom{NM-1}{i} \frac{(-1)^i}{i+1} e^{-\frac{i}{i+1}\frac{E}{N_o}} = 1 - \frac{1}{NM} e^{-\frac{E}{N_o}} \sum_{i=2}^{NM} (-1)^i \binom{NM}{i} e^{\frac{E}{iN_o}}$$

$$P_b = \Pr\left[X_{12} > \text{all } X_{ij} \text{ for } (i,j) \neq (1,2)\left|H_{11}\right.\right]$$

$$= \frac{2}{N_o} e^{-\frac{E}{N_o}} \int_0^{\infty} dX_{11}\, e^{-\frac{X_{11}^2}{N_o}} I_o\left(\frac{2E}{N_o} X_{11}\right) \frac{2}{N_o} \int_{X_{11}}^{\infty} dX_{12}\, e^{-\frac{X_{12}^2}{N_o}} X_{12} \left[\frac{2}{N_o} \int_0^{X_{12}} dX_{ij}\, e^{-\frac{X_{ij}^2}{N_o}} X_{ij}\right]^{NM-2}$$

$$= \sum_{i=0}^{NM-2} \frac{\binom{NM-2}{i}}{(i+1)} \frac{(-1)^i}{(i+2)} e^{-\frac{(i+1)}{(i+2)} \frac{E}{N_o}}$$

$$= \frac{1}{NM\ (NM-1)} e^{-\frac{E}{N_o}} \sum_{i=2}^{NM} \binom{NM}{i} (-1)^i e^{\frac{E}{iN_o}}$$

$$PE = 1 - [P_a + (N-1) P_b]$$

$$= \frac{1}{NM} - \frac{(N-1)}{NM\ (NM-1)} e^{-\frac{E}{N_o}} \sum_{i=2}^{NM} \binom{NM}{i} (-1)^i e^{\frac{E}{iN_o}}$$

$$PE = \frac{M-1}{M\ (NM-1)} e^{-\frac{E}{N_o}} \sum_{i=2}^{NM} (-1)^i e^{\frac{E}{iN_o}} \binom{NM}{i} \qquad \text{(A3-8)}$$

This is the exact error formulation for the suboptimal receiver in (A3-7). The sum in (A3-8) is upper bounded by its first term.

$$PE \leq \frac{N(M-1)}{2} e^{-\frac{E}{2N_o}} \qquad \text{(A3-9)}$$

The formula (A3-9) is a union-type bound; an error may occur only when the received signal projected on one of the (M - 1) non-signal classes exceeds the projection on the transmitted signal.

APPENDIX 4

BOUNDS TO POISSON DETECTION ERROR PROBABILITIES

a) Binary Detection

The two discrete valued independent random variables r_1 and r_o are conditionally Poisson distributed with means m_1 and m_o on H_1, or m_o and m_1 on H_o, with $m_1 > m_o$. Generally $m_o = n_B$ is the expected number of background counts and $m_1 = n_B + n_S$ is the expected number of background + signal counts. The optimal decision rule for MEP and equal a priori probabilities is

$$R_1 \underset{H_o}{\overset{H_1}{\gtrless}} R_o$$

The error probability is given by

$$PE = 1 - \sum_{n=1}^{\infty} \frac{e^{-m_1} (m_1)^n}{n!} \sum_{m=o}^{n-1} \frac{e^{-m_o}(m_o)^m}{m!} \qquad \text{(A4-1)}$$

assuming that equal counts results in an error. Equation (A4-1) may also be expressed as [7].

$$PE = e^{-(m_o+m_1)} \sum_{p=0}^{\infty} \left(\sqrt{\frac{m_o}{m_1}}\right)^p I_p(2\sqrt{m_o m_1}) \qquad \text{(A4-2)}$$

Bounds to Eqs. (A4-1) or (A4-2) are given below.

$$PE < e^{-(m_o+m_1)} \frac{\sqrt{m_1}}{\sqrt{m_1} - \sqrt{m_o}} I_o\left(2\sqrt{m_o m_1}\right) \tag{A4-3}$$

$$PE < \frac{1}{\sqrt{4\pi}} \sqrt[4]{\frac{m_1}{m_o}} \frac{1}{\sqrt{m_1} - \sqrt{m_o}} e^{-(\sqrt{m_1} - \sqrt{m_o})^2} \tag{A4-4}$$

$$PE < \frac{1}{\sqrt{4\pi}} \frac{1}{1 - m_o} \frac{1}{4\sqrt{m_o m_1}} e^{-(\sqrt{m_1} - \sqrt{m_o})^2} \tag{A4-5}$$

The bound in (A4-5) is valid only for $m_o < 1$

$$PE < e^{-(\sqrt{m_1} - \sqrt{m_o})^2} \tag{A4-6}$$

the bound in (A4-6) is known as the Chernov bound. Note the three above bounds have the same exponential dependence on the average counts. The Gaussian approximation is accurate for large m_o, m_1 and is given by

$$PE \simeq \text{erfc}\left[\frac{m_1 - m_o}{\sqrt{m_o + m_1}}\right] \tag{A4-7}$$

b) M-ary Detection

The optimal decision rule is again the largest count selection. The error probability is given by

$$PE = 1 - \sum_{n=1}^{\infty} \frac{e^{-m_1}(m_1)^n}{n!} \left[\sum_{M=0}^{n-1} \frac{e^{-m_o}(m_o)^m}{m!} \right]^{M-1} \qquad \text{(A4-8)}$$

The M-ary error probability is always upper limited by the union bound, using any binary error bound. Considering (A4-6) for the binary error, we have:

$$PE \leq (M - 1)\, e^{-(\sqrt{m_1} - \sqrt{m_o})^2} \qquad \text{(A4-9)}$$

This bound is tight when the (M - 1) possible binary errors are lowly correlated. In the case of low m_o however, the binary errors are highly correlated and (A9-9) may over-estimate PE by a factor of up to (M - 1). Another M-ary error bound is found by noting that no error occurs if the signal count is higher than the sum of all noise counts.

$$PE \leq e^{-(\sqrt{m_1} - \sqrt{(M - 1)\, m_o})^2} \qquad \text{(A4-10)}$$

This bound gives the exact PE for $m_o = 0$.

REPORT DOCUMENTATION PAGE		READ INSTRUCTIONS BEFORE COMPLETING FORM
1. REPORT NUMBER ESD-TR-84-016	2. GOVT ACCESSION NO.	3. RECIPIENT'S CATALOG NUMBER
4. TITLE *(and Subtitle)* Spatial Acquisition Algorithms and Systems for Intersatellite Optical Communication Links		5. TYPE OF REPORT & PERIOD COVERED Technical Report 6. PERFORMING ORG. REPORT NUMBER Technical Report 667
7. AUTHOR(s) Patrick Van Hove and Vincent W.S. Chan		8. CONTRACT OR GRANT NUMBER(s) F19628-85-C-0002
9. PERFORMING ORGANIZATION NAME AND ADDRESS Lincoln Laboratory, M.I.T. P.O. Box 73 Lexington, MA 02173-0073		10. PROGRAM ELEMENT, PROJECT, TASK AREA & WORK UNIT NUMBERS Program Element No. 63431F
11. CONTROLLING OFFICE NAME AND ADDRESS Air Force Systems Command, USAF Andrews AFB Washington, DC 20331		12. REPORT DATE 27 November 1984 13. NUMBER OF PAGES 132
14. MONITORING AGENCY NAME & ADDRESS *(if different from Controlling Office)* Electronic Systems Division Hanscom AFB, MA 01731		15. SECURITY CLASS. *(of this report)* Unclassified 15a. DECLASSIFICATION DOWNGRADING SCHEDULE

16. DISTRIBUTION STATEMENT *(of this Report)*

Approved for public release; distribution unlimited.

17. DISTRIBUTION STATEMENT *(of the abstract entered in Block 20, if different from Report)*

18. SUPPLEMENTARY NOTES

None

19. KEY WORDS *(Continue on reverse side if necessary and identify by block number)*

optical communication
spatial acquisition
laser communication
satellite cross links

20. ABSTRACT *(Continue on reverse side if necessary and identify by block number)*

Spatial acquisition strategies and technologies are analyzed for optical communication systems. Theoretical analysis is followed by examples and comparisons to aid system design. Examples are given for state-of-the-art technology appropriate for space applications.

Originator-supplied keywords include:

END

FILMED

4-85

DTIC